Graft Copolymer Stabilized Gold Nanoparticles and Their Applications and Chemically Cleavable Linkers and Their Applications

A THESIS
SUBMITTED TO THE FACULTY OF THE GRADUATE SCHOOL
OF THE UNIVERSITY OF MINNESOTA
BY

Jun Sung Kang

IN PARTIAL FULFILLMENT OF THE REQUIREMENTS
FOR THE DEGREE OF
DOCTOR OF PHILOSOPHY

T. Andrew Taton, Advisor

May 2013

Acknowledgements

I would like to thank all those who have helped, advised, supported, encouraged, and motivated me. With them, the time in University of Minnesota is valuable and unforgettable to me.

I would like to thank my advisor, T. Andrew Taton for his advices and supports. His distinguished insight, advice, and suggestion, from the beginning of my Ph.D course, have given me many opportunities to learn a lot of science, chemistry, and culture. Without him, I would not have been able to finish my Ph.D. I would also like to thank Prof. Distefano and Prof. Seelig for their valuable time and advice. I want to express my thanks to Barbara Beers for her help in my English improvement.

I would like to thank my past and present group members who have helped me, communicated with me, and contributed to my work. In particular, I am very grateful to Alexi Young, Walt Partlo, and Chandru Ramasubramanian, who have spent their valuable time for research discussion, great friendship, and memorable cheer. I would also like to thank my colleagues, including Santosh Khatwani, Kevin Landmark, Amanda Maxwell, Min Woo Jang, Jin-Hwa Chung, and Isaac Marks. I would like to express my gratitude for Aleardo Morelli in Prof. Seelig group who helped me for degradable PAGE. I have had a wonderful time with many Korean friends in Chemistry and CEMS. Particularly, I want to show my thanks to Juhee Cho, Sungjun Hong, Bong Soo Kim, Junha Jeon, Seongho Choi, Won Cheol Yoo, Jaebeom Han, Changyub Paek, Yong Wook Kim, Myungeun Seo, Youngmin Lee, Donghyuk Kim, and Soon Yong So, who have given productive discussion and broader insights into other chemical fields.

Most of all, I am really indebted to my parents, my wife, my sister, and my twin brother. I always feel that I have not got enough chance to show my gratitude to them. With their support and dedication, I can finish this work. I really thank all of them.

Abstract

This thesis consists of two parts: (1) graft copolymer stabilized gold nanoparticles (AuNPs) and their biological application in chapter 1~3 and (2) chemically cleavable α-azido ether and its biological application in chapter 4~6.

In the first part, poly(L-lysine)-*graft*-poly(ethylene glycol) (PLL-*g*-PEG) copolymers that bear multiple thiol groups on the polymer backbone are used for exceptional ligands to stabilize AuNPs. In general, these graft copolymer ligands stabilize AuNPs against environments that would ordinarily lead to particle aggregation. To characterize the effect of copolymer structure on AuNP stability, we synthesized PLL-*g*-PEGs with different backbone lengths, PEG grafting densities, and number of thiols per polymer chain. AuNPs were then combined with these polymer ligands, and the stabilities of the resulting AuNP@PLL-*g*-PEG particles against high temperature, oxidants, and competing thiol ligands were characterized using dynamic light scattering (DLS), visible absorption spectroscopy, and fluorescence spectrophotometry. Our observations indicate that thiolated PLL-*g*-PEG ligands (PLL-*g*-[PEG:SH]) combine thermodynamic stabilization via multiple Au-S bonds and steric stabilization by PEG grafts, and the best graft copolymer ligands balance these two effects. This new ligand system enables AuNPs to be used for solid phase polymerase chain reaction (SP-PCR) that requires harsh reaction conditions, such as, elevated temperature and competing thiol molecules. Azide functionalized PLL-*g*-[PEG:SH] were conjugated to oligodeoxy-nucleotide (ODN) primers via click chemistry and bound to AuNPs to yield AuNP-primers that successfully primed target DNA synthesis on the surface of the AuNPs through PCR, as demonstrated by gel electrophoresis, DLS, and fluorescent analysis. Moreover, the graft copolymer stabilized AuNPs were applied to rapid DNA diagnostics in a single PCR tube with magnetic particles through color change without any instrumental analysis.

In the second part, bioorthogonal, chemically cleavable α-azido ether has been studied and used to develop novel degradable materials. In order to understand the

chemistry of the α-azido ether, model molecules bearing the α-azido ether were prepared. Hydrolytic stability of the model molecules was investigated by measuring their degradation rate using ^{1}H-NMR, which leads to the relationship between the stability and chemical structures. Additionally, the cleavage kinetics of the model molecule, which was triggered by a couple of azide reducing reagents, was studied by ^{1}H-NMR and UV-Vis absorption spectroscopy. The kinetic studies enable us to develop mechanistic investigation of the chemical cleavage as well as optimal cleavage conditions. Furthermore, the products after the chemical cleavage of the α-azido ether were characterized using ^{1}H-NMR. The novel α-azido ether was then incorporated into degradable polyacrylamide gel electrophoresis (PAGE), in which biological macromolecules, including plasmid, microRNA, and proteins, were separated electrophoretically and recovered from the gel matrix with the optimal cleavage conditions. The kinetics of the recovery was quantitatively studied using UV-Vis absorption spectroscopy and fluorescence spectrophotometry. Furthermore, the recovered biological macromolecules were analyzed to investigate biocompatibility of our system. We anticipate further expansion of the α-azido ether to a broad range of biological applications based on the fundamental studies and the representative example in PAGE.

Table of Contents

List of Figures

Chapter 1

Chapter 2

Chapter 4

Chapter 5

provide the image. (top) RNA band using a conventional 5 %C Bis polyacrylamide gel. (bottom) RNA band using a degradable 8 %C N_3EG_2 polyacrylamide gel. (**B**) Secondary denaturating urea gel electrophoresis of ssRNA ladder, original and isolated microRNA (400nt). After gel electrophoresis using a Bis gel, the gel was stained with SYBR green II solution and fluorescence image was taken under UV illumination. The isolated microRNA had the same migration as that of original microRNA, maintaining their size after degradation. The result indicated the degradation condition was compatible with RNA even in high temperature resulting in no effect on the RNA band migration.

List of Tables

Chapter 2

Chapter 3

Abbreviations

APS	ammonium persulfate
AuNP	gold nanoparticle
BAC	*N,N'*-bisacrylylcystamine
BHT	butylated hydroxytoluene
Bis	*N,N'*-methylene bisacrylamide
B-PE	B-phycoerythrin
CAPS	*N*-cyclohexyl-3-aminopropanesulfonic acid
CNT	carbon nanotube
DCM	dichloromethane
DHLA	dihydrolipoic acid
DIBO	dibenzylcyclooctyne
DIPEA	*N,N*-diisopropylethylamine
DLS	dynamic light scattering
DMF	*N,N*-dimethylformamide
DMSO	dimethylsulfoxide
DNA	deoxyribonucleic acid
dNTP	deoxyribonucleotide triphosphate
dsDNA	double strand DNA
DSS	4,4-dimethyl-4-silapentane-1-sulfonic acid
DTT	dithiothreitol
EDC	1-ethyl-3-(3-dimethylaminopropyl)carbodiimide
EDTA	ethylenediaminetetraacetic acid
ELISA	enzyme-linked immunosorbent assay
EtBr	ethidium bromide
FAM	fluorescein
FAM-PEG-SCM	fluorescein poly(ethylene glycol)-succinimidyl carboxymethyl

FAM-PEG-SH	fluorescein poly(ethylene glycol)-thiol
FRET	Fluorescence resonance energy transfer
Gd-DOTA	gadolinium-tetraazacyclododecanetetraacetic acid
GFP	green fluorescent protein
GPC	gel permeation chromatography
IEF	isoelectric focusing
IgG	immunoglobulin G
LA	lipoic acid
LLC	Lewis lung carcinoma
MEHQ	methyl ether hydroquinone
MMP	matrix metalloproteinase
mPEG-SCM	methoxy-poly(ethylene glycol)-succinimidyl carboxymethyl
mPEG-SH	methoxy-poly(ethylene glycol)-thiol
MRI	magnetic resonance imaging
MsCl	methanesulfonyl chloride
MWCO	molecular weight cut-off
N_3EG_2	*N*-(2-(2-acrylamido-1-azidoethoxy)ethyl)acrylamide
NMR	nuclear magnetic resonance
ODN	oligodeoxyribonucleotides
PAAm	polyacrylamide
PAGE	polyacrylamide gel electrophoresis
PBS	phosphate buffered saline
PCL	poly-caprolactone
PCR	polymerase chain reaction
PDI	polydispersity index
PDP	pyridyldithiopropionate
PEG	poly(ethylene glycol)
PGA	poly-glycolic acid
PHA	polyhydroxylalkanoate

PLA	poly(lactic acid)
PLL	poly(L-lysine)
PLL_{11}-*g*-[PEG:PDP]	poly(L-lysine)-*g*-[poly(ethylene glycol):(2-pyridyldithio) propionamide]
PLL_{11}-*g*-[PEG:SH:FAM]	poly(L-lysine)-*g*-[poly(ethylene glycol):thiol:fluorescein]
PLL_{11}-*g*-[PEG:SH]	poly(L-lysine)-*g*-[poly(ethylene glycol):thiol]
PLL-*g*-PEG	poly(L-lysine)-graft-poly(ethylene glycol)
PP	polypropylene
PTFE	polytetrafluoroethylene
RDS	rate determining step
RNA	ribonucleic acid
RP-HPLC	reversed phase high-performance liquid chromatography
SDS	sodium dodecyl sulfate
siRNA	small interfering RNA
SNP	single-nucleotide polymorphism
SPDP	*N*-succinimidyl 3-(2-pyridyldithio)-propionate
SP-PCR	solid phase polymerase chain reaction
SPR	surface plasmon resonance
ssDNA	single strand DNA
Taq	*Thermus aquaticus*
TBE	Tris-borate-EDTA
TCEP	tris(2-carboxyethyl)phosphine
TCEP=O	tris(2-carboxyethyl)phosphine oxide
TE	Tris-EDTA
TEM	transmission electron microscopy
TEMED	tetramethylethylenediamine
TEV	tobacco etch virus protease
THF	tetrahydrofuran
TMS-N_3	trimethyl silyl azide

Tris	tris(hydroxymethyl)aminomethane

Chapter 1. Gold Nanoparticles and Polymerase Chain Reaction

1.1 Gold nanoparticles (AuNPs)

A nanomaterial is a material whose size is in the 1 – 100 nm range at least in one dimension. The size of a nanomaterial falls into a range which is larger than atoms and molecules other than polymers and smaller than bulk materials. As a consequence, the physical behaviors of nanomaterials are unique compared to those of atomic or bulk materials. After the conceptual beginning of nanomaterials (without using the word itself) by Richard Feynman's lecture in 1959 titled "There's Plenty of Room at the Bottom",[1-2] nanomaterials have been of great interest in a wide range of research fields, including chemistry, physics, biology, electronics, engineering, and materials, during the last three decades. Due to the confined nanoscale size, nanomaterials show extraordinary optical, electrical, magnetic, mechanical, and catalytic properties. For example, noble metal nanoparticles of Au and Ag have been used as sensing probes in analytical tools and biodiagnostics due to their incomparably intense color as well as size dependent color change.[3-4] Colloidal quantum dots consisting of semiconducting materials show excellent photoluminescence and tunable bandgaps, depending on their size and composition, and can be used in light-emitting devices[5] and fluorescent imaging and sensing of biological events.[6] Magnetic nanoparticles made of inorganic oxides have been applied in magnetic

separation of biological molecules[7] and contrast agents in magnetic resonance imaging (MRI).[8] Carbon nanotubes (CNT) have served as excellent reinforcers in composite materials providing better mechanical properties with low mass compared to glass-fibers.[9] Furthermore, electrical conductivity of CNT promises transparent, flexible, and conductive films in electronics.[10] Nanosized structures show high catalytic activity and selectivity depending on their size and shape in many organic reactions.[11-12]

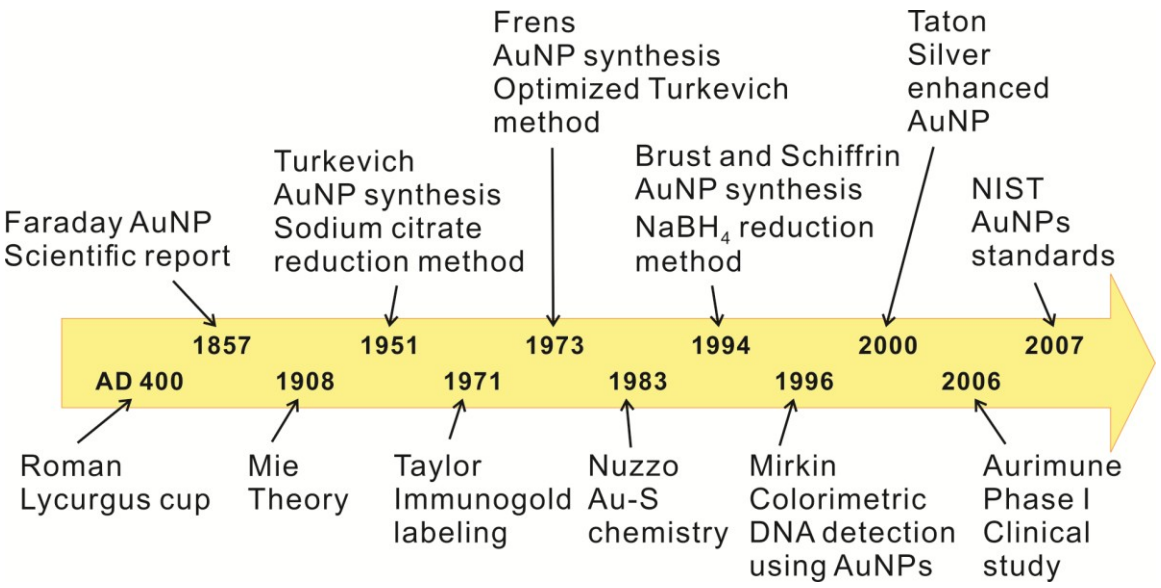

Figure 1-1. The timeline of gold: major discoveries and applications related to AuNPs. The figure was adapted with permission from *Acc. Chem. Res.* **2012**, *46*, 650. Copyright 2012 American Chemical Society.[13]

Among various nanomaterials, gold nanoparticles (AuNPs) are one of the most studied nanomaterials due to their simple preparation, novel properties, and facile functionalization. AuNPs have a long history based on these characteristics since the

ancient Roman times. AuNPs were used as color pigments in the Lycurgus cup of Roman glass and stained-glass windows of medieval cathedrals because of their intense red colors under transmitted light and dark green colors under reflected light.[14] At one time, gold colloidal solution was used as "the Elixir of Life" due to its blood-red color which brought to mind life-essence materials.[15] After Faraday published the first scientific report of a AuNP red-solution in 1857,[16] Turkevich[17] and Frens[18] developed a simple method to prepare AuNP using sodium citrate reduction of gold ions to generate uniform and size-controlled AuNPs, which is still one of the standard methods for AuNPs synthesis. Antibodies-functionalized AuNPs have been applied as contrast agents in electron microscopy to label cellular macromolecules to elucidate their *in vivo* biochemical functions, which has been called immunogold labeling since 1971 by Taylor.[19] In 1983, Nuzzo et al. reported evidence of fairly strong chemical bonding between Au and thiol (or disulfide) that contributed to facile functionalization of Au surface using thiol molecules. Before that time, it was believed that "Gold [was] recognized to be one of the least active metals in chemisorptions as evidenced by its inertness toward molecular oxygen." as Nuzzo et al. commented.[20] Later, the Au-thiol chemistry was applied to functionalize AuNPs with DNA by Mirkin[21] and Alivisatos[22] groups in 1996. In particular, Mirkin et al. inaugurated the use of AuNPs as optical probes based on their extraordinary optical properties to visually detect target DNA without any instrumental analysis other than eye examination. Since then, AuNPs have played a significant role for instrument-free detection assays in analytical chemistry and medical diagnostics.[4] The Mirkin group has further expanded the use of AuNPs to

various applications, such as, DNA detection assays using silver enhanced AuNPs,[23] AuNP arrays for electrical detection,[24] and Raman-active dye labeled AuNPs for Raman scattering,[25] and basic building blocks for ordered AuNP assembly.[26] AuNPs have further been studied as essential materials in many other applications, including catalytic systems[12] and nano-medicines,[27-28] resulting in AuNPs as key components in nanomaterials.

This thesis deals with use of the unique properties that AuNPs bear, especially, optical properties and facile Au-S surface chemistry. It is investigated to integrate the excellent properties into a biological technology, particularly polymerase chain reaction (PCR), as a means of instrument-free DNA detection, which reduces analysis time and removes the additional tasks that are required in most current DNA detection methods. However, the facile Au-S chemistry needs to be improved for this purpose because PCR requires harsh reaction conditions like high temperatures up to 95 ^{o}C in which the Au-S chemistry is restricted. The following sections describe a short discussion on the optical properties and surface chemistry of AuNPs as well as polymerase chain reaction.

1.1.1 Optical properties of AuNPs

AuNPs in the size range of 1 – 100 nm have been extensively studied due largely to their unique optical properties compared to bulk and atomic gold. When light interacts with bulk Au, it appears yellow due to a reduction of reflectivity at the blue region of the visible spectrum.[29] AuNPs, on the other hand, have intense and distinctive colors, covering the range from red to violet depending on their size (Figure 1-2).[30-31] This array

of colors is due to a phenomenon called surface plasmon resonance (SPR), which is the result of the collective oscillation of the free electrons being induced by an electromagnetic field. The incident light induces a polarization of the free electrons in the conduction band relative to the heavier nuclei. As a result, there is a resonance that correlates with the specific frequency of the incident light. A theoretical description for SPR of the AuNPs was reported by Mie in 1908.[31-32] The theory predicts that there is a linear relationship between ln(diameter) and ln(extinction coefficient (ε)). As a result, the value of the extinction coefficient of spherical AuNPs increases from 10^5 to 10^{10} $M^{-1}cm^{-1}$ with respect to their size ranging from 2 to 100 nm in diameter from both theoretical calculation and experimental data.[33-34] That means AuNPs are more useful as optical probes for bio-applications than organic dyes because the ε value of AuNPs is 4 - 5 orders of magnitude larger than that of organic dye molecules, (i.e. 1.16 x 10^5 $M^{-1}cm^{-1}$ at 530 nm of Rhodamine-6G). Therefore, AuNPs show promise in replacing organic optical tags for bio-applications as well as developing color based detection of subjects even in very low concentration.[4,21]

Another useful and interesting property of SPR is that the resonance and consequently AuNP colors can be readily tuned by size, shape, and distance between the AuNPs.[21,30,35] For instance, the size of AuNPs affects the frequency of the SPR band such that it is shifted according to the diameter of AuNPs. Both Mie theory prediction and experimental data indicate that as the size increases from 32 to 100 nm in diameter, the maximum extinction of SPR (λ_{max}) is shifted to longer wavelengths (525 to 569 nm),[33] and broadening of the SPR band occurs.[31] As a result, the color of AuNP solution

changes from red to violet with the increase of the AuNP size.[36] Another way of tuning the SPR band is by changing the shape of the gold from spherical particles to nanorods.[37] For gold nanorods, there are two λ_{max} corresponding to the oscillation of the conduction electrons along the short and long axis. Accordingly, the SPR bands are affected by the aspect ratio: the ratio of length to width. The SPR bands also vary according to the interparticle distance between the AuNPs. The SPR bands are red-shifted as the distance decreases because of the interaction between particle surface plasmons. Based on this, Alivisatos et al. developed a molecular ruler using this SPR band shift depending on the interparticle distance to monitor the kinetics of biological events.[35]

In order to use the unique optical properties of the AuNPs, it is a prerequisite that AuNPs are stable in application conditions. This can be achieved through chemical modification of the AuNPs, which can also introduce various functionalities on the AuNPs. Below is a short overview for why stabilization is required and how AuNPs can be stabilized.

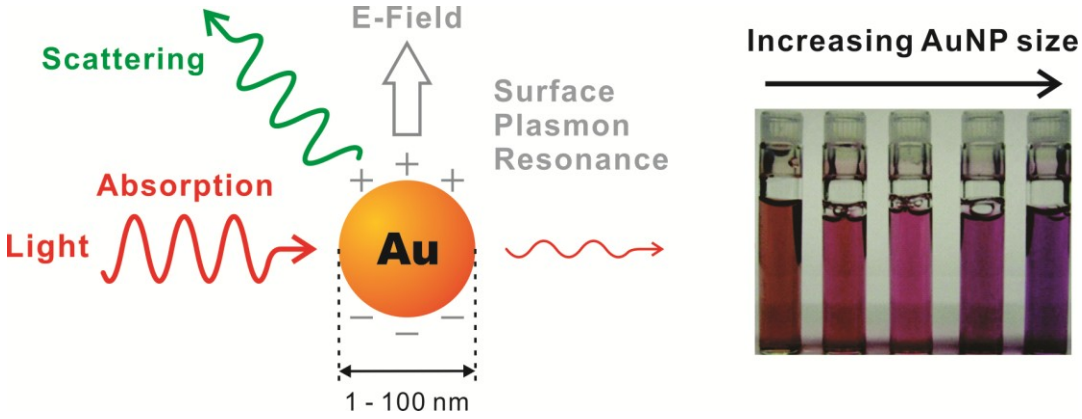

Figure 1-2. (**Left**) Optical properties of gold nanoparticles (AuNPs). AuNPs interact with light strongly through absorption and scattering as a result of surface plasmon resonance (SPR), which is the collective oscillation of the free electrons induced by an electromagnetic field of light. The incident light induces a polarization of the free electrons in the conduction band relative to the heavier nuclei, which is shown in positive and negative charges due to E-field. As a result, there is a resonance that correlates with the specific frequency of the incident light. (**Right**) Photographs of AuNP solutions with respect to the size. The color of AuNP solutions is intense even in low concentration. As the AuNP size increases, the color changes from red to violet. The photographs reprinted with permission from *Acc. Chem. Res.*, **2008**, 41 (12), 1721.[38] Copyright 2008 American Chemical Society.

1.1.2 Surface chemistry of AuNPs

AuNPs have become important tools in material science and biotechnology due to their unique properties. In order to preserve the unique properties, AuNPs should be stabilized to maintain their size during the application conditions. AuNPs have high surface-to-volume ratio and the surface has excess free energy compared to the bulk because a certain portion of surface atoms interacts with the surrounding environment and this interaction is normally weaker than that in the bulk.[39] Assuming AuNPs are spherical in shape, as the diameter of AuNPs decreases, the percentage of surface atom increases: 0.2% for 1000 nm, 11.5% for 100 nm, and 88% for 1.3 nm.[40] That means nano-sized Au has huge amounts of surface energy, which makes nanoparticles eventually fuse or aggregate to reduce the surface energy.[41] Thus, surface stabilization of AuNPs has been investigated to overcome the surface energy. Commonly, there are two methods to make a stable suspension: electrostatic repulsion and steric stabilization.

The first method is achieved by electrostatic repulsion by the introduction of charged species on the surface of AuNPs.[42] When ionic species, including NR_4^+, PO_4^-, and RCO_2^-, are present on the surface, the electrical potential of ionic species produces repulsive forces to separate AuNPs through electrostatic repulsion. However, it often does not make AuNPs stable enough for biological applications because even in low salt concentration the electrical potential decreases so rapidly that AuNPs form aggregates. In contrast, steric stabilization, which uses physical barriers on the surface, makes AuNPs more resistant to high salt concentration.[42] The physical barrier can be introduced using

stabilizing molecules, such as, small organic molecules and polymers,[43-46] including DNA, protein, and synthetic polymers.

Electrostatic repulsion and/or steric stabilization for AuNPs have been achieved by anchoring surface ligands.[42] In order to be a good surface ligand, the surface ligand should bind to Au strongly through the interaction between specific functional groups in the ligands and the Au surface. Although there are many functional groups,[47] such as, phosphine, phosphine oxide, amine, and carboxylate, strong interaction between Au and thiol has been widely used. The evidence of strong Au-S bond was first discovered by Nuzzo et al. in 1983 through their adsorption study of disulfide molecules on Au surface.[20] Afterwards, a homolytic Au-S bond strength is ~50 kcal/mol in a vacuum condition, which is fairly strong considering ~62 kcal/mol is a typical S-S homolytic bond strength.[40] Later, a couple of seminal papers were released consecutively in 1996, in which the strong Au-S bond was adapted to stabilize AuNPs for colorimetric DNA detection[21] and 3D AuNP nanoassembly.[22] The Au-S bond has then become the most widely used chemistry for the anchor group of AuNP stabilizing ligands. As a result, many thiol functionalized macromolecules have been utilized to generate stable AuNPs, including natural macromolecules,[21-22,48-49] synthetic homopolymers, in which AuNPs are connected by either terminal[50-58] or side-chain[59-62] thiols, and synthetic copolymers, including random,[63-64] alternating,[65] graft,[66-67] and block[50,68-71] copolymers.

However, the mono-thiol ligands are not always bound to the AuNPs surface under certain conditions, such as, high temperature[72-74] and in the presence of competing thiol species[75-78] or oxidants,[72,79-81] in an extremely good solvent for the ligands. Based on

measured energy barrier values of thiolate desorption process from the Au surface (15-30 kcal/mol),[40,82-84] thiol ligands are thermodynamically dissociated from the AuNP surface at high temperature. For example, Herdt in the Taton group reported that mono-thiol DNA ligands on AuNPs desorbed and degraded at high temperature. Grzybowski et al. used the thermal desorption of mono-thiol ligands from Au surface to form fused AuNPs.[73,85] In this approach, 1,8-octanedithiols crosslinked AuNPs forming spherical aggregates with nano-void between AuNPs, and then desorbed from the surface by heating the solution to form nanoporous materials. It is also reported that mono-thiol ligands are replaced with external thiol species via ligand exchange reaction. Mirkin et al. released mono-thiol DNA ligands from the AuNP surface by addition of external thiols like DTT through ligand exchange reaction. Moreover, Rotello et al. designed AuNP carriers in which mono-thiol functionalized fluorophore ligands were released from the AuNP surface via a glutathione-mediated exchange reaction, which is one of the most abundant thiol species in cytoplasm.

Chapter 2 in this thesis shows how stable ligands for AuNP can be achieved against the experimental harsh conditions, such as, high temperature, oxidants, and competing thiol species.[86] It is reported that as the number of thiols in a stabilizing ligand increases, enhanced stability is obtained.[87-90] For instance, Randall et al. showed that tridentate thiol ligand stabilized AuNPs had better thermal stability as well as resistance to ligand exchange reaction with competing thiol species, compared to monodentate and bidentate ligands.[91] Based on this idea, multi-thiolated graft copolymers have been developed for the stable AuNPs. Graft copolymers have advantages compared with small

molecules because of their straightforward synthesis and facile control of thiol ratio in a graft copolymer through which an optimal thiol ratio is readily investigated. The graft copolymer stabilized AuNPs are designed as a support in a polymerase chain reaction (PCR) that is operated in high temperature. Thus, the basic principles of PCR and advanced PCR technique are briefly overviewed.

1.2 Polymerase Chain Reaction (PCR)

1.2.1 Basic principles

DNA is an essential biological molecule that contains the genetic information to construct every component needed for life. Consequently, detecting specific DNA, which means recognition of specific sequence of ATGC molecules, has impacted molecular biology, clinical diagnostic, forensics, and so on. Traditionally, DNA detection has been achieved through hybridization assays using detection of specifically designed probes (*i.e.* radioactively or fluorescently labeled probes) or distinguishing the lengths of hybridized dsDNA and non-hybridized ssDNA via electron microscopy.[92] However, these methods have restrictions in terms of sensitivity and reproducibility, caused by the extremely small amounts of DNA samples. This has led to the investigation of a novel method to amplify the amounts of DNA samples using an enzymatic reaction called polymerase chain reaction (PCR).[93-94]

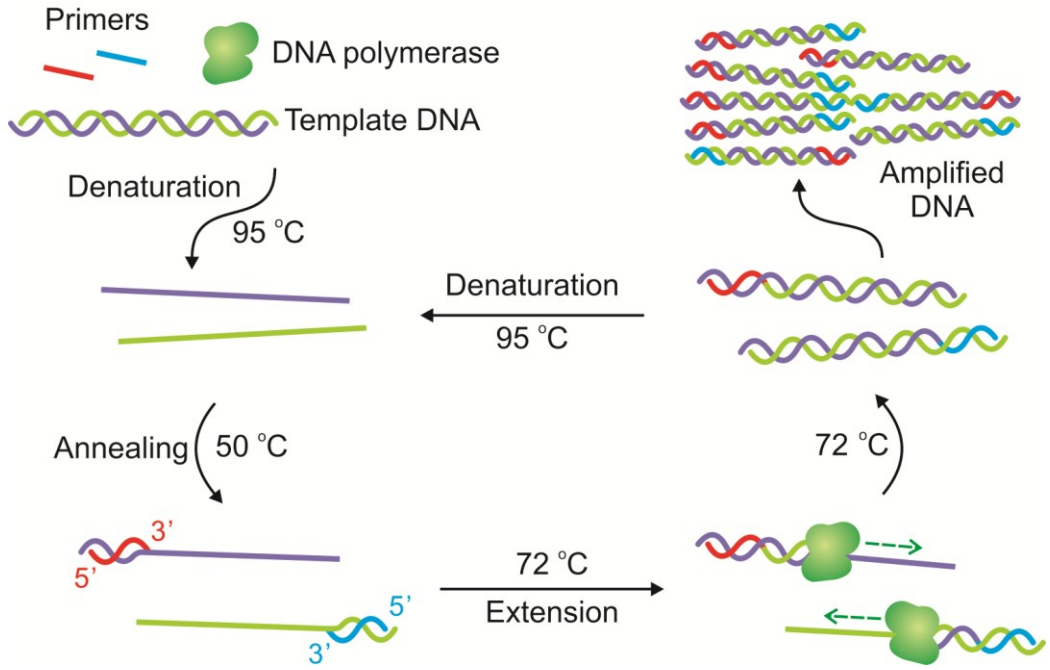

Figure 1-3. A schematic representation of thermal cycling PCR. Target DNA is amplified via successive thermal cycles of denaturation, annealing, and extension steps from minute amounts of DNA template to the level at which amplified DNA can be analyzed.

PCR has revolutionized modern molecular biology and clinical diagnostics by providing a practical method to amplify target DNA, theoretically, from a single copy of DNA. In contrast to the early hybridization assays, PCR provides a rapid, sensitive, and specific method for DNA detection. In a basic process, successive thermocycles are performed to copy the target DNA sequence from a DNA template. Each cycle synthesizes two copies of the target DNA from one template and the synthesized DNA serves as a new template for the next cycle, resulting in exponential amplification of the target DNA. PCR components consist of (1) DNA template, (2) a pair of forward and reverse primers that is oligo-deoxyribonucleotide and designed to be hybridized with a

specific sequence of a template, (3) a polymerase enzyme, (4) deoxyribonucleotide triphosphates (dNTP), and (5) reaction buffer. Each cycle consists of three steps: (1) denaturation, (2) annealing, and (3) extension. In the first denaturation step, the DNA template is unwound to generate two ssDNA templates at ~95 ^{o}C. During the annealing step, each primer is hybridized with the ssDNA templates through the double helix formation in the specific sequences at 40-65 ^{o}C. In the extension step, the polymerase copies complementary sequences from the ssDNA templates, usually accomplished at 72 ^{o}C. During this step, the polymerase catalyzes the primers' 3'-OH attack on α-phosphate of dNTP via two-metal ion mechanism, leading to 5' to 3' direction of DNA synthesis (Figure 1-4).[95] As a result, the amount of target DNA is doubled through the thermocycle. The thermocycle is then repeated to create enough DNA to be analyzed.

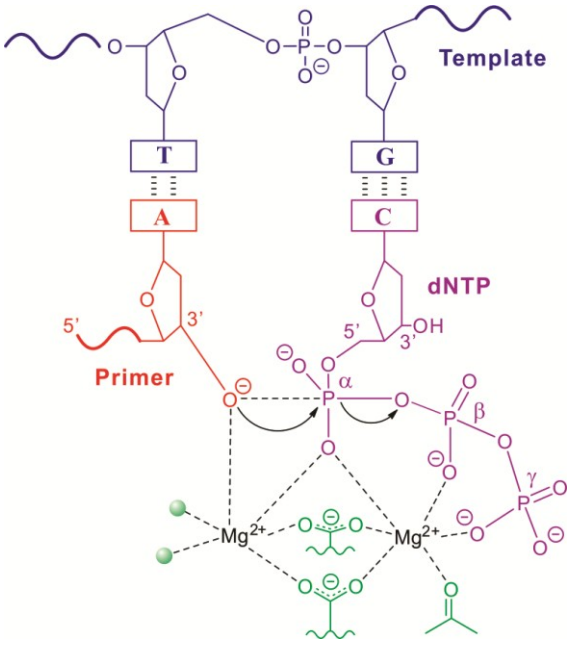

Figure 1-4. The two-metal ion mechanism of DNA polymerase.[95] Divalent metal ions like Mg^{2+} are bound to polymerase enzyme through typically carboxylate residues. The 3'-OH in the primer is deprotonated by the interaction with one of the metal ions. The deprotonated hydroxyl attacks the α-phosphate of the incorporated dNTP, which leads to covalent connection between 3'-OH of the primer and 5'-phosphate of the complementary nucleotide.

Historically, the basic concept of DNA amplification was already described prior to the development of thermocycling PCR. The Klenow fragment of *E. coli* DNA polymerase I was employed to amplify DNA; however, it needs to add fresh enzyme after each cycle because the Klenow fragment is not stable at the high temperature required for the denaturation step.[94] Moreover, the optimal temperature for the enzymatic reaction is 30 ^{o}C, which results in a broad range of DNA sizes due to non-specific interaction between primers and a template. Later, a thermostable DNA polymerase derived from *Thermus aquaticus* (Taq polymerase) was introduced into PCR protocols in the late 1980s[93,96] even if Taq polymerase was previously discovered in 1976.[97] Thus, it is not necessary to add fresh enzyme after each cycle avoiding a time-consuming and tedious task. Furthermore, the enzymatic reaction is performed at ~70 ^{o}C, which leads to elimination of the non-specific interaction and improves sensitivity and specificity. It has become integrated into an automated system using a machine called PCR thermocycler, which contributed to a ubiquitous, versatile, and invaluable biological technique.

The standard methodology of PCR thermocycling was then followed by the development of PCR techniques: adding multiple pairs of primers for simultaneous amplification of multiple target DNA (multiplex PCR),[98] modifying the concentration of either forward or reverse primer (asymmetric PCR),[99] incorporating probes in PCR mixture which generate signal based on the amounts of amplified DNA (real-time PCR),[100] shifting to a heterogeneous reaction system called solid-phase PCR (SP-PCR), and so on. Among them, SP-PCR will be briefly overviewed because this thesis will deal with PCR on AuNPs.

1.2.2 Solid phase PCR (SP-PCR)

Solid phase PCR (SP-PCR) involves immobilized forward and/or reverse primers on a solid support. The primers are extended to have target DNA sequence through PCR cycles. The solid support includes a planar surface, such as, glass[101-103] and polymer,[104-108] and a curved surface in micro/nano-particles of sepharose,[109] polyacrylamide,[110] magnetic polystyrene beads (i.e. Dynabead),[111] magnetic particles,[112] silica particles,[113] and gold nanoparticles.[74,114-115] The SP-PCR generates immobilized target DNA resulting in facile purification and separation, simple detection protocol, further manipulation, and promise for an automated system. As a consequence, SP-PCR has been used in many applications, including specific DNA detection[116] and SNP detection,[110] solid phase DNA colony construction followed by gene sequencing,[109,117] and mRNA profiling.[118] For example, a commercially available Nucleolink coated tube, which is composed of a thermostable polymer and can be used for EDC-amine coupling reaction for an immobilized primer, in microwells has been used for SP-PCR, followed by DNA detection.[116] Recently developed DNA sequencing technologies, called the next generation sequencing, have utilized SP-PCR through which DNA colonies are constructed on microparticles[109,111] or local flat surfaces[103,107] and analyzed to elucidate gene sequences.

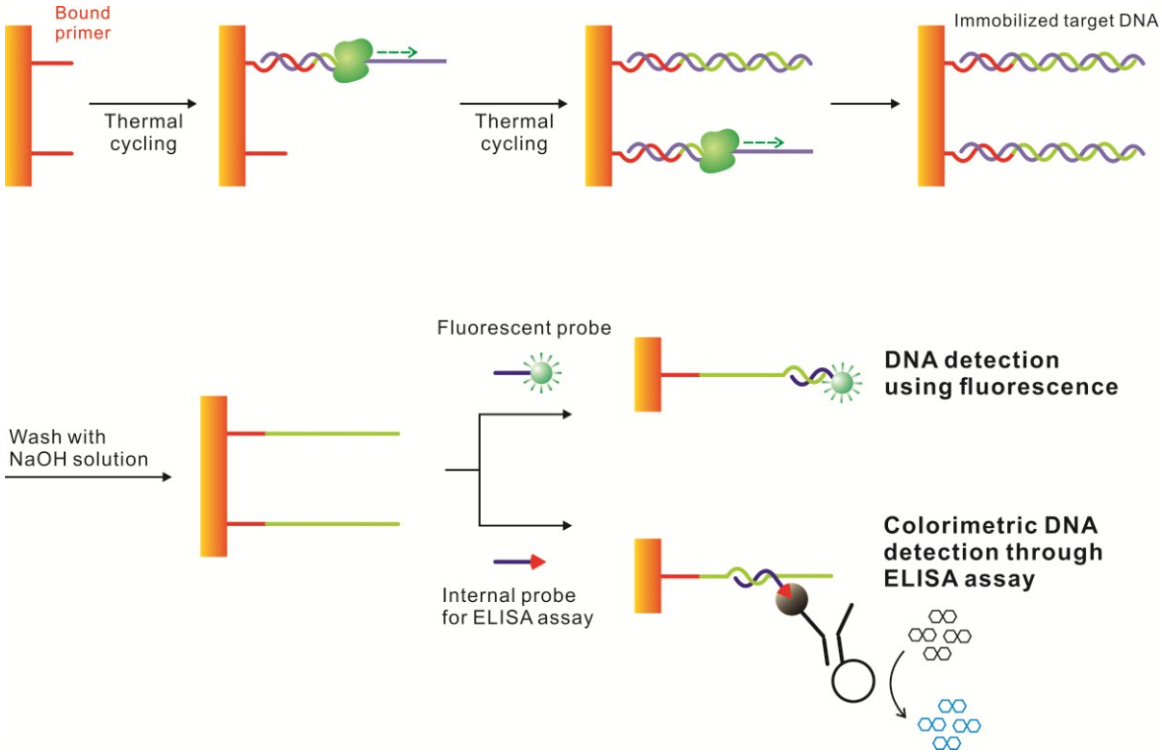

Figure 1-5. Representative illustration of SP-PCR and DNA detection after SP-PCR. Surface bound primers are amplified to have target dsDNA through SP-PCR. The dsDNA is denaturated to form ssDNA in which fluorescent probes or ELISA probes are hybridized. The presence of the target DNA is then analyzed using fluorescence or colorimetric ELISA assay.

In spite of its potential, SP-PCR has limitations caused by its low yield and efficiency[113,119-120] and need of additional instrumentation[121-122] or subsequent tasks[104,116] even in target DNA detection, which is already achieved without any instrumentation except eye examination (Figure 1-5). It has been suggested that molecular crowding on a solid support could decrease the probability of duplication depending on the density of the grafting chain.[119] Moreover, steric hindrance between DNA polymerase and grafting

chains can lower the efficiency of SP-PCR.[120] Currently developed DNA detection assay using SP-PCR requires additional instrumentations to measure the fluorescence of hybridized probes.[122] It is possible to eliminate additional instrumentation if immobilized target DNA is analyzed through color change using enzyme-linked immunosorbent assay (ELISA).[116] However, this method requires additional procedures for ELISA, including denaturation of target DNA, hybridization of probes into target DNA, conjugation of enzyme to the probes, and enzymatic reaction.

Chapter 3 of this thesis deals with a colorimetric DNA detection assay through SP-PCR without any additional instrumentation or any secondary reactions except magnetic attraction of positive target DNA within 5 min. It leads to facile and rapid amplified DNA detection compared to currently developed DNA detection via SP-PCR. To approach this goal, AuNPs are used because of their excellent optical properties allowing eye examination even in low concentrations, such as 1 nM. However, in order to incorporate AuNPs into SP-PCR, the thermal stability of the conjugate between the immobilized primer and the AuNP surface should be satisfied. Otherwise, the dissociation of primers from the solid supports may lead to low yield and non-reproducible results.

The thermal stability of conjugation and entire entities has been issues for other solid supports. Although thermally unstable conjugates or solid supports have been applied to SP-PCR and showed positive results,[105,112] improving the thermal stability has been proven to increase SP-PCR yield as well as give reproducible results. Consequently, there were attempts to improve thermal stability by modifying the chemistry. For

example, CovaLink is a chemically modified polystyrene surface for primer immobilization in micro-tubes or wells through a carbodiimide coupling reaction between 5'-phosphorylated primers and covalently connected secondary amino groups to the surface[123]; however, its half-life is 30 m at 94 ^{o}C leading to low yield and requiring careful handling in SP-PCR.[105] Later, NucleoLink was invented to resolve the thermal instability of CovaLink, which led to a better yield (~10 fold higher S/N ratio) and handling, compared to CovaLink.[106] The modification of the primer can improve the thermal stability as well. The interaction of the mono-biotin/streptavidin conjugate in biological applications has been used to connect streptavidin-coated particles and DNA. However, Dressman et al. reported the dissociation of mono-biotin tagged primers from the streptavidin-coated beads during thermal cycling although mono-biotin/streptavidin is a strong conjugate at room temperature.[124] The chemical modification from mono-biotin to dual-biotin was performed to increase the thermal stability, which has been adapted in one of the next generation sequencing technologies in the market.[111,124]

Au surface has usually been conjugated to DNA through Au-S chemistry. However, it is well-known that the Au-S bond is not stable at high temperatures.[72] It is easily expected that if mono-thiol conjugated AuNPs are incorporated in PCR, thermal instability of Au-S bond may reduce the yield and give non-reproducible results. Thus, there are a few reports in which mono-thiolated AuNPs are used in SP-PCR for 3D nano-architecture[114] and real-time monitoring of SP-PCR using surface plasmon resonance shift,[115] whereas it is also reported that mono-thiolated AuNPs inhibit the SP-PCR

reaction.[74] As a result, thermally stable conjugates are required to apply AuNPs in SP-PCR for reproducible colorimetric DNA detection assay.

The thermally stable conjugates between AuNP and primers can be accomplished using multi-thiolated graft copolymer as mentioned above. In chapter 3, it is described how a graft copolymer is used to conjugate AuNP and primer, followed by its application towards the colorimetric DNA detection through SP-PCR.

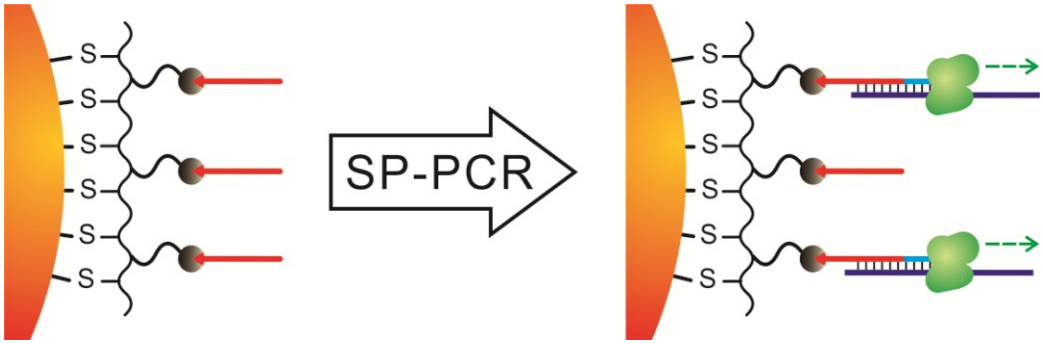

Figure 1-6. Schematic illustration of SP-PCR using oligothiol graft copolymer stabilized AuNPs as solid supports. Primers (red) are extended to have target DNA through SP-PCR.

1.3 Overview

The next two chapters, 2 and 3, of this thesis deals with graft copolymer stabilized AuNP and its biological application in SP-PCR (Figure 1-6).

Chapter 2 outlines the strategy of multi-thiolated graft copolymer stabilized AuNPs and describes our fundamental study about stability of the AuNPs against experimental harsh conditions, such as, high temperature, competing thiols, and chemical

etchants. It also explores relationship between the stability and the ratios of thiol and hydrophilic graft chains like poly(ethylene glycol) (PEG) in a graft copolymer.

Chapter 3 investigates a practical example of the multi-thiolated graft copolymer stabilized AuNPs as a solid support in one of the most versatile biological technologies, PCR. It describes how primers are conjugated and extended through SP-PCR as well as our novel strategy for rapid post-PCR colorimetric DNA detection without any instrumentation.

Chapter 2. Oligothiol Graft-Copolymer Coatings Stabilize Gold Nanoparticles Against Harsh Experimental Conditions[1*]

2.1 Introduction

The stability of a nanoparticle suspension is often critically dependent on the structure of ligands that are bound to the nanoparticle surface.[2-3] Surface ligands stabilize nanoparticle suspensions in a variety of ways—they block physical and chemical access to the nanoparticle surface, compatibilize the nanoparticle with solvent, sterically and/or electrostatically inhibit particle-particle interactions, slow the loss of surface atoms to solution or other particles (via Ostwald ripening), and provide functional groups for conjugating biological or other molecules to the particle without interfering with the particle surface. Because of the many roles that surface ligands play, and the different types of materials they are bound to, there is no single ligand structure that stabilizes all nanoparticles in every application. However, the most successful nanoparticle ligands do have some structural features in common. Good surface ligands typically have functional groups that bind the nanoparticle surface strongly, self-interacting (often solvophobic)

[*] Reproduced with permission from Jun Sung Kang and T. Andrew Taton, *Langmuir* **2012**, *28*, 16751. Copyright 2012 American Chemical Society.[1]

segments that discourage ligand dissociation, and charged and/or polymer segments that provide electrostatic and steric stabilization.

Designing surface ligands for Au nanoparticles (AuNPs) is easier than for other nanoparticles because of the strong interaction between the Au surface and thiol functional groups.[4] As a result, many thiol-functionalized macromolecules have been used to stabilize Au nanoparticle suspensions,[5] including DNA[6-7] and RNA,[8] peptides[9] and proteins,[10] oligo-saccharides,[11] and synthetic homopolymers (connected to Au via either terminal[12-13] or repeat-unit[14-16] thiols) and copolymers, including random,[17] alternating,[18] graft,[19] and block[20-21] copolymers. Among the polymers, poly(ethylene glycol) (PEG) chains and segments have been used extensively in biotechnological and biomedical applications involving AuNPs[22-23] because of PEG's biocompatibility, its solubility in a broad range of solvent conditions, and the degree of steric stabilization it confers to bound particles. As a result, AuNPs used in room-temperature aqueous buffers are very commonly passivated with thiolated PEG ligands.

However, we and others have found that monothiol ligands, including monothiolated PEGs, are not always stably bound to AuNP surfaces at high temperatures,[24-26] in the presence of competing thiols[27-30] or oxidizing agents,[24,31] and in solvents where the ligand is extremely well solvated—conditions that are often encountered in biotechnological protocols. Nuzzo et al. measured the enthalpy of desorption of thiolates (as disulfides) from Au surfaces into the gas phase to be only ΔH_{des} = -28 kcal/mol,[32] and others have measured even smaller ΔH_{des} (or related T_{des}) values for solvophilic thiols desorbing into solution.[33-34] The desorption of hydrophilic

polymer or biomolecular thiols into water or aqueous buffer from nanoparticle surfaces have small enough ΔH_{des} values that, even though stable Au-S bonds are formed at room temperature, the ligand-surface bonds are thermodynamically disfavored at higher temperature. In biological or biotechnological environments, ligands are also readily displaced from Au surfaces by competing thiols[35-36] such as glutathione, mercaptoethanol and dithiothreitol, or by oxidation,[37-38] and this exchange is accelerated at high temperatures.

One way to enhance the stability of solvophilic, thiol-functionalized ligands on Au surfaces[39] and nanoparticles[40-43] has been to increase the number of thiols per ligand. Researchers have investigated the relative stability of AuNPs passivated with ligands bearing two to four thiols per ligand, and have found that they are generally more stable to harsh experimental conditions than AuNPs protected with monothiol ligands.[41,44] However, to our knowledge there has been no systematic demonstration of the relationship between the stability of an AuNP in aqueous suspension against heat, corrosion and competing ligands, and the number of thiols in a hydrophilic ligand greater than four.

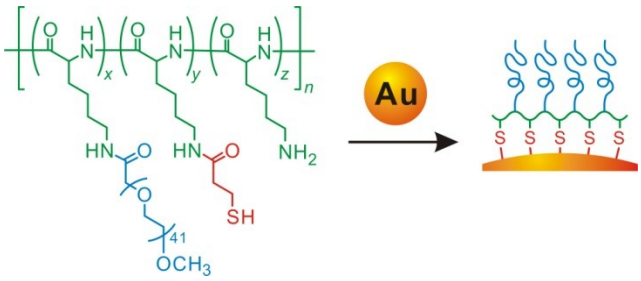

Figure 2-1. Schematic representation of the stabilization of AuNPs by oligothiolated graft copolymers.

Herein, we describe the synthesis of different thiolated poly(L-lysine)-*graft*-poly(ethylene glycol) (PLL-*g*-PEG) copolymers and the use of these graft copolymers to passivate the surfaces of AuNPs (Figure 2-1). We also describe how different numbers of thiols in a ligand affect the thermal stability of AuNPs under harsh conditions—including high temperatures, competing thiols, and chemical etchants. Dynamic light scattering (DLS) analysis and visible absorption spectroscopy were used to monitor the kinetic stability of AuNP suspensions under these conditions. In addition, fluorescence spectrophotometry was used to characterize the desorption of the different graft copolymer ligands at the molecular level. KCN etching experiments were performed to investigate how surface coverage by graft copolymers was related to the resistance of the AuNP surface against chemical attack. Our results provide important guidelines for the design of thiolated ligands for AuNPs, and especially for those used in biotechnological applications,[5] such as thermocycled PCR, that require harsh experimental conditions.

2.2 Experimental Methods

2.2.1 General

Poly(L-lysine) trifluoroacetate (PLL_{11}, M_n 2700, PDI 1.1; PLL_{34}, M_n 8200, PDI 1.05; PLL_{50}, M_n 12100, PDI 1.04) was purchased from Alamanda Polymers, Inc. (Huntsville, AL). Methoxy-poly(ethylene glycol)-succinimidyl carboxymethyl (mPEG-SCM, MW 2000), methoxy-poly(ethylene glycol)-thiol (mPEG-SH, MW 2000), and fluorescein poly(ethylene glycol)-succinimidyl carboxymethyl (FAM-PEG-SCM, MW 3400) were purchased from Laysan Bio, Inc. (Arab, AL). *N*-succinimidyl 3-(2-pyridyldithio)-propionate (SPDP) was purchased from ProteoChem, Inc. (Denver, CO). All other reagents were purchased from Aldrich (St. Louis, MO) unless otherwise noted. Ultrapure water was generated from a Milli-Q water purification system (Millipore Inc.; Billerica, MA, R > 10 MΩ·cm). PD-10 desalting columns were purchased from GE Healthcare (Pittsburgh, PA). ^{1}H NMR spectra were recorded on a Varian Unity (500 MHz) using solvent peaks as internal standards. Visible absorption spectra were obtained on a Hewlett-Packard 8453 UV-Vis spectrophotometer. Gel permeation chromatography (GPC) was conducted on an Agilent 1100 HPLC system (Santa Clara, CA) equipped with two Waters HT4 Styragel columns (7.8 × 300 mm, 10 μm bead size, Milford, MA) in series, and a refractive index detector (G1362A, Santa Clara, CA). GPC experiments were performed using DMF (0.1 M LiBr) as the eluent with a flow rate of 0.4 mL/min at 50 °C. GPC data was calibrated using linear PEG standards (Agilent Tech., Santa Clara, CA). When GPC traces showed multiple peaks, the traces were deconvoluted by

assuming multiple polymer populations, and each peak was separately analyzed by fitting to an independent Gaussian lineshape.[45] Transmission electron microscopy (TEM) images were obtained on a JEOL 1210 electron microscope equipped with a Gatan video camera and a Gatan Multiscan CCD camera (1024×1024 pixels). One drop of nanoparticle solution was placed on copper grid (formvar/carbon, 300 mesh, Electron Microscopy Science) and air-dried. All images were obtained at an operating voltage of 120 kV.

2.2.2 Synthesis

Synthesis of PLL_{11}-*g*-PEG_x. PLL_{11} (100 mg) and *N,N*-diisopropylethylamine (100 μL) were dissolved in DMSO (2.3 mL) in a 4 mL polypropylene (PP) vial, and the solution was stirred until the polymer was completely dissolved. Aliquots of this solution were transferred into separate 4 mL PP vials. With stirring, different concentrations of mPEG-succinimidyl carboxymethyl (mPEG-SCM, MW 2000) in DMSO (150 μL) were then added dropwise to each aliquot (Table 2-1). After reaction overnight, each solution was dialyzed against water using a 2000 Da molecular weight cut-off (MWCO) membrane for 1 d, and then lyophilized to obtain product as a white powder. The resulting polymers were characterized by ^{1}H NMR (D_2O) and GPC. Both methods indicated that the polymer product contained a small amount (< 10 wt%) of mPEG-COOH, presumably due to hydrolysis of mPEG-SCM, that could not be removed by purification; this impurity was retained in subsequent experimental steps. We refer to the

product graft copolymers as PLL_{11}-*g*-PEG_x, where *x* represents the fraction of PLL lysines converted to PEG, as measured by NMR.

Table 2-1. Synthesis of PLL_{11}-*g*-[PEG_x:SH_y].

	PLL_{11}-*g*-PEG_x synthesis					**PLL_{11}-*g*-[PEG_x:PDP] synthesis**		
x^a	PLL_{11}		mPEG-SCM		x^b (NMR)	PLL_{11}-*g*-PEG_x	SPDP	
	μL	μmol	mg	μmol		mg	mg	μmol
0.1	575	9.3	20.4	10.2	0.18	8.0	8.3	26.6
0.2	460	7.4	32.6	16.3	0.22	9.3	7.3	23.4
0.3	345	5.6	36.7	18.4	0.28	10.0	5.8	18.6
0.4	276	4.4	39.1	19.6	0.32	11.5	5.6	17.9
0.5	230	3.7	40.7	20.4	0.37	13.0	4.5	14.4
0.6	230	3.7	48.9	24.5	0.45	13.6	4.4	14.2
0.8	184	3.0	52.1	26.1	0.60	16.6	2.6	8.3

[a]Expected fraction of PLL lysines converted to PEG. [b]Measured fraction of PLL lysines converted to PEG of PLL_{11}-*g*-PEG_x by NMR.

Synthesis of PLL_{11}-*g*-[PEG_x:PDP]. PLL_{11}-*g*-PEG_x was dissolved in 1X phosphate-buffered saline (PBS, 60 μL) in a 1.5 mL Eppendorf tube. Excess SPDP (at least 1.5 equiv) in DMSO (70 μL) was added into the solution (Table 2-1). For the synthesis of higher graft ratios of pyridyldithiopropionate (PDP), an additional 100 μL of DMSO was added to dissolve the SPDP. After 10 h, the reaction mixture was dialyzed against water using a 2000 Da MWCO membrane for 1 d and then lyophilized. This yielded polymer products as white powders. Incorporation of PDP groups was confirmed by ^{1}H NMR (D_2O).

Synthesis of PLL_{11}-*g*-[PEG_x:SH_y]. PLL_{11}-*g*-[PEG_x:PDP] (6.0 mg) was dissolved in 1X PBS (900 μL) in an Eppendorf tube. Then, excess dithiothreitol (DTT; 0.389 M, 100 μL 1X PBS) was added to the solution. After 2 h, the resulting polymer was isolated

from small-molecule reactants with a PD-10 size exclusion column, using water as the eluent, according to the manufacturer's instructions. Water was removed by lyophilization to yield product as a white powder, which was characterized by ^{1}H NMR (D_2O). We refer to these polymers as PLL_{11}-*g*-[PEG_x:SH_y], where *x* and *y* represent the fractions of PLL lysines converted to PEG and thiol groups, respectively, as measured by NMR.

Synthesis of PLL_{34}-*g*-PEG_x. PLL_{34}-*g*-PEG_x polymers with $x < 0.6$ were synthesized as described above for PLL_{11}-*g*-PEG_x (Table 2-2), using PLL_{34} as the starting material. For polymers with $x > 0.6$, pre-formed PLL_{34}-*g*-PEG_x with $x < 0.6$ was used as a starting material in place of PLL_{34}. To the solution of PLL_{34}-*g*-PEG_x in DMSO (150 μL) was added DIPEA (0.8 μL) and mPEG-SCM in DMSO (200 μL). After reaction overnight, the solution was dialyzed against water using a 3500 Da molecular weight cut-off (MWCO) membrane for 1 d. Finally, the dialyzed solution was lyophilized to obtain product as a white powder. The product PLL_{34}-*g*-PEG_x was characterized by ^{1}H NMR (D_2O) and GPC.

Synthesis of PLL_{34}-*g*-[PEG_x:SH_y]. PLL_{34}-*g*-[PEG_x:SH_y] polymers were synthesized as described above for PLL_{11}-*g*-[PEG_x:SH_y] (Tables 2-2 and 2-3).

Table 2-2. Synthesis of PLL_{34}-*g*-[PEG_x:SH_y], where $x < 0.6$.

	PLL_{34}-*g*-PEG_x synthesis					**PLL_{34}-*g*-[PEG_x:PDP] synthesis**		
x^a	PLL_{34}		mPEG-SCM		x^b (NMR)	PLL_{34}-*g*-PEG_x	SPDP	
	μL	μmol	mg	μmol		mg	mg	μmol
0.4	500	3.1	82.1	41.1	0.17	14.4	16.9	54.1
0.6	400	2.4	98.6	49.3	0.25	15.0	10.4	33.3
0.8	300	1.8	98.6	49.3	0.35	12.8	5.3	17.0

[a]Expected fraction of PLL lysines converted to PEG. [b]Measured fraction of PLL lysines converted to PEG of PLL_{34}-*g*-PEG_x by NMR.

Table 2-3. Synthesis of PLL_{34}-*g*-[PEG_x:SH_y], where $x > 0.6$.

	PLL_{34}-*g*-PEG_x synthesis					**PLL_{34}-*g*-[PEG_x:PDP] synthesis**		
x^a	PLL_{34}-*g*-PEG_x		mPEG-SCM		x^b (NMR)	PLL_{34}-*g*-PEG_x	SPDP	
	x	mg	mg	μmol		mg	mg	μmol
0.6	0.25	37.1	38.6	19.3	0.63	21.7	3.7	12
0.8	0.35	25.5	19.6	9.8	0.77	24.1	2.1	6.9

[a]Expected fraction of PLL lysines converted to PEG. [b]Measured fraction of PLL lysines converted to PEG of PLL_{34}-*g*-PEG_x by NMR. [c]Measured fraction of PLL lysines converted to PEG of PLL_{34}-*g*-[PEG_x:SH_y] by NMR. [d]Measured fraction of PLL lysines converted to thiol groups of PLL_{34}-*g*-[PEG_x:SH_y] by NMR.

Synthesis of PLL_{50}-*g*-[PEG_x:SH_y]. The graft copolymers were synthesized as described above for PLL_{11}-*g*-[PEG_x:SH_y], except that no attempt was made to isolate or purify intermediate polymers PLL_{50}-*g*-PEG_x or PLL_{50}-*g*-[PEG_x:PDP] (Table 2-4). PLL_{50} (30 mg) and *N,N*-diisopropylethylamine (30 μL) were dissolved in DMSO (0.6 mL) in a vial, and the solution was stirred until the polymer was completely dissolved. Aliquots of this solution were transferred into separate vials. While stirring, mPEG-succinimidyl carboxymethyl (mPEG-SCM, MW 2000) in DMSO (150 μL) was then added dropwise to

each aliquot. After 6 h, excess SPDP in DMSO (70 μL) was added to the aliquots. After the reaction overnight, the crude solution was diluted to 500 μL with DMSO. A portion of this solution (200 μL) was combined with excess TCEP·HCl (10 mg, 35 μmol) for 3 h. The resulting polymers were purified by centrifugal filtration (3000 Da MWCO) using D_2O as solvent. This D_2O solution was characterized by ^1H NMR, and then used directly in subsequent experiments.

Table 2-4. Synthesis of PLL_{50}-*g*-[PEG_x:SH_y].

x^a	PLL_{50}		mPEG-SCM		SPDP	
	μL	μmol	mg	μmol	mg	μmol
0.2	210	9.3	16.7	8.4	20.8	66.6
0.4	210	7.4	33.3	16.7	15.6	49.9
0.6	105	5.6	25.0	12.5	5.2	16.6
0.8	105	4.4	33.3	16.7	2.6	8.3

[a]Expected fraction of PLL lysines converted to PEG.

Synthesis of fluorescein (FAM)-modified graft copolymers. PLL_{11}-*g*-[PEG_x:SH_y:FAM] graft copolymers were synthesized by the method described above for PLL_{11}-*g*-[PEG_x:SH_y], with some modification. Before incorporating PEG grafts or thiol groups, PLL_{11} (100 mg, 37 mol) was initially combined with 5(6)-carboxyfluorescein *N*-hydroxysuccinimide ester (1.8 mg, 3.8 mol, 0.1 equiv) and *N*,*N*-diisopropyl-ethylamine (100 μL) in DMSO (1.1 mL) to modify a fraction of the polymer with fluorescein groups. Aliquots of this solution were then used directly as starting materials in reactions with mPEG-SCM as described above. The resulting solutions were loaded onto a PD-10 size exclusion column, using water as the eluent. Two separate fluorescent

fractions were collected, corresponding to fluorescein-labeled PLL-*g*-PEG (eluting first) and free fluorescein. The first fraction was combined with excess SPDP and reduced using DTT as described above for PLL_{11}-*g*-[PEG_x:SH_y] to yield samples of graft copolymer containing a minority of fluorescein groups. Incorporation of fluorescein into the polymer was confirmed by ^{1}H NMR.

Synthesis of FAM-modified PEG-SH. FAM-PEG-SH was synthesized by the reaction between cystamine and amine-reactive FAM-PEG-NHS. Cystamine dihydrochloride (2.2 mg, 9.8 μmol) was dissolved in a mixture of 1-methyl-2-pyrrolidinone (200 μL) and *N*,*N*-diisopropylethylamine (20 μL). FAM-PEG-SCM (100 mg, 29.4 μmol) was added, and this mixture was allowed to react overnight. The solution was loaded onto a PD-10 size exclusion column, using water as the eluent, and the initial colored fraction (~7 mL) was collected. This fraction was extracted with dichloromethane (3 × 20 mL). The organic extracts were combined, dried over anhydrous sodium sulfate, and filtered, and solvent was removed *in vacuo*. The remaining solids were recrystallized from cold ethanol. The recrystallized material was redissolved in 1X PBS (1 mL), and combined with DTT (0.1 mmol) overnight to reduce disulfide bonds. The reaction mixture was dialyzed against water using a 1000 Da MWCO membrane for 1 d and then lyophilized. This yielded FAM-PEG-NHS as a yellow-orange powder (11.6 mg, 17 %). Successful incorporation of the thiol group was confirmed by ^{1}H NMR (D_2O).

Grafting ratio determination by ^{1}H NMR. The PEG grafting ratio, *x*—defined as the fraction of PLL sidechains that bear a PEG group—and the thiol grafting ratio, *y*—

the fraction of PLL sidechains that are thiol-modified—were calculated from peak integrals (I) in the NMR spectrum, according to the equations below:

$$x = \frac{I(\mathrm{mPEG-OC}\boldsymbol{H_3})}{\mathrm{N_{PLL}} \times I(\mathrm{PLL-NHC_5H_{10}C}\boldsymbol{H_3})}$$

$$y = \frac{I(-\mathrm{NHCOCH_2C}\boldsymbol{H_2}\mathrm{SH})\ /\ 2}{\mathrm{N_{PLL}} \times I(\mathrm{PLL-C_5H_{10}C}\boldsymbol{H_3})\ /\ 3}$$

Preparation of citrate-capped AuNPs. AuNPs were prepared by sodium citrate reduction of $HAuCl_4$.[46] All glassware was cleaned with aqua regia and all H_2O used was ultrapure and filtered through a 0.02-μm pore nylon membrane. A roundbottom flask was charged with 470 mL H_2O and 10 mL of 11.9 mM $HAuCl_4$. This solution was stirred vigorously and refluxed. After 30 min, 20 mL of 40 mM sodium citrate was quickly added. As the solution was refluxing, the color of the solution changed from colorless to deep red within 10 min. After refluxing for 1 h, the solution was allowed to cool, and the AuNPs were analyzed by absorption spectroscopy, TEM and DLS; λ_{max} = 519 nm, d(TEM) = 17.0 ± 1.1 nm, and d_z(DLS) = 20.3 ± 0.5 nm. The amount of Au used in the synthesis and d(TEM) were used to calculate the particle concentration of AuNPs.[47]

Surface modification of AuNPs with PLL-*g*-[PEG:SH]. The solution of AuNPs was reacted with graft copolymers to modify the surface. To 20 mL of AuNP solution (1 nM) was added excess graft copolymer (at least 1000 polymer molecules/particle) in a 20 mL vial. After vigorous mixing at room temperature, 10 mL of the solution was transferred to a 15 mL screw-top vial, and the vial was heated to 90 °C in a sand bath. Both the room-temperature and 90 °C solutions were incubated for three days. Solutions were then cooled, transferred to a 15 mL centrifuge tube, and centrifuged at 8000 × g for

30 min. The supernatant was discarded to remove unreacted polymer, and the AuNP centrifugate was re-dispersed in 15 mL H_2O. Centrifugation, supernatant removal, and re-dispersion were repeated 3 times.

2.2.3 Dynamic light scattering (DLS) analysis

The intensity (z)-averaged hydrodynamic diameter (d_z) of AuNPs in solution was measured with a Nano ZS instrument (Malvern, Worcestershire, England). All AuNP samples were centrifuged briefly (3000 × *g*, 60 s) to remove dust. The concentration of PBS (1X, 10 mM) and DTT (10 mM) were adjusted by addition of 10X PBS and 100 mM DTT solution, respectively. The diameter d_z was obtained by cumulant fitting, using an initial decay time of up to 100 μs to obtain the best fit.

2.2.4 Fluorescence experiments

For fluorescence experiments on polymers bound to AuNPs, the absorbance of the solution was adjusted to 0.1 to minimize inner-filter effects. All samples contained 1X PBS (pH 7.3). The temperature of each capped fluorescence cuvette was controlled in an oil bath. Fluorescence data were collected by a Quantamaster fluorimeter (PTI, London, Ontario; λ_{ex} = 470 nm) using optical filters (FF01-492/SP-25 and BLP01-488R-25, Semrock) to eliminate scattered light. Before and after each measurement, the cuvette was shaken and inverted to homogenize the solution. After 6 h of measurements, AuNPs were etched by adding 50 μL of 10 M KCN to each sample, incubating at 90 °C for 1 h,

and then at room temperature overnight, in order to release all fluorophore still bound to the particles. The fraction of polymer dissociated from the particles over time was calculated by dividing fluorescence intensity at 523 nm by the final fluorescence intensity at 523 nm after KCN etching.

2.3 Results and Discussion

The primary goal of this research was to evaluate thiolated PLL-PEG graft copolymers as stabilizing ligands for Au nanoparticles, and to determine the contributions of different copolymer characteristics—backbone lengths, PEG grafting densities, and number of thiol groups per polymer chain—on the effectiveness of the copolymer ligands. Non-thiolated PLL-PEG graft copolymers have been previously shown to passivate both monolithic[48-49] and colloidal[50-51] surfaces against adhesion of proteins and cells; a goal of this work was to translate the advantages of PLL-*g*-PEG copolymers to the passivation of AuNPs. Detailed experimental[48] and theoretical[52-53] studies on PLL-*g*-PEG-coated surfaces are consistent with past work on the general biocompatibility of PEG coatings, which resist nonspecific adsorption via steric and excluded-volume effects.[54-55] PLL-*g*-PEG has also been used to stabilize suspensions of inorganic nanoparticles,[56] where the same steric and entropic effects are responsible.[2] In all of these studies, PLL-*g*-PEG was anchored by electrostatic or covalent interactions between lysine side-chains on the polymer and the material surface. We found that combining citrate-capped Au nanoparticles with unmodified PLL-*g*-PEG yielded colloid that was

stable at room temperature, similar to previous studies performed with other PEGylated polyamines.[57] But we found that the PLL-*g*-PEG did not significantly improve the nanoparticles' stability against high temperatures or etchants, presumably because the interaction between the polymer lysine groups and the Au surface was not strong enough to ensure a dense layer under these conditions.

2.3.1 Synthesis of oligothiolated graft copolymers

In order to strengthen the interaction between PLL-*g*-PEG and Au colloid surfaces, we incorporated thiol groups onto the PLL backbone to convert the polymer into a multidentate ligand for Au. This was accomplished by sequential addition of NHS-ester-terminated PEG (mPEG-SCM) and NHS-ester-containing thiol linker (SPDP) to monodisperse PLL backbone starting materials, similar to the method reported by Kataoka and coworkers.[58] The goal of the synthesis was to convert every lysine in the original PLL to either a PEG or thiol group, but we anticipated that some lysine groups would remain unconverted by this approach. As a result, we expected $x + y \leq 1$ for products PLL_n-*g*-[PEG_x:SH_y], accounting for incomplete conversion of lysine groups in the PLL starting material.

Prior to introducing thiol groups, intermediate PLL-*g*-PEGs were characterized by NMR and GPC to verify the grafting ratio (x) of PEG (Figure 2-2 and Table 2-5). These intermediate copolymers were then combined with excess SPDP to exhaustively convert remaining lysine groups to pyridyldithiopropionate (PDP) groups. Although the incorporation of PDP groups into PLL-*g*-[PEG_x:PDP] could be verified by NMR, it was

impossible to calculate the degree of PDP incorporation because of band broadening in the NMR spectra. However, once the PDP groups were reduced to reveal thiols, grafting ratios in the resulting PLL$_n$-*g*-[PEG$_x$:SH$_y$] copolymers were characterized by integration of the sharp peaks in their NMR spectra (Figure 2-3 and table 2-6). These results showed that we were only able to synthesize thiolated graft copolymers for $0.25 < x < 0.65$. For $x < 0.25$, no polymer was isolated from the synthesis, presumably because addition of PDP groups made the polymer too hydrophobic or subject to oxidative (disulfide) crosslinking; and for $x > 0.65$, the procedure returned PLL-*g*-PEG$_x$ intermediates with no thiol groups attached, possibly due to steric crowding by the attached PEGs.[59]

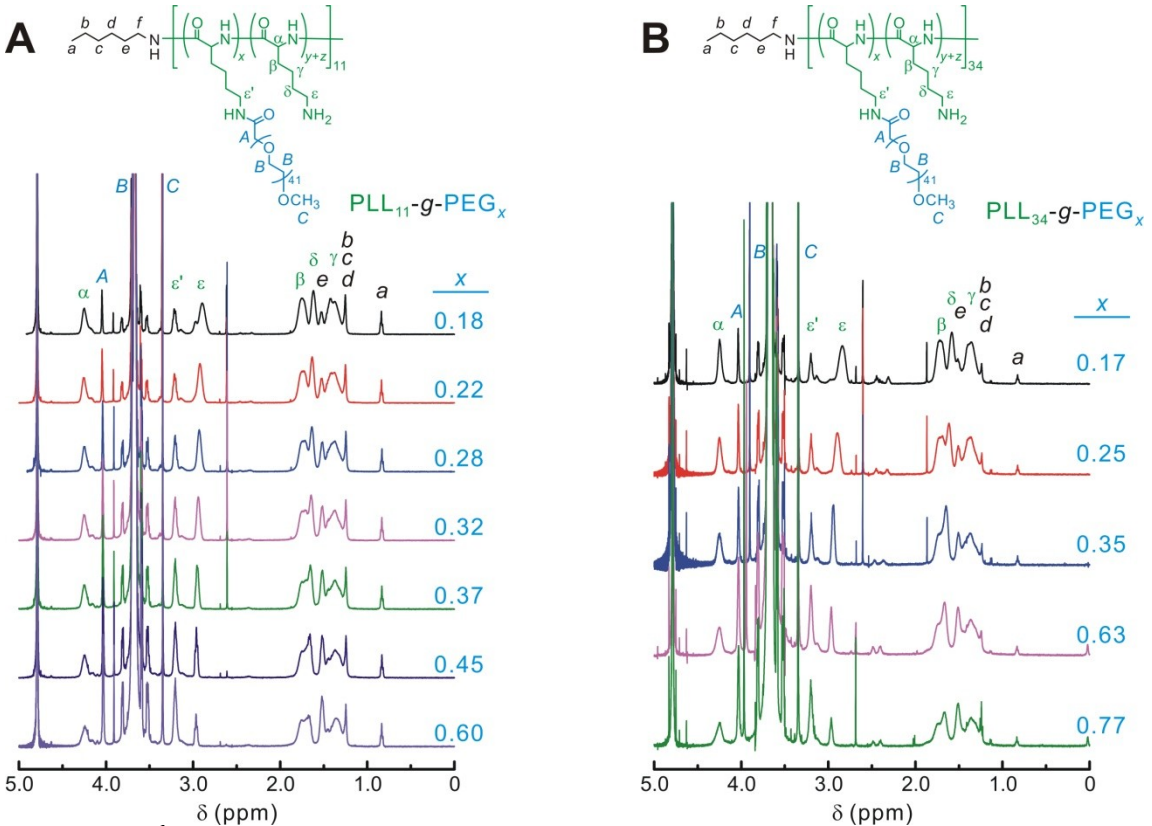

Figure 2-2. ^{1}H NMR spectra of (**A**) PLL$_{11}$-*g*-PEG$_x$ and (**B**) PLL$_{34}$-*g*-PEG$_x$ in D_2O.

Table 2-5. Characteristics of PLL_n-*g*-PEG_x and PLL_n-*g*-[PEG_x:SH_y]

PLL_n	PLL_n-*g*-PEG_x				PLL_n-*g*-[PEG_x:SH_y]	
	x_{NMR}	$M_{n,NMR}$ (g/mol)	$M_{n,GPC}$ (g/mol)	PDI_{GPC}	*x*	*y*
PLL_{11}	0.18	5200	4900	1.13	0.28	0.64
	0.22	6100	6100	1.28	0.27	0.61
	0.28	7300	6500	1.24	0.32	0.60
	0.32	8100	7200	1.22	0.37	0.51
	0.37	9200	8200	1.19	0.44	0.36
	0.45	11000	8600	1.21	0.50	0.29
	0.60	14000	10000	1.19	0.58	0.21
PLL_{34}	0.17	15000	20000	1.13	0.29	0.61
	0.25	20000	20000	1.11	0.31	0.67
	0.35	27000	21000	1.09	0.41	0.58
	0.63	45000	26000	1.12	0.56	0.28
	0.77	54000	28000	1.10	0.63	0.20
PLL_{50}	[a]				0.25	0.67
					0.33	0.57
					0.52	0.32
					0.63	0.19

[a]Synthetic PLL-*g*-PEG intermediates were not isolated for PLL_{50}-based copolymers.

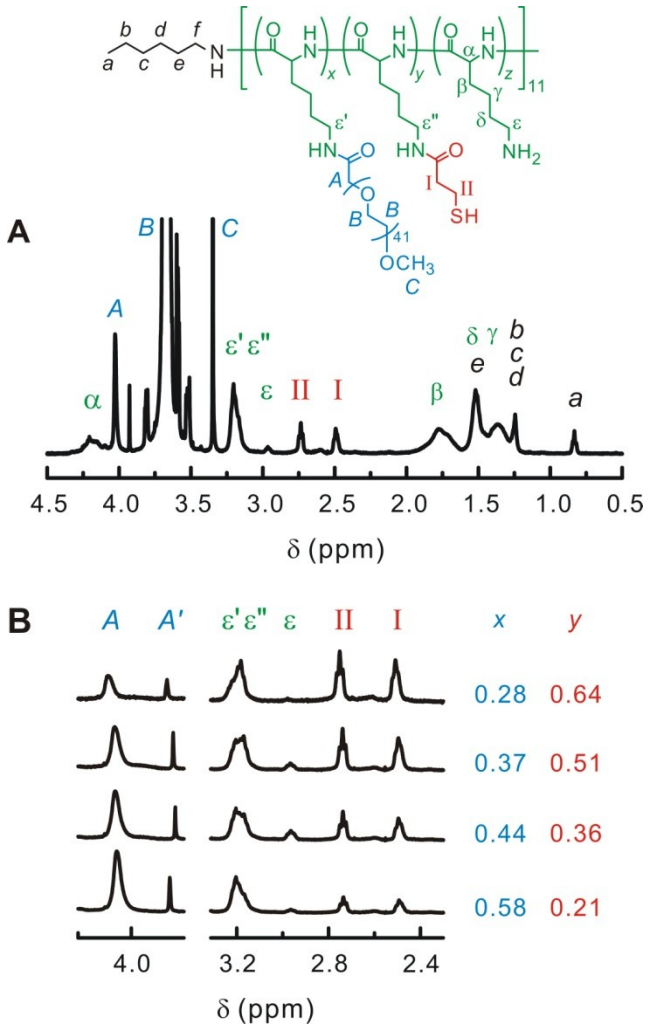

Figure 2-3. (**A**) ^{1}H NMR spectrum of PLL_{11}-*g*-[$PEG_{0.58}$:$SH_{0.21}$] dissolved in D_2O. (**B**) Closeups of ^{1}H NMR spectra for PLL_{11}-*g*-[PEG_x:SH_y], illustrating integration of PEG-C$\underline{H_2}$-CONH- (*A*), lysinyl -C$\underline{H_2}$$NH_2$- (ε, ε', and ε"), and thiopropionate -C$\underline{H_2}$C$\underline{H_2}$SH (I and II) protons. Grafting ratios *x* and *y* are calculated from these integrals. The spectra also show a peak corresponding to a small amount of PEG-C$\underline{H_2}$-COOH impurity (*A'*).

Table 2-6. Characteristics of AuNP@PLL$_n$-*g*-[PEG$_x$:SH$_y$].

					prepared at RT		prepared at 90 °C	
PLL$_n$	x	y	thiols per chain	$M_{n,NMR}$ (g/mol)	d_z (nm)	λ_{max} (nm)	d_z (nm)	λ_{max} (nm)
	0.28	0.64	7.04	7900	46.81	524	35.89	527
	0.27	0.61	6.71	7700	32.96	524	33.00	526
	0.32	0.60	6.60	8700	32.51	523	33.48	526
PLL$_{11}$	0.37	0.51	5.61	9700	34.28	524	35.19	524
	0.44	0.36	3.96	11000	33.20	523	36.73	524
	0.50	0.29	3.19	12000	33.10	524	36.66	524
	0.58	0.21	2.31	14000	30.98	523	33.00	523
	0.29	0.61	20.77	25000	31.69	523	31.98	524
	0.31	0.67	22.84	26000	31.63	522	32.71	523
PLL$_{34}$	0.41	0.58	19.88	33000	31.34	522	33.61	522
	0.56	0.28	9.43	41000	31.29	521	33.48	522
	0.63	0.20	6.96	45000	30.90	521	31.55	523
	0.25	0.67	33.50	33000	32.96	523	36.78	522
	0.33	0.57	28.50	40000	32.47	522	36.53	523
PLL$_{50}$	0.52	0.32	16.00	57000	34.67	522	38.45	523
	0.63	0.19	9.50	67000	34.26	522	36.85	522

2.3.2 Surface modification of AuNP with PLL_n-*g*-[PEG_x:SH_y]

Citrate-capped Au nanoparticles were combined with PLL_n-*g*-[PEG_x:SH_y] polymers in H_2O at room temperature for 3 d to yield polymer-capped AuNPs that withstood cycles of centrifugal concentration and heating. No color change or precipitation was observed during surface modification, indicating that the oligothiol polymers did not aggregate the AuNPs by crosslinking. After excess copolymer was removed by centrifugation and redispersion in aqueous solution, the polymer-stabilized AuNPs were characterized by DLS analysis and visible absorption spectroscopy (Table 2-6). The absorption spectra of all polymer-stabilized AuNP suspensions were red-shifted relative to that of the original, citrate-protected particles ($\lambda_{max,\ AuNP\text{-}citrate}$ = 519 nm; $\Delta\lambda_{max}$ = +2-5 nm). This shift in the surface plasmon resonance absorption of the AuNPs is consistent with a change in their surface dielectric, induced by surface functionalization.[60] DLS was used to measure the z-averaged hydrodynamic particle diameter (d_z) of the nanoparticles before and after polymer stabilization.[61] In general, polymer functionalization consistently increased d_z of the AuNPs by 10-14 nm over the diameter of the original particles. The grafted PEG chains on all of the PLL-PEG copolymers used in this study had a starting degree of polymerization of 41, and assuming the structural model in Figure 2-1, we estimate that these chains would extend from the particle-bound PLL backbone into solution between 3 nm (random coil) and 14 nm (fully extended). The measured increases in d_z are consistent with this model,[62] though it is difficult to draw firm structural conclusions from hydrodynamic measurements. Not all of the polymers tested were successful; one, PLL_{11}-*g*-

[$PEG_{0.28}$:$SH_{0.64}$], generated AuNP suspensions with anomalously large d_z and polydispersity index (PDI) values. This polymer had the highest thiol functionalization density in the PLL_{11} series, and the high d_z value may be due to particle crosslinking by multiple functional groups on the polymer. All of the other polymers tested generated monodisperse particle dispersions (PDI < 0.10 for PLL_{11} and PLL_{34} graft copolymers and 0.25 for PLL_{50} graft copolymers). In addition, the graft copolymer stabilized AuNP suspensions were stable in the high ionic strength solution (1 M $MgCl_2$) over hours at room temperature due to the presence of PEG layers, while citrate stabilized AuNP suspension aggregated even in 2 mM $MgCl_2$ solution (Figure 2-4).

Previous studies have shown that ligand passivation of AuNPs can sometimes be improved by "annealing" the product particles at elevated temperatures.[63-64] To test the effect of temperature on the synthesis of PLL-PEG-protected AuNPs, we also combined AuNPs and PLL_n-*g*-[PEG_x:SH_y] copolymers at 90 °C for 3 d. After purification, the annealed particles exhibited slightly larger d_z and λ_{max} values than those prepared at room temperature, consistent with a denser degree of functionalization and a more extended corona of graft copolymer on the particle surface. One hypothesis of this study was that these characteristics would confer higher stability to the annealed, PLL-PEG-protected AuNPs.

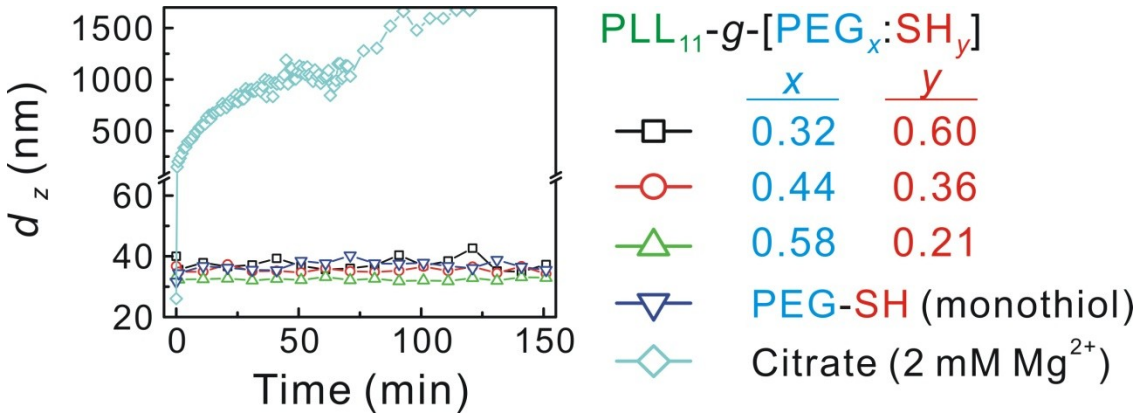

Figure 2-4. Intensity-averaged hydrodynamic diameter (d_z) of aqueous AuNP@PLL$_{11}$-*g*-[PEG$_x$:SH$_y$] and AuNP@PEG-SH particle suspensions containing 1 M $MgCl_2$ solution and AuNP@citrate particle suspensions containing 2 mM $MgCl_2$ solution, as a function of time, measured by DLS.

2.3.3 Comparative stability of AuNP@PLL-*g*-[PEG:SH] suspensions

A central goal of this work was to develop AuNPs that are stable to the presence of the free thiols and dithiols used in biotechnology, like DTT, which typically displace surface ligands from the AuNP surface and cause irreversible particle aggregation.[44] To test their stability, we gradually heated AuNP@PLL-*g*-[PEG:SH] suspensions in aqueous buffer to 90 °C in the presence of 10 mM DTT, and monitored the particles by DLS and visible absorption spectroscopy. In general, time-resolved DLS experiments (Figure 2-5) showed that most of the particle suspensions were stable (did not experience an increase in d_z corresponding to aggregation) over hours. An increase in d_z was observed for AuNPs modified with polymers containing either low or high ratios of PEG grafts to thiol

groups, and annealed particles were more stable than those prepared at room temperature. In addition, graft copolymers with shorter PLL backbones appeared to be marginally better at stabilizing AuNPs than longer ones. Importantly, all of the AuNP@PLL-*g*-[PEG:SH] particle suspensions were far more stable to heat and DTT than AuNPs functionalized with monothiolated mPEG-SH molecules, which were observed to aggregate even before the solution reached high temperature.

These DLS studies were supported by visible absorbance spectroscopy experiments using the same solution conditions and temperature ramp to 90 °C (Figure 2-6). Using a standard 1-cm cuvette, we observed that all of the particle suspensions exhibited a slow decrease in optical absorbance (~30% over 90 min) as particles adhered to the cuvette walls (and out of the optical path of the instrument); this is frequently observed for polymer- and biomolecule-stabilized AuNPs.[65] But the λ_{max} of most of these particle samples was not changed by heating in the presence of DTT. We did observe large increases in λ_{max} for AuNPs modified with PLL$_n$-*g*-[PEG$_x$:SH$_y$] copolymers with the lowest thiol-to-PEG ratios. These large increases in λ_{max} are characteristic of aggregating AuNPs.[66]

From this data, we argue that PLL-*g*-[PEG:SH] graft copolymers successfully stabilize AuNP suspensions by a balance of steric stabilization by PEG chains and thermodynamic stabilization by the oligothiol polymer ligands. In principle, polymers with too many thiol groups might crosslink the target AuNPs, and offer insufficient steric shielding by PEG against agglomeration; polymers with too few thiols might not bond strongly enough to the particle surfaces, or even at all, if the thiolated PLL backbone

were occluded by too many grafted PEG chains. Our DLS and absorption spectroscopy experiments do not provide information on the molecular details of the polymer-particle interaction, but they are consistent with this hypothesis of a balance between steric and thermodynamic stabilization.

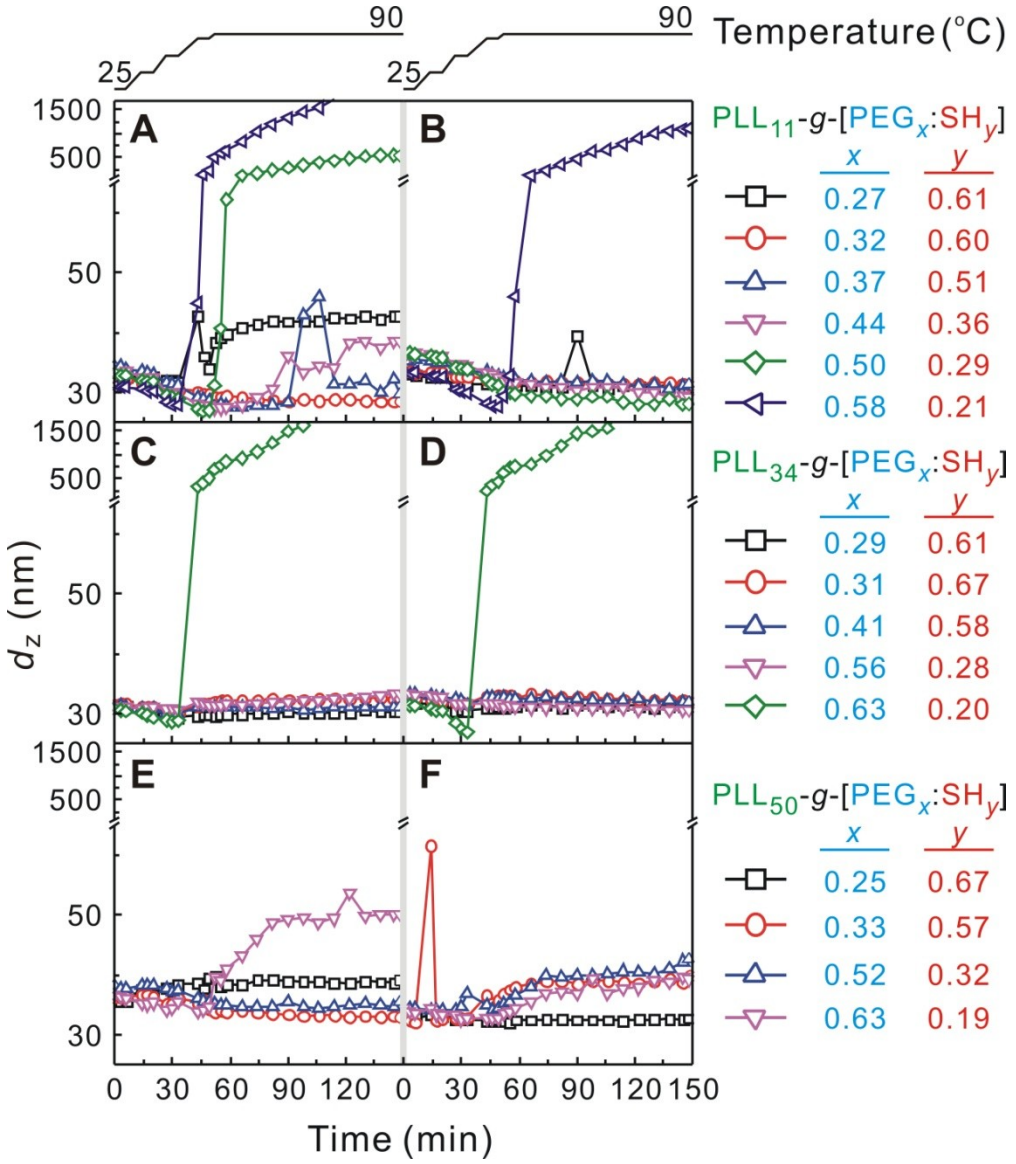

Figure 2-5. Intensity-averaged hydrodynamic diameter (d_z) of aqueous AuNP@PLL_n-*g*-[PEG_x:SH_y] particle suspensions containing 10 mM DTT and 10 mM PBS (pH 7), as a function of time and temperature, measured by DLS. Suspensions were prepared at room temperature (**A**, **C**, **E**) or annealed at 90 °C (**B**, **D**, **F**) with graft copolymers made from PLL_{11} (**A**, **B**), PLL_{34} (**C**, **D**) or PLL_{50} (**E**, **F**) backbones. In each experiment, the solution temperature was increased stepwise from 25 °C to 90 °C as shown in the legend at the top.

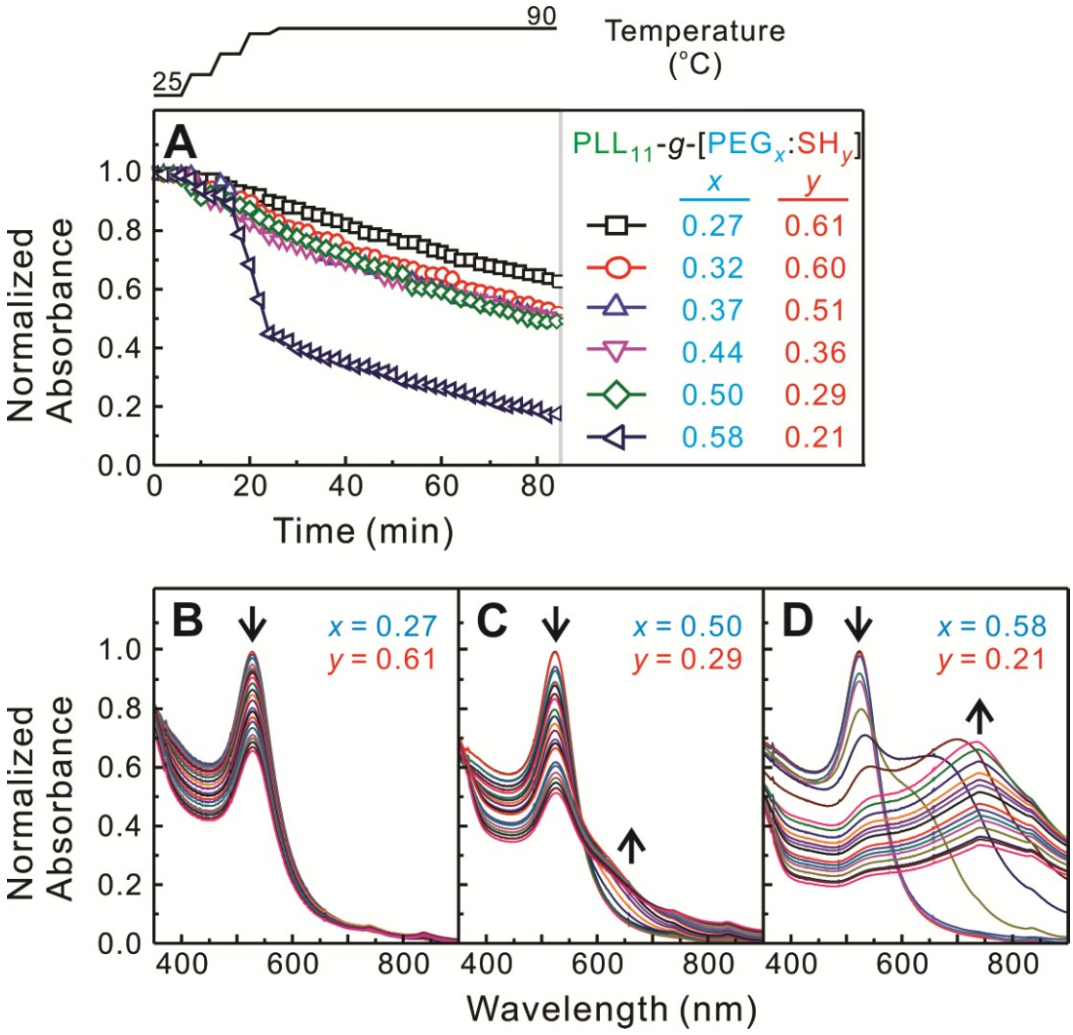

Figure 2-6. (**A**) Absorbance at 524 nm of aqueous AuNP@PLL_{11}-*g*-[PEG_x:SH_y] particle suspensions containing 10 mM DTT and 10 mM PBS (pH 7), as a function of time and temperature. In each experiment, the solution temperature was increased stepwise from 25 °C to 90 °C as shown in the legend at the top. (**B-D**) Full absorption spectra of AuNP@PLL_{11}-*g*-[PEG_x:SH_y] suspensions from (**A**).

2.3.4 Stability of AuNP-copolymer interactions

In order to more specifically characterize the interaction between graft copolymers and AuNP surfaces at the molecular level, we performed time-resolved fluorescence experiments on the dissociation of fluorescein-labeled PLL-*g*-[PEG:SH] from AuNPs. AuNPs are outstanding fluorescence quenchers,[67] and so fluorescent graft copolymer molecules bound closely to AuNP surfaces show no observable fluorescence intensity.[24] However, as the polymers desorb from the surface of the AuNPs into solution, their fluorescence is recovered. Thus, monitoring fluorescence intensity provides a proportional measure of the amount of polymer bound to and released from the AuNP surface.[30] In these experiments, AuNP@PLL-*g*-[PEG:SH] suspensions were heated to 90 °C, either in the presence or absence of DTT, and the fluorescence intensity of the suspension was monitored over time (Figure 2-7). We also performed the same experiments on AuNPs modified with monothiolated FAM-PEG-SH for comparison. Then, at the end of the experiment, the total amount of fluorophore present in each sample was determined by etching away the supporting AuNPs with KCN, and measuring the final fluorescence. In this way, the fractional fluorescence intensities shown in Figure 2-7 should represent the fraction of polymer dissociated from the particle surface over time.

Even in the absence of competing DTT, a substantial fraction (30%) of bound, monothiol FAM-PEG-SH was released from AuNPs at 90 °C within 30 min, and 100% of the monothiol dissociated in the presence of 1 mM DTT over the same period. By contrast, oligothiolated PLL-*g*-PEG graft copolymers showed dramatically less

desorption under all conditions, demonstrating stronger binding than PEG-SH. Among the different PLL$_{11}$-*g*-[PEG$_x$:SH$_y$] polymers studied, ligand desorption was inversely related to the number of thiols per polymer. For example, only 20% of polymers with an average of 6 thiols per PLL chain (y = 0.55) dissociated from the AuNP surface at 90 °C over 6 h, while 60% of those with an average of 4 thiols per chain (y = 0.35) dissociated over the same time (Figure 2-7B). Increasing the concentration of DTT led to more rapid ligand dissociation, but even at high temperature and DTT concentrations, some oligothiolated PLL-*g*-PEG remained on the AuNP surface (Figure 2-7C). These results are consistent with a model for ligand binding in which multivalency leads to stronger surface interactions and resistance against ligand loss.[15,68]

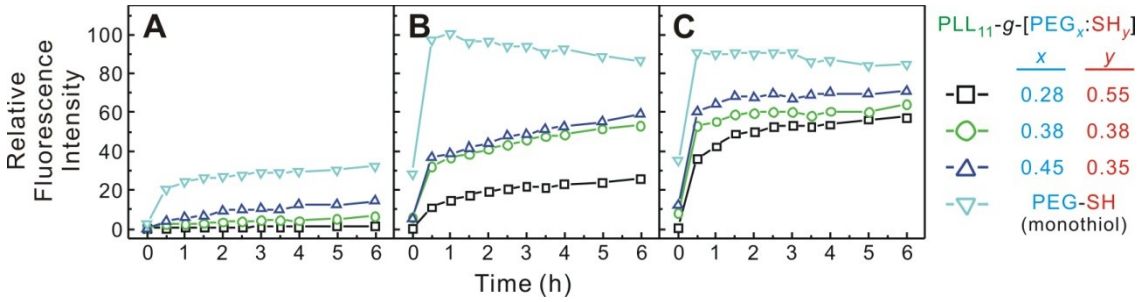

Figure 2-7. Relative fluorescence intensity of AuNP@PLL$_{11}$-*g*-[PEG$_x$:SH$_y$:FAM] particle suspensions, incubated at 90 °C, as a function of time. Solutions contained (**A**) no DTT, (**B**) 1 mM DTT, and (**C**) 10 mM DTT.

2.3.5 Stability of AuNP@PLL-*g*-[PEG:SH] against chemical etching

The instability of ligand-protected AuNPs can often be traced to chemical reactions at the nanoparticle surface. As a result, AuNP suspensions can be stabilized by restricting physical access to nanoparticle surfaces. One general way to test this access to chemical attack is to observe cyanide-induced Au etching in water.[69] Even though cyanide is not used in typical biotechnology protocols, it is a good proxy for other small molecules that react with Au surfaces, and cyanide etching of AuNPs can be easily monitored by absorption spectroscopy of the disappearing Au surface plasmon band.[70] We found that the rate of cyanide etching of AuNP@PLL$_n$-*g*-[PEG$_x$:SH$_y$] particles depended upon the relative fraction of thiol groups in the copolymer (Figure 2-8). For example, AuNP@PLL$_{11}$-*g*-[PEG$_x$:SH$_y$] particle suspensions prepared at room temperature lost 80% of their absorbance at λ_{max} within 2 h for $y < 0.5$, but just 20% of their absorbance for $y > 0.6$ (Figure 2-8A). Particles made with longer PLL backbones were generally less stable to etching for similar grafting ratios (Figure 2-8B). All AuNP@PLL-*g*-[PEG:SH] particles were made more resistant to KCN etching by first annealing them at 90 °C (Figure 2-8C). All of these results point to a relationship between the density of thiol functionalization of the AuNP surface—achieved either by controlling the number of thiols per PLL-*g*-[PEG:SH] chain, or by thermodynamically annealing the modified particles—and protection against chemical attack.

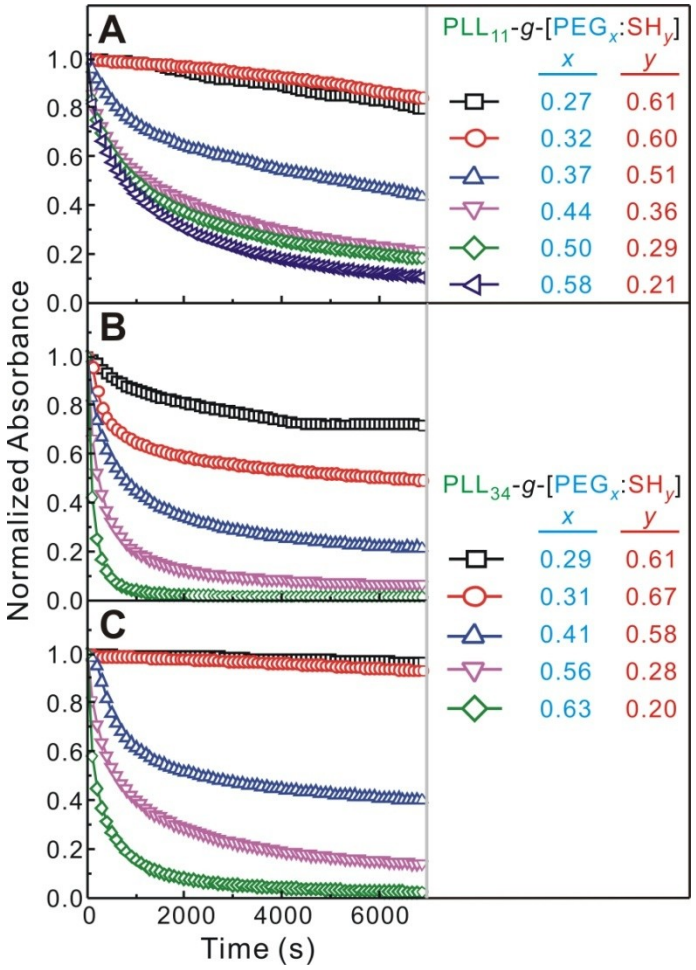

Figure 2-8. Absorbance at 520 nm of AuNP@PLL_{11}-*g*-[PEG_x:SH_y] suspensions exposed to 10 mM KCN, as a function of time. (**A**) AuNP@PLL_{11}-*g*-[PEG_x:SH_y] prepared at room temperature; (**B**) AuNP@PLL_{34}-*g*-[PEG_x:SH_y] prepared at room temperature; and (**C**) AuNP@PLL_{34}-*g*-[PEG_x:SH_y] annealed at 90 °C.

2.3.6 Steric and thermodynamic stabilization in AuNP@PLL-*g*-[PEG:SH] particles

We chose thiolated PLL-*g*-PEG graft copolymers as stabilizers for AuNPs because of the potential for combining steric stabilization of the colloidal suspension by PEG chains with strong ligand attachment by multiple thiol groups. This same combination has previously been studied for PLL-*g*-PEG adsorption on flat surfaces. Textor and co-workers have analyzed the effect of grafting ratios on PLL-*g*-PEG$_x$ adsorption on oxide surfaces, and found that the density of the protective PEG layer and resistance against non-specific protein adsorption was maximized at intermediate values of x.[48,52] In these authors' analysis, this represented a balance between affinity of lysine amines for the oxide surface on the one hand, and steric shielding by PEG on the other. Although stabilization of AuNP suspensions by PLL-*g*-[PEG:SH] copolymers is different from passivation of flat oxide surfaces, we argue that many of the same factors that make PLL-*g*-PEG copolymers effective coatings for oxides also apply to the success of the AuNP@PLL-*g*-[PEG:SH] materials reported here. Researchers have also shown that, if the ends of the grafted PEG chains in PLL-*g*-PEG are appropriately functionalized, it is possible to use PLL-*g*-(PEG-X) coatings as scaffolds for attaching other molecules—including proteins and peptides, affinity tags, and small organic molecules —to inorganic surfaces.[71-72] Otherwise, the unconverted lysine groups in the PLL-*g*-[PEG:SH] could be used to conjugate other molecules, even if PEG chains might shield the molecules. Although we have not demonstrated this for AuNPs in this report, one could imagine

AuNP@PLL-*g*-[PEG-X:SH] as a vehicle for combining the recognition properties of biomolecules and the unique physical properties of AuNPs into an extremely stable nanobioconjugate.

2.4 Summary

We have demonstrated that thiolated PLL-*g*-PEG graft copolymers are exceptional stabilizers for AuNPs, and have explored the relationship between graft copolymer structure and colloidal stability. In general, this study illustrates a balance between thermodynamic and steric factors in graft copolymer stabilization of AuNPs. On the one hand, having multivalent interactions between multiple thiol groups on the graft copolymer and the AuNP surface helps prevent ligand dissociation under extreme conditions, and isolates the surface from chemical attack. On the other hand, grafted PEG chains provide steric stabilization of the colloidal suspension, and keep AuNPs from aggregating. As a result, we predict that future optimization of PLL-*g*-[PEG_x:SH_y] ligands for biotechnological applications will involve balancing x and y. Moreover, we anticipate that the PLL-*g*-[PEG:SH]-stabilized AuNPs could be useful as nanoparticle supports in applications such as PCR, which require harsh experimental conditions including high salt concentrations, elevated temperature, and thiols that typically compete for surface ligands.

Chapter 3. Oligothiol Graft Copolymer Stabilized Gold Nanoparticles as Solid Supports in PCR

3.1 Introduction

The polymerase chain reaction (PCR) is an indispensable technology in modern molecular biology and diagnostics, and has been applied to DNA cloning, genetic engineering, DNA sequencing, and diagnostics of infectious and genetic disease. In PCR, a DNA polymerase enzyme extends a short, primer oligonucleotide to complement a full-length DNA template, and amplifies the target DNA sequence exponentially via temperature-controlled cycles from just a few copies of the template.[1] The PCR amplicons are then typically detected by additional instrumental analysis, including fluorescence detection of fluorescent DNA intercalating dyes or fluorophore-labeled DNA probes.[2]

Because PCR is instrument-intensive, it has been challenging to translate PCR to low-cost, portable analysis of DNA sequence targets. One approach to reducing the impact of instrumentation on PCR has been to replace fluorescence detection with visual inspection methods. A variety of visible-contrast detection methods have been developed for post-PCR analysis of DNA amplicons, including visualization of microbead aggregation,[3] colorimetric detection by association of conjugated polymers,[4] signal

amplification by polymer deposition on surfaces,[5] and a variety of colorimetric and reporter-deposition techniques based on metal nanoparticles. Gold nanoparticles (AuNPs), in particular, are attractive as visible labels for DNA detection schemes because of their unique physical and chemical properties. The large extinction coefficients of AuNPs[6] make it possible to visually determine concentrations of AuNP-tagged DNA molecules in solution that are similar to those determined for fluorophore-labeled DNA by benchtop fluorescence instruments.[7] On solid substrates, AuNP-labeled DNA can be observed directly at high surface concentrations, and autometallography at AuNP surfaces translates low surface concentrations of AuNP-tagged DNA into clearly visible, black spots.[8] For all of these techniques, sequence-specific AuNP-DNA probes (analogous to the fluorescent oligonucleotide probes used in fluorescence assays) are relatively easy to construct from unmodified AuNPs and thiol-terminated oligonucleotides.[9-10]

Taking advantage of these properties, researchers have developed post-PCR colorimetric detection assays for specific DNA targets using AuNP-based sequence probes.[11-14] In most of these assays, the AuNP-DNA probes were not included in the PCR step, and were only used after PCR amplicons were isolated from the PCR reaction. There have been a few reports in which AuNPs modified with thiolated oligonucleotide primers have been used in single-tube, solid-phase PCR.[15-19] Other researchers,[14,20] however, have reported that standard PCR reactions are poisoned by including AuNP-DNA conjugates made from thiolated oligonucleotides. We have previously reported that thiolated DNA does not stay bound to AuNP surfaces at the high temperatures[21-23] or in

the presence of competing thiols[24-28] that are common to PCR reactions, and this may be one reason why PCR reactions commonly fail with AuNP-bound primers. Monothiolated DNA is also known to degrade at high temperatures in the presence of AuNPs.[23,29-30] DNA polymerases adsorb and denature on AuNP surfaces,[31] and this causes PCR enzymes to lose their activity when AuNPs are included in the PCR reaction. In principle, these issues might be addressed by changing the chemistry that connects oligonucleotide primers to the AuNP surface. Lee and coworkers have very recently reported that coating AuNPs with a silica shell,[32] and then connecting DNA primers to this shell, allows the resulting ultra-stable AuNP-DNA conjugates to be used in single-tube colorimetric analysis of PCR.[14] It is not clear, however, how much of the attached or PCR-amplified DNA survived this process, or how many bound primers participated in the PCR reaction.

We report that an alternative strategy for connecting DNA to AuNPs, using multivalent, oligothiolated poly(L-lysine)-*graft*-poly(ethylene glycol) (PLL-*g*-PEG) copolymers as extremely strong ligands for the AuNP surface, enables the resulting AuNP-DNA conjugates to be used directly and stably as primers in PCR reactions. In order to characterize the effect of AuNP surface chemistry on PCR priming, we have systematically investigated the relationship between AuNP-DNA conjugate structure and PCR conditions, and we have analyzed the AuNP-bound PCR products using gel electrophoresis, dynamic light scattering, and fluorescent spectrophotometry. Finally, we have developed a single-tube, magnetic-capture method that allows AuNP-DNA-primed PCR reactions to be read by visual inspection within five minutes. We hope that our

results may be used to develop novel DNA diagnostic assays and solid-phase DNA sequencing technologies using AuNPs as primer supports.

3.2 Experimental Methods

3.2.1 General

Poly(L-lysine) trifluoroacetate (PLL_{11}, M_n 2700) was purchased from Alamanda Polymers, Inc. (Huntsville, AL). Methoxy-poly(ethylene glycol)-succinimidyl carboxymethyl (mPEG-SCM, MW 2000) was purchased from Laysan Bio, Inc. (Arab, AL). *N*-succinimidyl 3-(2-pyridyldithio)-propionate (SPDP) was purchased from ProteoChem, Inc. (Denver, CO). Triethylamine (Et_3N) was distilled from calcium hydride and methanesulfonyl chloride (MsCl) was distilled from P_2O_5. Oligonucleotides (ODN) were synthesized on an Expedite Nucleic Acid Synthesizer, using reagents from Glen Research (Sterling, VA). 5'-modified ODN with dibenzylcyclooctyne (DIBO) was synthesized as previously described. 5'-modified ODN with thiols and fluorescein were synthesized according to the manufacturer's instruction (Glen Research, Sterling, VA). PCR reactions were conducted using AmpliTaq Gold DNA Polymerase (Applied Biosystems Inc., Grand Island, NY). Primers were designed to amplify nucleotides 7131-7230 or 7131-7530 of the bacteriophage Lambda genome. SYBR Green I dye and Streptavidin coated magnetic beads (Dynabeads) were purchased from Invitrogen (Carlsbad, CA). All other reagents were purchased from Aldrich (St. Louis, MO) unless

otherwise noted. Ultrapure water was generated from a Milli-Q water purification system (Millipore Inc.; Billerica, MA, R > 10 MΩ·cm). PD-10 desalting columns were purchased from GE Healthcare (Pittsburgh, PA). ^{1}H NMR spectra were recorded on a Varian Unity (500 MHz) using solvent peaks as internal standards. Visible absorption spectra were obtained on a Hewlett-Packard 8453 UV-Vis spectrophotometer. The intensity (z)-averaged hydrodynamic diameter (d_z) of AuNPs in solution was measured with a Nano ZS instrument (Malvern, Worcestershire, England). Fluorescence data were collected by a Quantamaster fluorimeter (PTI, London, Ontario; λ_{ex} = 470 nm) using optical filters (FF01-492/SP-25 and BLP01-488R-25, Semrock) to eliminate scattered light.

3.2.2 Synthesis

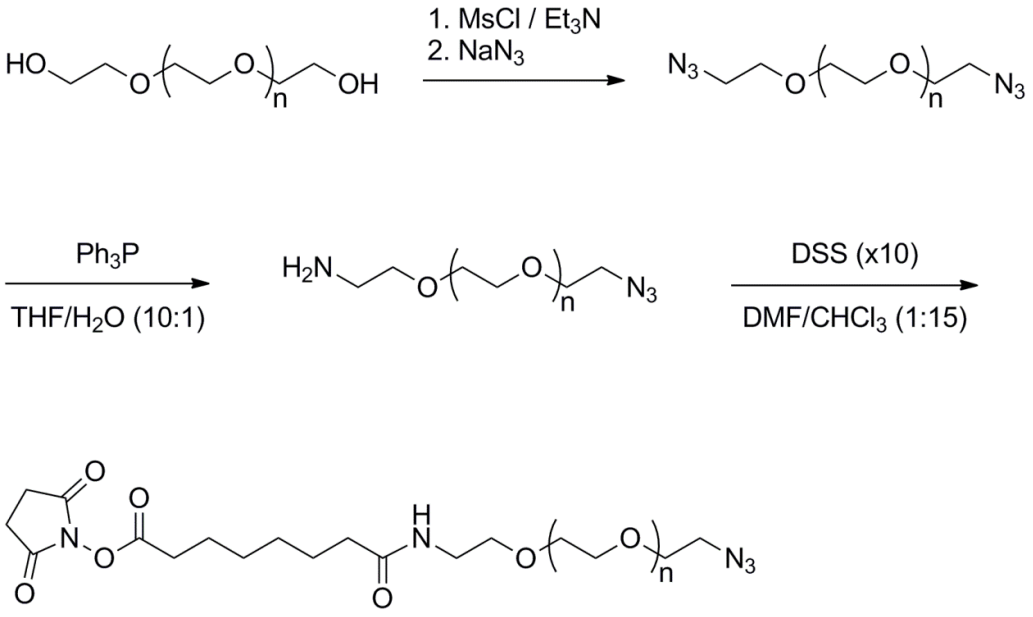

Figure 3-1. Synthetic scheme of α-amino ω-azido hetero functionalized PEG.

Diazido PEG Synthesis. Diazido PEG was prepared from PEG diol (MW 2,000) according to a method similar to that described by Schwabacher et al.[33] with the following modification. After PEG diol (50 g, 25 mmol) was dried by addition of 25 ml toluene and rotary evaporation, 120 ml of THF was added under N_2, and MsCl (4.3 ml, 56 mmol) then was added by a syringe. As the solution was cooled in an ice bath, Et_3N (7.7 ml, 56 mmol) in 5 mL of THF was added dropwise. The ice bath was removed 1 h later and the solution was stirred for about 4 h. To the mixture was added 150 mL H_2O, and the solution was cooled in an ice bath. Next, pH of the solution was adjusted to about 8 by the addition of $NaHCO_3$. NaN_3 (3.4 g, 52 mmol) was added to the solution while the solution was stirred. After THF was distilled at 80°C, the mixture was refluxed for 36 h. The aqueous layer was extracted with ether/DCM mixture (1:1) five times, and each organic layer was washed with brine. The organic layer was dried over Na_2SO_2 and dried by rotary evaporation. Residual solvent was removed by evacuation. (yield : 31.5 g, 50 %) ^{1}H NMR (500 MHz, $CDCl_3$, δ) 3.38 (t, CH_2N_3, J = 5.0 Hz), 3.47-3.78 (br s, CH_2CH_2O).

***α*-Amino *ω*-azido PEG synthesis.** Reduction of diazido PEG (5 g, 2.5 mmol) in 25 ml in THF/H_2O (10:1) was done statistically by dropwise addition of triphenylphosphine (656 mg, 2.5 mmol) in 5 mol of THF for 24 h under N_2. THF was distilled by rotary evaporation and 10 mL of H_2O was added into the solution. The solution was kept at 4 °C overnight. White precipitates then were filtered. To the solution was added by one pellet of NaOH. The aqueous layer was extracted by $CHCl_3$, and the organic layers were combined, dried over Na_2SO_4, and evaporated. The product was

purified by silica gel chromatography (DCM:methanol:NH_4OH 10:1:0.1, R_f = 0.2) to yield 0.95 g (19 %) after the elution of unreacted diazido PEG (R_f = 0.5), and leaving diamino PEG (R_f = ~0) in the silica gel. ^{1}H NMR (500 MHz, $CDCl_3$, δ) 2.86 (t, CH_2NH_2, J = 5.2 Hz), 3.38 (t, CH_2N_3, J = 5.0 Hz), 3.51 (t, $CH_2CH_2NH_2$, J = 5.2 Hz), 3.47-3.78 (br s, CH_2CH_2O).

RP-HPLC analysis. RP-HPLC was used to confirm the purity of *α*-amino *ω*-azido PEG because NMR analysis can not differentiate the desire product from the mixture of diamino and diazido PEG, according to a method similar to that described by Schwabacher et al. with the following modification.[33] Diazido PEG (500 mg, 0.25 mmol) was reacted with TCEP·HCl (150 mg, 0.52 mmol) in H_2O as a reference of diamino PEG. After 1 day, the pH was adjusted to about 10 by addition of 1 M NaOH. The product was extracted with $CHCl_3$. The organic layers were combined, dried over Na_2SO_4, and evaporated. This product and the purified *α*-amino *ω*-azido PEG (20 mg) were reacted with benzyl chloroformate (28 µl and 14 µl, respectively) in 200 µL of THF and trace amounts of DIPEA overnight. After ninhydrin test showed negative indicating no amine left, the mixture was dialyzed by a 1,000 MWCO membrane in 1 L of H_2O (three times) for 1 day. The product was analyzed by RP-HPLC (2:3 CH_3CN:H_2O with 0.05% CF_3CO_2H, 3 mL/min). The mixture from purified *α*-amino *ω*-azido PEG was eluted as one peak, while the mixture from diamino PEG showed a trace of carboxybenzylated *α*-amino *ω*-azido PEG followed by carboxybenzylated diamino PEG.

NHS-ester-PEG-N_3 synthesis. To the solution of di-(*N*-hydroxysuccinimidyl)-suberate (552 mg, 1.5 mmol) in 16 ml of DMF/$CHCl_3$ (1:15) was added α-amino ω-azido

PEG (300 mg, 0.15 mmol) in 5 ml of $CHCl_3$ and 2 μl of DIPEA slowly by syringe (8 ml/h) under N_2. As the addition proceeded, cloud solution became clear. After stirring overnight, the solution was evaporated and added by small aliquot of CH_2Cl_2. The product was precipitated by addition into cold ether and filtered. The product was dissolved in CH_2Cl_2, filtered, and precipitated into cold ether (twice). The white product was characterized by NMR. ^{1}H NMR (500 MHz, $CDCl_3$, δ), 1.36 (m, CH_2CH$_2$CH$_2$CONH, 2H), 1.43 (m, CH_2CH$_2$CH$_2$COO, 2H), 1.65 (m, CH$_2$$CH_2CH_2$CONH, J = 7.5 Hz, 2H), 1.75 (m, CH$_2$$CH_2CH_2$COO, J = 7.5 Hz, 2H), 2.18 (t, CH$_2$CH$_2$$CH_2$CONH, J = 7.5 Hz, 2H), 2.60 (t, CH$_2$CH$_2$$CH_2$COO, J = 7.4 Hz, 2H), 2.84 (br s, CO-CH_2CH_2-CO, 4H), 3.39 (t, CH_2N$_3$, J = 5.0 Hz, 2H), 3.45 (t, CONHCH_2, J = 5.2 Hz, 2H), 3.55 (t, CONHCH$_2$$CH_2$O, J = 5.2 Hz, 2H), 3.47-3.84 (br s, CH_2CH_2O), 6.10 (br s, CO*NH*, 1H).

PLL-*g*-[PEG-N$_3$:SH] synthesis. To the solution of PLL (10 mg) in 200 μl DMSO and 10 μl DIPEA was added 25 mg of NHS-PEG-N$_3$ in 500 μl THF. After shaking the solution for 2 h, the solution was added to 20 mg of SPDP and rinsed with 100 μl of 1x PBS and 100 μl of DMSO. The solution was shaken vigorously overnight. The solution was dialyzed in 2,000 MWCO membrane tubes for 1 day in 1 L of H_2O (three times). The product was lyophilized and redissolved in 500 μl of 1x PBS. To the solution was added 10 mg of DTT and shaken for 1 h. Then, the desired product was collected between 2 and 3 ml from PD-10 column using H_2O as an eluent. After lyophilization, the product was characterized by NMR analysis similar to the method in chapter 2.[34] The grafting ratios of PEG and SH were 0.29 and 0.53 using CH_2N$_3$ (δ = 3.37) and CH_2SH (δ = 2.75), respectively.

Copper free click DNA conjugation on AuNPs. AuNPs were functionalized with oligonucleotide primers using oligothiol conjugated graft copolymers via copper free click chemistry between 5'-dibenzocyclooctyne-modified oligonucleotides and azide groups in the polymers.[35] The solution of 5'-dibenzocyclooctyne-modified oligonucleotides (1.1 eq.) was mixed with the solution of PLL-*g*-[PEG-N_3:SH] for overnight. Then, to the solution of AuNPs was added the mixture followed by stirring for 1 h. The concentration of the mixture was brought to 10 mM phosphate buffer (0.15 M NaCl, pH 7.4). For annealed AuNPs after ~ 30 min, the solution in a glass vial was placed in a sand bath whose temperature was adjusted to ~ 90°C. The final concentration of NaCl and Tween20 was brought to 0.3 M and 0.01 %, respectively, 3 h later. The solution was incubated overnight. To remove excess amounts of ligands, the solution was cooled and centrifuged in 1.5 ml tubes. The supernatant was discarded and the pellet was resuspended in 1.5 ml 0.01% Tween20. This was repeated three times. The solution was kept in 4 °C refrigerator.

3.2.3 PCR conditions

PCR reactions were conducted using AmpliTaq Gold DNA Polymerase. Reagents were combined in 1X PCR buffer to target concentrations.

For experiments to determine whether AuNPs inhibit PCR or not, PCR samples contained 2.5 U/100 μL AmpliTaq Gold DNA polymerase, 2 μM of forward and reverse primers, 200 μM each dNTP, 1.5 mM $MgCl_2$, 1X PCR buffer (10 mM Tris-HCl (pH 8.3)

and 50 mM KCl), 0.01% Tween20, 1 ng/100 μL bacteriophage Lambda DNA, and different concentration of AuNPs@citrate, HS-T_{20}, HS-PEG-T_{20}, and PLL-*g*-[PEG-T_{20}:SH] from 0 to 4 nM. The thermal cycling protocol involved initial heating at 95 °C for 5 min; then 30 cycles of 95 °C for 15 sec, 60 °C for 30 sec, and 72 °C for 45 sec; and finally 72 °C for 6 min.

For SP-PCR using graft copolymer stabilized AuNPs, PCR samples included constant concentrations of 80 nM forward primer, 5 μM reverse primer, 5 pM of 400 bp DNA template, 0.01 % Tween20, 1X PCR buffer (10 mM Tris-HCl (pH 8.3) and 50 mM KCl), and 1 nM AuNPs. The concentration of AmpliTaq Gold DNA polymerase and $MgCl_2$ varied from 2.5 U/ 100 μL to 5 U/100 μL and from 1.5 mM to 4.5 mM, respectively. The same thermal cycling protocol was used as described above except number of thermal cycles, which varies from 30 to 50.

For colorimetric detection of SP-PCR using graft copolymer stabilized AuNPs, PCR samples included constant concentrations of 10 nM forward primer, 30 nM reverse primer, 1 ng/mL of Lambda DNA or 5 pM of 400 bp DNA template, 0.01 % Tween20, 1X PCR buffer (10 mM Tris-HCl (pH 8.3) and 50 mM KCl), and 1 nM AuNPs (total volume: 50 μL). The reverse primers were 5'-biotin labeled for Dynabead conjugation, which led to color change with magnetic attraction. Control experiments were performed by excluding template or using 5'-OH normal reverse primers. The concentration of AmpliTaq Gold DNA polymerase and $MgCl_2$ were 5 U / 100 μL and 4.5 mM, respectively. The thermal cycling protocol involved initial heating at 95 °C for 5 min;

then 30 cycles of 95 °C for 15 sec, 54 °C for 30 sec, and 72 °C for 75 sec; and finally 72 °C for 6 min.

3.2.4 SP-PCR characterizations

Agarose gel electrophoresis. PCR reactions were characterized by gel electrophoresis in 1.5% (PCR inhibition experiment) or 1.0% (SP-PCR experiments) agarose gel in 1X TBE. Wells were loaded with either 8 μL (PCR inhibition experiments) or 16 μL (SP-PCR experiment) of each PCR reaction, and the gel was electrophoresed for 1 h at 100 V. Photographs of the gels were taken using a digital camera. The gels then were stained with 50 g/mL ethidium bromide (EtBr) for 10 min, and washed with ddH_2O for 10 min, and imaged for EtBr fluorescence.

dsDNA characterization. dsDNA was characterized by DLS analysis and fluorescence using SYBR Green I. To extract AuNP-PCR from PCR mixture containing various chemicals, such as, DNA polymerase, dsDNA, primers, $MgCl_2$, etc., the PCR reaction mixture was diluted with 1.5 mL of 10 mM TE (10 mM Tris, 1 mM EDTA, and 0.01% Tween20, pH 7.5) and centrifuged at 7000 rpm (30 min). The supernatant was transferred into a new tube and centrifuged at 7000 rpm (30 min). After the supernatant was removed, all AuNP pellets were combined. This process was repeated once more with 10 mM TE (0.01% Tween20), twice with 1X TBE (0.01% Tween20). The concentration of AuNPs was determined by UV-Vis spectroscopy using the following equation; $\ln\varepsilon = k \ln D + a$, where $k = 3.32111$ and $a = 10.80505$.[36] The purified

AuNPs@dsDNA was used to determine the hydrodynamic size of the AuNPs by DLS analysis. The 0.1 nM of AuNP was incubated with 1X SYBR Green I and 10 mM KCN at 65°C (50 min) to etch the AuNPs. The fluorescent intensity was then measured and calibrated to standard curve to obtain the concentration of amplified dsDNA.

ssDNA characterization by DLS analysis and fluorescence using ODN-FAM. The purified AuNP@dsDNA was incubated with 1 mL of 0.1 M NaOH (0.01% Tween20) for 30 min. The mixture was then centrifuged at 7000 rpm (30 min). The supernatant was transferred into a new tube and centrifuged at 7000 rpm (30 min). After the supernatant was removed, all AuNP pellets were combined. This process was repeated once more with 0.01% Tween20, twice with 10 mM TE (0.01% Tween20). The concentration of AuNPs was determined by UV-Vis spectroscopy. The purified solution of AuNPs@ssDNA was used to determine the hydrodynamic size of AuNPs by DLS analysis. The solution of AuNP@ssDNA or AuNP@primer for control was then incubated with 20 nM of ODN-FAM in 10 mM TE (final volume 150 μL, Absorbance of AuNPs = 0.1 at λ_{max}, 0.3 M NaCl, and 0.01% Tween20) overnight 50 °C using PCR machine after 15 sec pre-heating at 95°C. The samples were then centrifuged at 10,000 rpm (20 min). The supernatant was transferred and centrifuged at 10,000 rpm (30 min). The combined AuNPs pellets were further purified by the same procedure using 10 mM TE (0.3 M NaCl and 0.01% Tween20) twice. The AuNPs were diluted in 10 mM TE (130 μL, 0.3 M NaCl and 0.01% Tween20). The AuNPs hybridized ODN-FAM (100 μL) were then mixed with 100 mM KCN (10 μL), and the mixture was incubated at 65 ^{o}C for 50 m

to etch the AuNPs. The solutions were characterized by PTI fluorometer to measure the fluoresecent intensity of ODN-FAM.

3.2.5 Colorimetric detection of AuNP SP-PCR

Streptavidin-coated Dynabeads solution (200 μL, 10 mg/mL) was mixed with 1 mL 10 mM TE (0.01 % Tween20). After magnetic beads were settled down using a magnet, the supernatants were discarded. This was repeated three times more. After these washing, the beads were mixed with 100 μL of 10 mM TE (0.01% Tween20), which resulted in 20 mg/mL solution.

After SP-PCR using the AuNPs, the photographs of the tubes were taken using a digital camera and UV-Vis spectra were measured. The solutions were then mixed with 15 μL of the washed Dynabeads solution and gently shaked for 5 min. Next, a magnet was placed on the bottom of the tubes to settle down the Dynabeads. The photographs of the tubes were taken and UV-Vis spectra were measured.

For waveguided optical analysis, 20 μL of the supertants from each tube was transferred into a 0.8 mm diameter capillary tube. The surface of the capillary tube was etched using commercially available glass-etching cream, which visualized the color of the solutions (1.2 cm etched surface, 1 cm non-etched surface, and 0.5 cm etched surface from the bottom). The tubes were placed in homemade dark room and white-light was illuminated from the top of the tubes. Photographs were then taken from the front of the tubes with and without a green optical filter made of green cellophane papers.

Table 3-1. PCR primers and probes sequences.

Forward primer	5'- GAT GAG TTC GTG TCC GTA CAA CTG G - 3'
Monothiol forward primer	5'- HS -(C6) - GAT GAG TTC GTG TCC GTA CAA CTG G - 3'
Monothiol forward primer	5'- HS -(C6) - TTT TTT TTG ATG AGT TCG TGT CCG TAC AAC TGG - 3'
DIBO tagged forward primer	5'- DIBO - GAT GAG TTC GTG TCC GTA CAA CTG G - 3'
Reverse primer (400bp)	5'- CCC GGC AGC ACA AAT GCC ACA GGT T -3'
Reverse primer (100bp)	5'- AGA CGG GCA ATC AGT TCA TCT TTC G –3'
Biotin tagged reverse primer (400bp)	5'- biotin - CCC GGC AGC ACA AAT GCC ACA GGT T -3'
Complementary FAM-ODN	5'- FAM - C CCG GCA GCA CAA ATG CCA C - 3'
Noncomplementary FAM-ODN	5'- FAM - GG TTA TCG AAA TCA GCC ACA - 3'

3.3 Results and Discussion

3.3.1 ODN functionalized AuNPs using oligothiol graft copolymer stabilizing ligands

The main goal of this study was to explore the relationship between multivalency of DNA surface ligands attached to AuNPs and the stability and utility of those ligands in PCR reactions. Previous work has shown that increasing ligand valency improves the stability of ligand-capped nanoparticles in general,[37] and of AuNP-DNA conjugates in particular.[27,38] Towards this aim, researchers have synthesized di- and tri-thiol modifier reagents for use in solid-phase oligonucleotide (ODN) synthesis, and then combined the resulting oligothiolated ODNs with AuNPs to form stable AuNP-ODN conjugates. We have previously attempted to use these conjugates in PCR reactions without success. In principle, this problem might be solved by attaching ODNs to AuNP surfaces via even more thiol groups. This hypothesis follows from our recent report that AuNPs survived harsh experimental conditions similar to those found in PCR when they were passivated with PLL-*g*-PEG graft copolymer ligands containing many thiols per polymer chain.[34] To apply these polymers to AuNP-ODN construction, we attached the copolymer ligands to ODN molecules via a strain-promoted, copper-free "click" chemistry method we reported recently (Figure 3-2),[35] to yield oligonucleotide-copolymer conjugates. PLL-*g*-PEG polymers containing both azide and thiol functional groups (PLL-*g*-[PEG-N_3:SH]) were prepared by sequentially combining monodisperse poly(L-lysine) trifluoroacetate (PLL_{11}, M_n 2700, PDI 1.1) with an azido-PEG-NHS ester (M_n 2000) and a protected thiol-NHS

ester (SPDP) in controlled ratios, followed by deprotection of the thiol groups. These azide-functionalized polymers were then combined with a 5'-dibenzocyclooctyne (DIBO)-modified ODN to yield multi-thiolated, oligonucleotide-grafted PLL. These polymers were then incubated for 3 d with 15-nm diameter, citrate-modified AuNPs to yield AuNP-DNA conjugates. Our previous work on graft-copolymer-modified AuNPs showed that particle suspensions were more stable if particles were incubated with polymer at 90 °C;[34] in this work, we formed AuNP-DNA conjugates at both room temperature and at 90 °C, in order to perform the same analysis. The hypothesis of this study was that polymer-oligonucleotide constructs would remain more strongly attached to AuNPs during PCR reactions than oligonucleotides bound by just one or a few thiol groups. To help make this comparison, we also synthesized AuNPs modified with 5'-monothiolated oligonucleotides using previously reported methods.

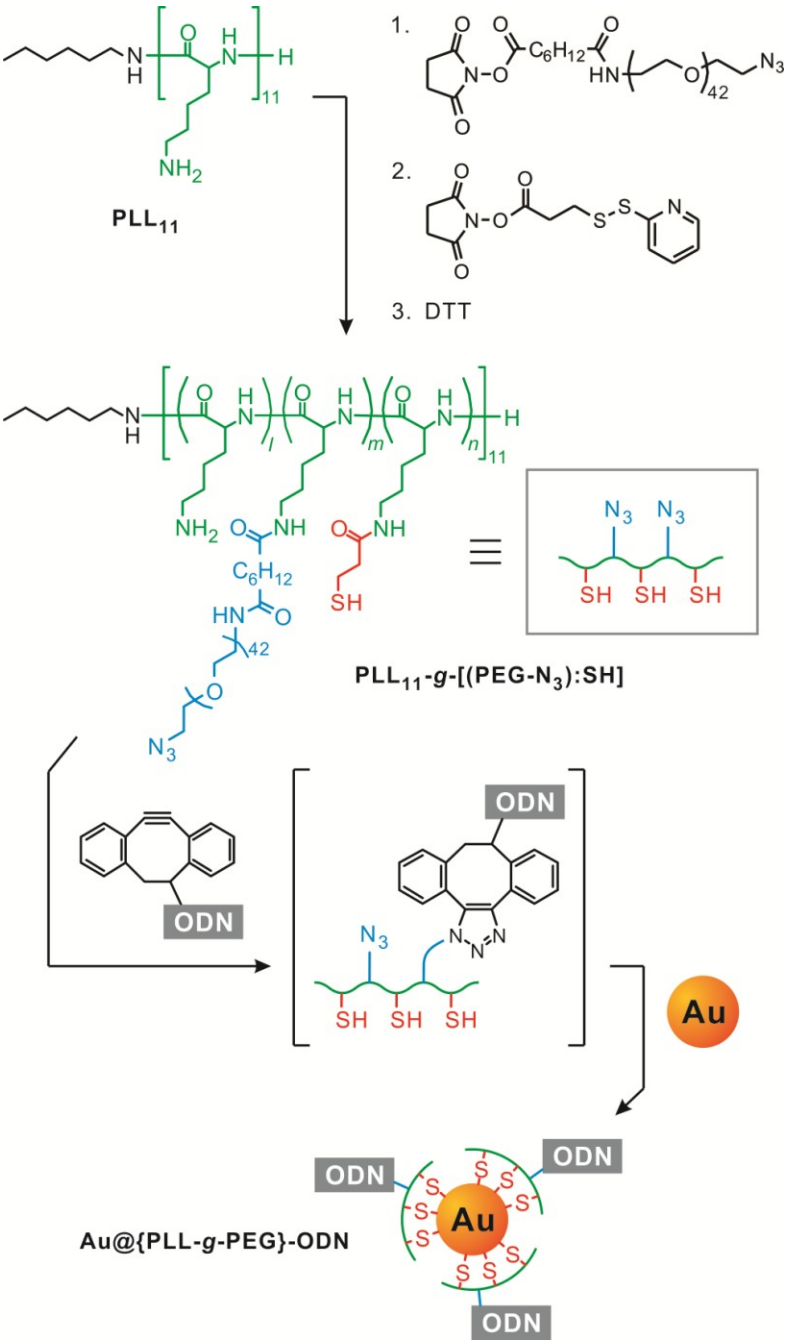

Figure 3-2. Schematic representation of AuNPs coated with ODN functionalized oligothiol graft copolymer.

3.3.2 PCR inhibition experiments

One requirement of the use of AuNP-ODN conjugates in PCR reactions is that they do not inhibit (or "poison") the PCR reaction. Storhoff and coworkers reported that DNA-modified AuNPs can inhibit PCR even when the bound DNA is not directly involved in the PCR reaction.[20] To test whether the AuNPs inhibited PCR through thermal cycles, AuNPs stabilized by T_{20} ODNs conjugated through either widely used mono-thiols or the graft copolymers were included in PCR. Figure 3-3 illustrated the mono-thiolated ODN (HS-T_{20}) stabilized AuNPs inhibited the amplification reaction during PCR even in the low concentration of the AuNPs (0.2 nM). It showed more migration of AuNPs bands in gel electrophoresis than PCR negative AuNPs and the absence of target DNA bands in the ethidium bromide (EtBr) staining gel image. When PEG layers were incorporated between thiols and ODNs, complete inhibition was observed above 1 nM of AuNPs (Figure 3-3). When the inhibition occurred, the AuNPs band showed more migration similar to the HS-T_{20} stabilized AuNPs. In contrast, multi-thiolated graft copolymers stabilized AuNPs had no effect on the PCR results even in the high concentration (4 nM). As a result, the positive DNA bands in EtBr staining gel image was observed as well as no migration changes of AuNPs bands before and after PCR (Figure 3-3). The Alivisatos group reported that further migration of DNA functionalized AuNPs resulted from lower DNA density on AuNPs.[39-40] The faster migration from electrophoresis analysis suggested that mono-thiolated ODNs could be degraded or desorbed from surface of AuNPs during thermal PCR cycles and polymerases interacted with AuNP surfaces, which completely inhibited extension and

amplification of DNA. Although introduction of PEG layers could reduce the PCR inhibition below 1 nM of AuNPs, which might be come from thermodynamically unfavored desorption of PEG layer to the water at elevated temperature,[41] the results suggested that AuNPs stabilized with mono-thiolated ODN was not suitable for colorimetric detection assays that required a certain concentration of AuNPs at which the color of solution should be distinguished by naked eyes.

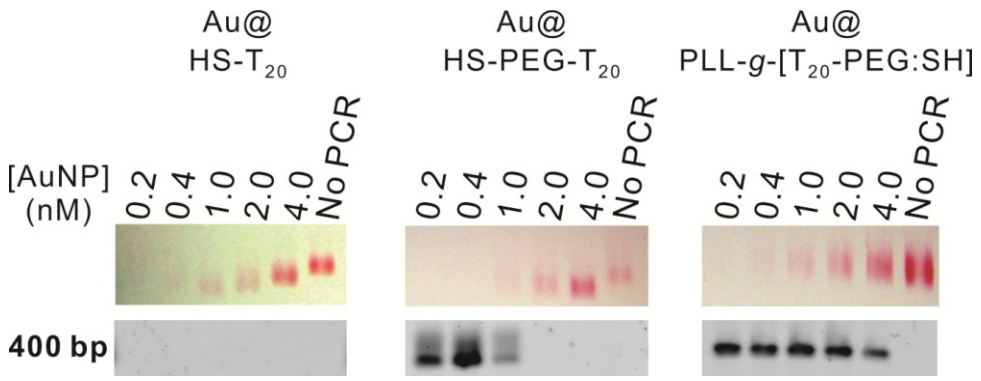

Figure 3-3. Agarose gel electrophoresis images of PCR inhibition experiments. After PCR was performed containing different concentrations of AuNPs that were stabilized by HS-T_{20}, HS-PEG-T_{20}, or PLL-*g*-[PEG-T_{20}: SH], the PCR products were analyzed aragose gel electrophoresis. **Top:** Visible images corresponding to AuNP red-bands stabilized with (**Left**) HS-T_{20}, (**Middle**) HS-PEG-T_{20}, or (**Right**) PLL-*g*-[PEG-T_{20}:SH]. **Bottom:** Fluorescence images corresponding to ethdium bromide staining 400bp DNA bands for AuNPs stabilized with (**Left**) HS-T_{20}, (**Middle**) HS-PEG-T_{20}, or (**Right**) PLL-*g*-[PEG-T_{20}:SH]. From left to right lanes, the concentration of AuNPs increases (0.2, 0.4, 1, 2, and 4 nM). In no PCR lanes, AuNPs were not performed for PCR as negative control.

3.3.3 Solid phase PCR on AuNPs

There have been a few reports of incorporation AuNPs into PCR mixture[14,42-43] as well as reports of using AuNP bound oligodeoxyribonucleotides (ODNs) as primers in PCR, which is called solid phase PCR (SP-PCR). This strategy has been attracted because they offer not only simple and rapid colorimetric detection without post-PCR instrumentation, but also further subsequent applications using immobilized amplicons. Particularly, immobilized amplicons via SP-PCR have been exploited for DNA cloning, high-throughput DNA sequencing, and protein identification and become popular and powerful tools for biotechnology.[44-48] The SP-PCR on AuNPs have more advantages than other solid-phases, including a microbead,[44,46] a flat surface,[49] and a microtiter plate,[50] due to features of AuNPs. The unique optical properties of AuNPs can be used as optical tags for bio-physics study using interparticle distance dependent plasmonic band shifts.[51-52] In addition, nano-sized characteristics yield larger curvature on surface that can provide more space and employ denser genes on the unit surface area than micro-size particles or flat surfaces.[53] Moreover, it may solve the limitation of SP-PCR caused by steric masking of primers to polymerases.[54-56] In addition, nano-sized materials have more diffusive characteristic in the solution than microbead or flat surface, resulting in more efficient amplification via enzymatic reaction.[57] Nonetheless, there are few reports in which AuNPs are used as solid-phase for PCR because of the imcompatibility of widely used AuNP-monothiolated DNA conjugates in PCR conditions, which leads to degradation and desorption of the DNA[23,29-30] as well as the loss of DNA polymerase activity,[31] as mentioned before.

We believed that our graft copolymer stabilized AuNPs could overcome these problems and be successfully used as supports for PCR. In addition, the graft copolymer stabilized AuNPs did not affect on DNA polymerase activity from the PCR inhibition experiments, resulting in the target DNA synthesis. Therefore, we performed SP-PCR using the graft copolymer stabilized AuNPs on which forward primers were immobilized. It is reported that the efficiency of SP-PCR depends on the concentration of initial DNA template.[58] As a result, SP-PCR frequently uses simultaneous amplification of the target DNA in the liquid phase and the solid phase.[46,59] The amplified target DNA in the liquid phase increases the concentration of the DNA templates, which improves the efficiency of SP-PCR. We also included unbound forward primers in the PCR mixture for this strategy.

Thoughout SP-PCR, primers bound to AuNP surface are extended by DNA polymerase to have target DNA sequences without changing AuNP properties. As a result, AuNP amplicons should not only show intact AuNP optical properties (red color), but also have larger hydrodynamic size than that of AuNP-primers. Gel electrophoresis migration length was used to study the size change before and after SP-PCR.[39-40] In addition, complementary characterization of the size change was performed using DLS, because the migration in gel electrophoresis is related to both size and charge of AuNP amplicons. We used DLS for this characterization because DLS analysis is related to the hydrodynamic size of suspensions, not the charge in most cases.[60-61] Furthermore, amplified double strand DNA (dsDNA) from positive SP-PCR was quantified using fluorescent DNA intercalating dyes, which have fluorescence in the presence of

dsDNAs.[62] To avoid false indication that would be caused by the hybridization between the immobilized primers and the amplified single strand DNA (ssDNA) in the liquid phase, the dsDNA bound to AuNPs was denaturated by basic solution, and the resulting ssDNA on AuNP surfaces was analyzed. We used DLS based size change from the stiff dsDNA to the flexible ssDNA for this purpose. Moreover, to know whether target DNA was amplified on the AuNP surfaces, we used complementary ODN probes bearing fluorophores and characterized the fluorescence of the hybridized complementary ODN probes (Figure 3-4).

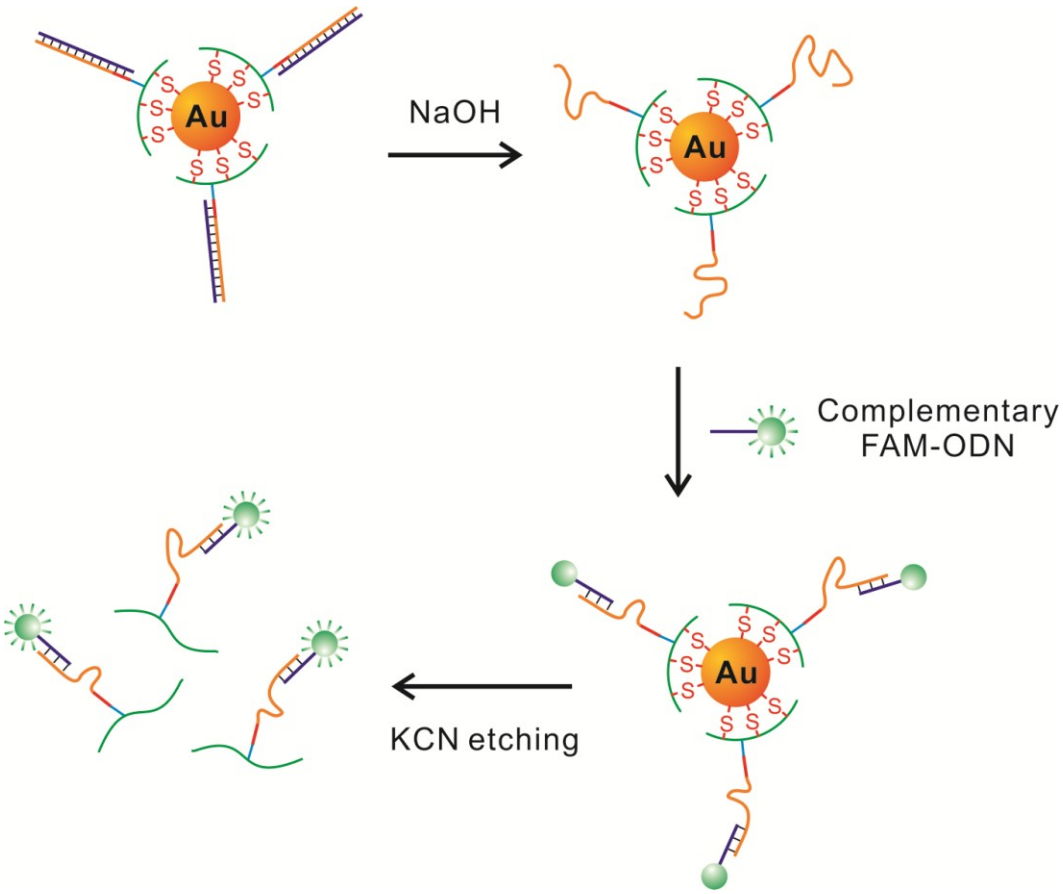

Figure 3-4. Schematic illustration of AuNP-ssDNA characterization using fluorophore tagged complementary ODN probes. dsDNA on the AuNP-amplicons is denaturated by basic solution, resulting in immobilized ssDNA. FAM-ODN probes containing complementary sequence to the immobilized ssDNA are mixed with the AuNP-ssDNA. When the FAM-ODNs are hybridized, the fluorescence is quenched due to FRET by AuNPs. After purification of the solution to remove excees amount of free FAM-ODNs, the AuNPs are etched to turn on the fluorescence that is measured by a fluorometer.

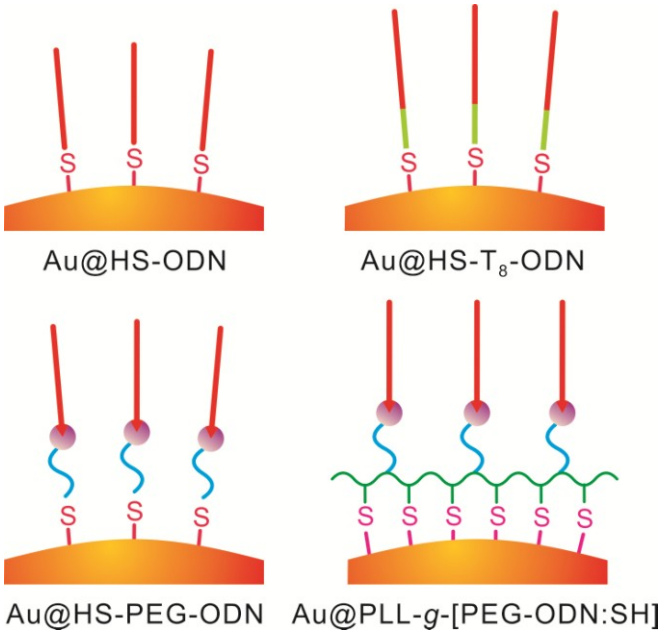

Figure 3-5. Schematic demonstrations of AuNPs stabilized by different types of thiol primers; **Au@HS-ODN.** monothiol primer, **Au@HS-T_8-ODN.** monothiol T_8 primers, **Au@HS-PEG-ODN**. monothiol PEGylated primers, and **Au@PLL-*g*-[PEG-ODN:SH].** oligothiol graft copolymers conjugated with primers

We performed SP-PCR on AuNPs (1 nM) surfaces that were attached to different types of thiol primers, including monothiol primers (Au@HS-ODN), monothiol T_8 primers (Au@HS-T_8-ODN) in which T_8 spacers had similar molecular weight (2,400 g mol^{-1}) to that of PEG layer (2,000 g mol^{-1}), monothiol PEGylated primers (Au@HS-PEG-ODN) and oligothiol graft copolymers conjugated with primers (Au@PLL-*g*-[PEG-ODN:SH]) (Figure 3-5). The PCR amplicons were analyzed by gel electrophoresis to characterize the target DNA amplification in the liquid phase and the solid phase (Figure 3-6A). Electrophoretic patterns of the red AuNP bands showed all monothiol stabilized AuNPs had more migration after SP-PCR. In addition, these AuNPs did not produce the

target DNA in the liquid phase from the EtBr staining image. In contrast, Au@PLL-*g*-[PEG-ODN:SH] not only showed a different electrophoretic pattern after PCR, that is, less migration AuNP bands, but also produced the target DNA in the EtBr staining image. These results indicate that only Au@PLL-*g*-[PEG-ODN:SH] yielded the positive SP-PCR in both liquid phase and solid phase because the less migration of AuNP bands is an evidence of the denser DNA layers on the AuNPs, which is similar to the previous PCR inhibition experiments. Compared to the previous PCR inhibition experiments, the incorporation of PEG layer in monothiol ODNs (Au@HS-PEG-ODN) resulted in the negative PCR result even in 1 nM of AuNPs, at which concentration partial target DNAs were amplified in the previous PCR inhibition experiments. We believed that the primer directed the DNA polymerase located proximal to the surface of AuNPs. As a result, the DNA polymerase interacted with the AuNPs surface, was deactivated, and led to complete PCR inhibition.

The AuNP-amplicons were further characterized by size change and fluorescent DNA intercalating dyes (SYBR green I) (Figure 3-6B). Intensity-averaged hydrodynamic diameter (d_z) of AuNP-amplicons was measured using DLS after removal of excess PCR reagents that might cause false results. The purified AuNP-amplicons showed consistent results from DLS analysis. All monothiol stabilized AuNPs did not show any distinct size change after SP-PCR, whereas Au@PLL-*g*-[PEG-ODN:SH] provided significant increase of d_z from 49 to 80~115 nm in a diameter, depending on PCR conditions (discussed later). Similarly, the amounts of immobilized dsDNA, quantified using SYBR green I that has green fluorescence in the presence of dsDNA after AuNPs etching,

significantly increased only in the case of Au@PLL-*g*-[PEG-ODN:SH]. These observations suggested that monothiol ligands were not suitable under PCR conditions.

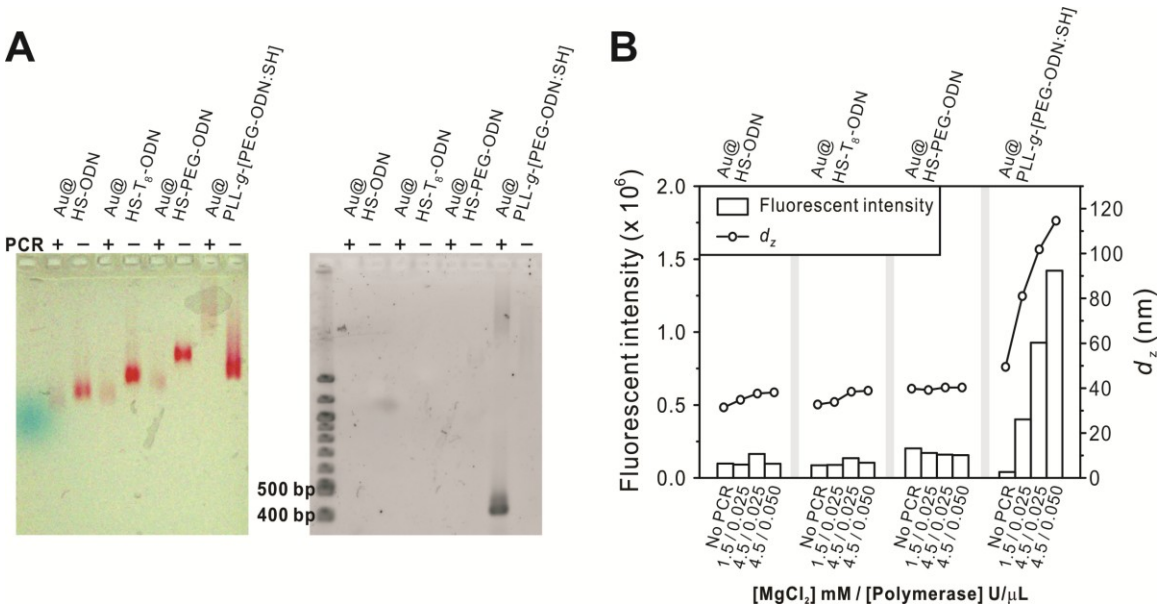

Figure 3-6. (**A**) Agarose gel electrophoresis images of bright field (**Left**) and EtBr staining (**Right**) of AuNP-amplicons after 30 thermal PCR cycles with 4.5 mM of $MgCl_2$ and 0.025 U/μL of DNA polymerase. Top legends include AuNP solid supports with different types of primers. (**B**) Fluorescence intensity of the intercalated SYBR green I with the amplified dsDNA on the AuNPs and intensity-averaged hydrodynamic size (d_z) of the AuNP-amplicons before and after SP-PCR varying the concentration of $MaCl_2$ (1.5 and 4.5 mM) and DNA polymerase (0.025 to 0.050 U/μL).

PCR efficiency relies on the concentrations of $MgCl_2$ and DNA polymerase.[1,63] Thus, the concentrations of $MgCl_2$ and DNA polymerase varied from 1.5 mM to 4.5 mM and 0.025 U/μL to 0.050 U/μL, respectively, to optimize PCR conditions (Figure 3-6B). Similar to the previous SP-PCR, all monothiol stabilized AuNPs resulted in the negative SP-PCR due to little change of the fluorescent intensity and the size. On the other hand,

Au@PLL-*g*-[PEG-ODN:SH] yieled increasing amounts of the immobilized dsDNA as the concentration of polymerase $MgCl_2$ and DNA polymerase increased. For example, the amount of the immobilized dsDNA increased by 2.3 times more when the concentration of $MgCl_2$ was tripled from 1.5 to 4.5 mM, based on the fluorescence intensity of intercalated SYBR green I dyes. Doubling the concentration of DNA polymerase (0.025 to 0.050 U/μL) produced 1.5 times higher fluorescent intensity with constant concentration of $MgCl_2$ (4.5 mM). DLS analysis also showed consistent results; the size of AuNP-amplicons was increased from 81 to 102 nm with three times more concentration of $MgCl_2$, and 102 to 115 nm with doubled amounts of DNA polymerase.

Furthermore, increasing the number of thermal cycles produced more immobilized target dsDNA. For instance, with 4.5 mM $MgCl_2$ and 0.050 U/μL DNA polymerase, 50 of thermal cycles produced 28.1 strands of the immobilized dsDNA per one AuNP and larger AuNPs (d_z 138 nm, Figure 3-7C), whereas 30 of thermal cycles generated 11.5 strands and 115 nm of d_z. Moreover, when the template length decreased from 400 bp to 100 bp (30 cycles, 4.5 mM $MgCl_2$, and 0.050 U/μL DNA polymerase), the number of the immobilized target dsDNA increased from 11.5 to 36.4 using SYBR green I quantification method, presumably, because the smaller size of the target DNA led to less crowding on the solid surface. By the way, the smaller size of 100 bp showed further migration in gel electrophoresis and smaller d_z (92.4 nm) by DLS (Figure 3-7A and C).

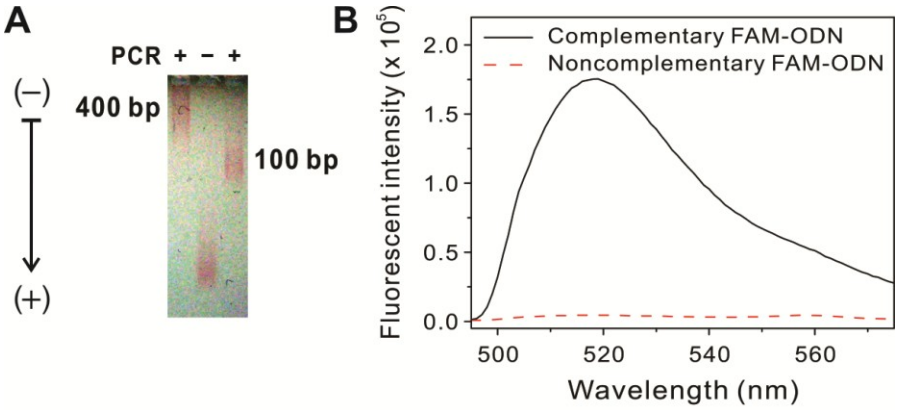

C

Target DNA size (bp)	Number of cycles	d_z (nm) dsDNA	d_z (nm) ssDNA
100	30	92.4	73.6
400	30	118.9	80.5
400	50	137.5	105.4

Figure 3-7. (**A**) Agarose gel electrophoretic patterns of the AuNP-amplicons after SP-PCR using different length of templates: 400 bp (left lane) and 100 bp (right lane). The middle lane included Au@PLL-*g*-[PEG-ODN:SH] without SP-PCR for comparison. (**B**) Fluorescent intensity of complementary (black solid line) and non-complementary (red dot line) FAM-ODNs that were incubated with the denaturated AuNP-amplicons, after AuNP etching with KCN. (**C**) Size change of AuNP-amplicons depending on target DNA size and number of thermal cycles, measured by DLS.

In order to know whether these results come from the positive SP-PCR rather than the false characterization, which might be caused by the hybridization between the forward immobilized primers and the reverse target ssDNA, we characterized the immobilized ssDNA after denaturation of the immobilized dsDNA. First, we used DLS to monitor the size change, because ssDNA has a flexible conformation that leads to

decrease of d_z, compared to a stiff dsDNA.[64] The size of AuNP-amplicons decreased from 118.9 to 80.5 nm for the 400 bp target DNA and 92.4 to 73.6 nm for the 100 bp target DNA (Figure 3-7C). These values were still larger than that of Au@PLL-*g*-[PEG-ODN:SH] (49.5 nm), suggesting primer extension on the AuNP surface rather than hybridization between the immobilized primers and the reverse ssDNA. Furthermore, in order to determine the presence of proper sequences, either complementary or non-complementary fluorescein modified ODN probes (FAM-ODN) were incubated with the immobilized ssDNA (Figure 3-4). The complementary ODN-FAM resulted in much higher fluorescent intensity due to sequence specific hybridization, whereas the non-complementary FAM-ODN showed negligible fluorescence, which indicated the proper target sequence amplification through SP-PCR (Figure 3-7B).

3.3.4 Digitalized DNA diagnostic assay through SP-PCR

Next, we developed a rapid and facile DNA diagnostic assay through the color change of AuNP-amplicons from red to colorless in a single PCR tube. First, we tried to use hybridization between the immobilized ssDNA of AuNP-amplicons, which were generated through the denaturation and purification steps of the immobilized dsDNA as discussed before, and the complementary ODN tethered to magnetic nanoparticles. However, the hybridization was slow and it required additional efforts for the denaturation and purification steps. Instead, we designed a novel system in which faster DNA detection could be achieved without any additional efforts other than simple mixing

of magnetic beads, followed by magnetic attraction (Figure 3-8A). We chosen a conjugation reaction between streptavidin-biotin because its reaction rate is faster (k_b = 10^6~10^7 $M^{-1}s^{-1}$)[65] than that of DNA-DNA hybridization (k_b = 10^4~10^5 $M^{-1}s^{-1}$).[66] For this purpose, the reverse primers are tagged with biotin groups that lead to biotin tagged AuNP-amplicons thoughout SP-PCR. After SP-PCR, the PCR mixture is mixed with streptavidin-coated magnetic beads to capture biotin tagged AuNP-amplicons using the magnetic beads. As a result, when a magnet is placed on the bottom of the PCR tube, the AuNP-amplicons-magentic beads are settled down, generating disappearance of red color in the solution. In contrast, if target DNA templates are not present in the SP-PCR mixture, there is no extension of the bound primers as well as no biotin tagging on the AuNPs. Thus, magnetic attraction does not induce any color change in the SP-PCR solution.

As the proof-of-concept, we performed SP-PCR containing 1 nM of AuNP-primers and 30 nM of biotin tagged reverse primers whose concentration was reduced compared to the previous SP-PCR conditions because higher concentrations require more amounts of streptavidin-coated magnetic beads. After SP-PCR with and without target DNA, the AuNP-amplicons were mixed with the magnetic beads for five minutes in which any purification of the AuNP-amplicons was not performed. When the target DNA was present the color of the solution disappeared after magnetic attraction, whereas when the target DNA was absent the color was retained as red (Figure 3-8B). These observations indicated that the color change came from the streptavidin-biotin conjugation as a consequence of positive SP-PCR. The magnetic beads can be included

before SP-PCR at the cap and stayed on the cap by the surface tension of the solution, or can be added after PCR. If the magnetic beads were included prior to SP-PCR, capturing biotinylated AuNP-amplicons showed less efficiency, presumably, because of the partial denaturation of streptavidin at high temperature.[67] Nonetheless, the color change was clear enough for the colorimetric detection by eye examination.

Furthermore, when normal reverse primers (5'-OH) were replaced for biotin tagged primers, the magnetic attraction did not induce color change, meaning that the color change solely relies on streptavidin-biotin conjugation rather than non-specific absorption of AuNP-amplicons to the magnetic beads. This control experiment also confirmed that the chelation of ssDNA via magnesium ion bridges did not occur during the conjugation. For further characterization, the supernatant was discarded and the pellets were washed, followed by addition of denaturation basic solution. The conjugated AuNP-amplicons with the magnetic beads were recovered due to the denaturation of double helix, recovering red color (Figure 3-8B). It also proved that SP-PCR led to enzymatic synthesis of the target dsDNA on AuNP surface.

Next, we enhanced the color of the solution using waveguided optical analysis. The small volume of the solution (20 μL) was placed in capillary tubes (0.8 mm diameter) whose glass surfaces were etched to scatter the light and visualize color of the scattered light. When light goes through the capillary tube from top to bottom, the increase of light path length provides more extinction of light, resulting in enhanced red color compared to light illumination at right angle to the capillary tubes (Figure 3-8C). Moreover, the color was readily translated into digitalized signals (0 and 1), using a green

optical filter that removed red color. As a result, the positive SP-PCR generated green color for 1 signal, whereas the negative SP-PCR did not show any color for 0 signal (Figure 3-8C). The digitalized AuNP-PCR could be extended to a massive and rapid DNA diagnostic assay if automated systems were developed by reading 1 and 0 signals for positive and negative of target DNA presence, respectively.

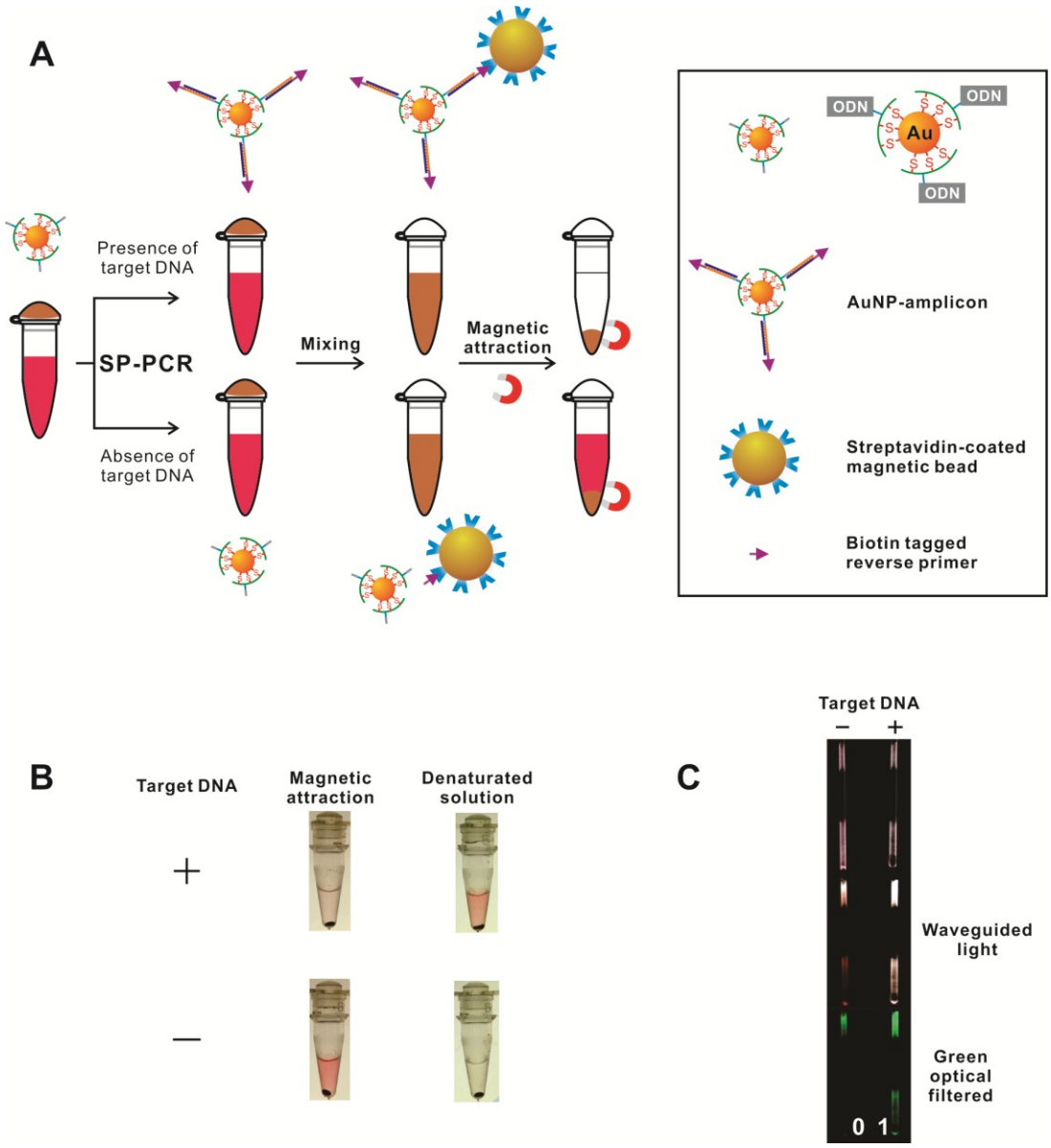

Figure 3-8. (**A**) Schematic diagram of colorimetric detection of SP-PCR on AuNPs. When target DNA exists, AuNP-amplicons are tagged with biotin thoughout SP-PCR. The biotin tagged AuNP-amplicons are then captured by streptavidin-coated magnetic beads. When magnetic field applied, the captured AuNPs are settled down, providing color change from red to colorless. On the other hand, if the target sequence is absent, AuNPs do not have biotin tags, resulting in the retention of red color. (**B**) Experimental results of (**A**). The presence of target DNA in SP-PCR mixture induced color change

from red to colorless, which was distinguishable by eye examination. On the other hand, the red color was retained when target DNA was not present in SP-PCR conditions. (**C**) Photographs of AuNP-amplicons in capillary tubes after magnetic attraction in (**B**). (**Top**) Light was illuminated at right angle to the tubes. (**Middle**) Waveguided light illumination was used through capillary tube from top to bottom. (**Bottom**) Digitalized images of waveguided light color using green optical filter. Negative SP-PCR showed dark for 0 signal, whereas positive SP-PCR had green color for 1 signal.

3.4 Summary

We described solid phase PCR using immobilized primers on AuNPs, and investigated primer extension and amplification using different types of ligands. The positive SP-PCR was achieved and characterized when thermally stabilized AuNPs by oligothiol graft copolymers. In addition, the stabilized AuNPs were used to develop a facile and rapid DNA diagnostic assay based on color change without any additional analysis other than eye examination. It should be noted that the virtue of this assay is that it requires a few minutes for DNA diagnosis without any tedious or expensive instrumental analysis and a skilled technician. Moreover, we developed a cheap process for digitalized data extraction from the AuNP SP-PCR, which might be applied to an automated massive DNA diagnostic platform. The stable AuNPs for PCR could be expanded to other PCR based technologies, including DNA mapping, single-nucleotide polymorphism analysis, and generic disease diagnostics. Furthermore, the nano-sized AuNP amplicons could be one of the promising SP-PCR solid substrates for the next generation DNA sequencing platforms using hybridization sequencing method. It should be noted that AuNP amplicons may offer an alternative approach to reduce the DNA translocation speed for currently developed nanopore based a DNA sequencing technology.

Chapter 4. Bioorthogonal, Chemically Cleavable α-Azido Ether.

4.1 Degradable material and cleavable linker

Degradable material is a material that disintegrates under certain conditions, including environmental conditions, light illumination, and specific chemical triggers, with a reasonable and demonstrable timescale.[1] Scientific and technological demand for degradable materials has increased to improve human life by preserving our environment[2] and health.[3-4] As a consequence, degradable materials have played an important role as eco-friend biodegradable plastics that can minimize damage to our environment,[2] degradable biological media for analytical and fundamental studies to understand biological functions,[5-6] and biocompatible and healing materials for biomedical applications.[3,7] Degradable materials can be made from inorganic and organic materials based on natural origin or man-made synthetic sources. There are many degradable inorganic materials, such as, porous calcium phosphates,[8] silica,[9] metal-organic frameworks,[10] and organic materials based on natural sources like gelatin.[11] This thesis mainly focuses on degradable organic materials from synthetic polymers, especially, in biological applications.

The degradation mechanism of synthetic polymeric materials solely depends on the chemical characteristics of the cleavable linker that makes up the material. In other

words, the cleavable linker determines what conditions act as cues to disintegrate the material.[12] For example, because an ester functional group can be hydrolyzed to acid and alcohol, degradable materials composed of esters decompose in the presence of water.[7,13] Likewise, a hydrogel having a disulfide crosslinker can be dissolved by the addition of mild reducing reagents like thiol species to break the disulfide crosslinker.[14]

The cues to trigger cleavage can be categorized based on where they exist; inside an organism or outside the body; endogenous sources (water,[7,13] enzyme,[15] and biologically abundant chemicals[12]) and exogenous sources (light[6,16] and biologically rare chemicals[12,17-21]). In addition, the interaction between a cleavable linker and its triggers varies in terms of reaction conditions and cleavage kinetics. Both the origin of triggers and the cleavage interactions determine applications of cleavable linkers and degradable materials. For instance, water is the most abundant source in our bodies and ester hydrolysis is very slow in the absence of a catalyst.[13] Consequently, ester linkers have been incorporated into biodegradable fixation devices, including resorbable pins, screws, and plates, which need slow degradation until the defect is healed.[7] Light labile linkers have been utilized to make 3D-patterns in a hydrogel[22] or manipulate physical strength of a hydrogel[6,23] because light can penetrate a transparent media to trigger the cleavage of the linker.

Many degradable materials have been developed to degrade based on the endogenous sources in biological applications. Although these materials have advantages like natural degradation without injecting triggers, they often have disadvantages in terms of degradation control after implementation, especially, in *in vivo* applications. On the

other hand, degradable materials that degrade on exposure to exogenous sources can have benefits in terms of degradation control after implementation by manipulating the external triggers. Thus, it is possible to make a specific pattern by post-degradation control using exogenous light source within demonstrable timescale.[23] However, degrading materials by exogenous chemical triggers have not been well-developed. We believe that the materials which degrade by exogenous chemical triggers would be suitable for various applications, such as, a degradable polymeric network for cell-culture media and a degradable polymer for biomedical devices and drug delivery.

The rest of this thesis deals with the investigation of a linker that can be cleaved by exogenous chemicals, a degradable polymeric material comprised of the linker, and its application to biological technology. The chemistry of the degradable material is based on the α-azido ether functional group and its cleavage triggers, such as, phosphine and dithiol. It will be shown how stable the cleavable linker is without the cleavage triggers and how rapid the cleavage reaction occurs in the presence of the triggers. Next, the α-azido ether is incorporated into a crosslinked polymeric network of a polyacrylamide hydrogel that is one of the most widely used supports in gel electrophoresis.[24] The degradation of hydrogel with the cleavage triggers will be explored to show how an exogenous chemically cleavable linker can be associated with biological technology. This chapter gives a brief background about cleavable linkers and their applications, followed by polyacrylamide gel electrophoresis.

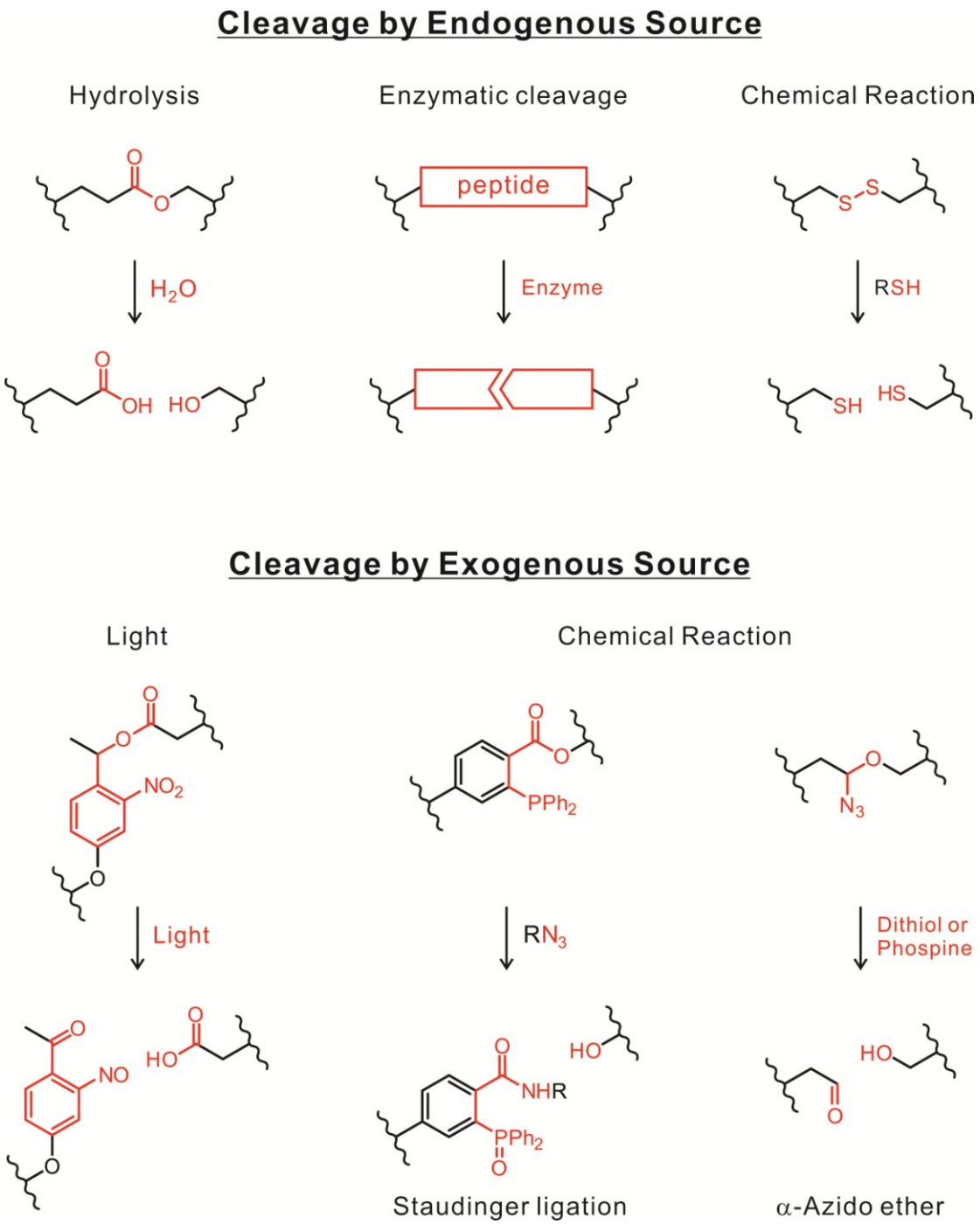

Figure 4-1. Cleavable linkers in biological applications. (**Top**) Linkers that can be cleaved by endogenous sources, such as, water, enzyme and biologically abundant chemicals. (**Bottom**) Linkers that can be cleaved by exogenous sources, such as, light and biologically rare chemicals.

4.2 Cleavable linkers and its applications

4.2.1 Cleavage by endogenous source

Hydrolytic cleavage. One of the widely used cleavable linkers by endogenous triggers involves a hydrolytic mechanism; water attacks the cleavable linker to break the bond with or without a catalyst.

Ester is a representative linker that is cleaved through hydrolysis. The cleavage reaction rate is too slow without a catalyst like a base. In *in vitro* applications, it has been utilized in solid-phase biological molecule synthesis in peptides and nucleic acids. Merrifield first chemically synthesized a peptide chain via stepwise additions of an amino acid monomer to a chain on a crosslinked polystyrene resin and removed the synthesized peptide from the resin using base catalyzed hydrolysis of an ester linker, which brought a Nobel Prize award to him.[25] Later, nucleic acids were chemically synthesized via a similar concept using ester cleavage from a controlled pore glass support.[26] This linker has become a standard cleavable linker in the solid-phase synthesis until now. In *in vivo* applications, the ester has played an essential role with its slow reaction rate[13] in biodegradable polymers, such as, poly(lactic acid) (PLA), poly-glycolic acid (PGA), poly-caprolactone (PCL), polyhydroxylalkanoate (PHA), and their copolymers.[2-3,7] For example, PLA has been studied as a suitable bioadsorbable material for a fixation device being a replacement for a metallic device because of its long retention of strength, biocompatibility, and slow biodegradability, which promise no secondary surgery after fixation.[7]

In contrast to slow hydrolysis of ester in the absence of base catalyst, acid catalyzed rapid hydrolysis has been utilized in various linkers, such as, *p*-alkoxybenzyl alcohol,[27] silyl ether,[28] orthoester,[29] acetal,[30-31] ketal,[32] hydrazone,[33] and so on.[12,34] Similar to the ester, the acid catalyzed hydrolysis was applied to solid-phase synthesis for *in vitro* biological molecule synthesis through the cleavage of *p*-alkoxybenzyl alcohol developed by Wang.[27] On the other hand, the acid-labile linkers have been actively studied for a pH responsive drug delivery system. Because there are pH gradients in *in vivo* system (*i.e.* tumors: pH 5.7 to 7.8), pH sensitive biomaterials containing acidic labile cleavable linkers have been investigated for drug delivery to tumors.[31,34] For example, Griset *et al.* showed that the anticancer drug, paclitaxel, was released effectively and inhibited the growth of LLC tumors in C57B1/6 mice by acidic catalyzed cleavage of acetal groups, which induced hydrophobic to hydrophilic transformation, swelled crosslinked nanoparticles, and released the drugs.[31]

Enzymes mediated cleavage. Because enzymatic cleavage is highly selective and efficient to a specific peptide sequence and is performed under mild conditions, enzymes have been integrated into cleavable linkers in *in vitro* and *in vivo* applications.[4,12,15,35-37] For *in vitro* applications, a specific peptide sequence like ENLYFQG was used as a cleavable linker, which could be cleaved by a tobacco etch virus protease (TEV). Speers *et al.* developed a probe containing the ENLYFQG sequence and cleaved the sequence by TEV to analyze samples by mass spec and identify the sites where the probe recognized the protein.[35] For *in vivo* applications, enzymatic cleavable linkers were incorporated into a degradable hydrogel in which growth factors were released by enzymatic cleavage to

regenerate tissues in rats.[37] Moreover, dendrimeric nanoparticles containing PLGLAG cleavable linkers were used to image fluorescence Cy5 and Gd-DOTA MRI probes for tumors in animals, in which matrix metalloproteinase (MMP) cleaved the sequence during the tumor invasion and metastasis process.[38]

Chemically triggered cleavage. Chemicals that are biologically abundant can be a source to trigger cleavage. One of the most studied endogenous chemical triggers is a thiol because it is biocompatible and often associated with disease,[39] which has been used to design a targeted imaging agent[40] and drug delivery system.[41] Although there are a few linkers (*i.e.* nitrobenzenesulfonamide[42] and thiolphenylester[43]) that can be broken by the thiol trigger, a disulfide bridge has been widely explored; because it is naturally occurring to reserve a protein structure indicating biocompatibility; its synthesis is simple; and its cleavage is rapid in mild conditions.[12,44] As a result, the disulfide has been utilized as a linker for catch-and-release regents to analyze proteins in *in vitro* application.[45] Moreover, small interfering RNA (siRNA) was conjugated with cholesterol via a disulfide linker to deliver the siRNA to cells in the brain and show efficient gene knockdown using animal subjects.[46] Nonetheless, the disulfide linker is often restricted due to its instability. Since the cleavage occurs through rapid thiol exchange reaction,[44] biologically abundant thiols (*i.e.* cysteine amino acid) can lead to non-specific cleavage.[12]

4.2.2 Cleavage by exogenous source

Cleavage can be triggered by exogenous sources, such as, light illumination and chemicals. These linkers have benefits compared to the endogenous triggered linkers because its cleavage can be controllable by changing exposure time and concentration of triggers.

Light driven cleavage. Light driven cleavage has been extensively used in many applications, such as, organic synthesis, photolithography, coating industry, and photo-switching.[16,47] Recently, these photolabile linkers have been incorporated into biological applications because of their excellent temporal and spatial control. For example, Luo *et al.* created biochemical channels in a photodegradable hydrogel by UV-light illumination with spatial control to cleave the photolabile linkers and generate reactive sulphydryl groups in which biological molecules were conjugated to the channels.[22] Later, Anseth group incorporated a nitobenzyl ether crosslinker, which was cleaved under 365 nm light, into a hydrogel.[6,23] The hydrogel was used for an *in vitro* cell encapsulation platform and its properties were tuned by photo-cleavage. Vivero-Escoto *et al.* used photolabile groups to change surface charges from positive to negative to induce the release of anticancer drugs inside of human cells.[48] Nonetheless, use of photo-cleavable linker is often limited because of potential damage to biological components[49] and the penetration depth of light.[50-51] We believe that these facts presumably are the reason why there are only a few reports about the use of photolabile linkers inside a living organism: transparent zebrafish embryos in which photolabile protecting groups were released by light illumination to control concentration of biological components,[52-53] and bioluminescence imaging in

living mice through photo-cleavage by nanoparticle guided photon upconversion from near-IR to UV to overcome the issue of penetration depth.[51]

Chemically triggered cleavage. There are a few linkers that can be cleaved by exogenous chemical triggers in biological applications, including 1,2-diol and sodium periodate ($NaIO_4$) trigger,[17] azo and sodium dithionite ($Na_2S_2O_4$) trigger,[18,54] and azide and reducing reagents (phosphines or dithiols) in Staudinger ligation[19] and α-azido ether.[20-21,55-58] Because $NaIO_4$ can damage biological molecules like RNA[59] and $Na_2S_2O_4$ is decomposed in physiological conditions,[60] 1,2-diol and azo linkers are not used in living organism. On the other hand, the azide reduction can be used for *in vitro* and *in vivo* applications because its chemical reaction is biocompatible and bioorthogonal.

The azide reduction chemistry has initiated "bioorthogonal chemistry", which means "a chemical reaction that neither interacts with nor interferes with a biological system",[61-62] because azide is a non-naturally occurring functional group and the concentration of its triggers are too low for the azide reduction.[63] As a result, the azide reduction has played an important role in *in vitro* and *in vivo* bioconjugation methods through Staudinger ligation. Although the main purpose of Staudinger ligation is to connect two entities through an amide bond, there is one example, to the best of my knowledge, in which Bertozzi group expanded the Staudinger ligation to cleave a quencher moiety and turn on fluorophore for live cell imaging.[19] However, nowadays, the Staudinger ligation has been replaced with azide-alkyne click chemistry due to its slow reaction rate.[61,64]

Chemical triggered cleavage of α-azido ether has been utilized in DNA sequencing technology[20] and DNA detection platform,[21,55-58] and played an essential role in the next generation sequencing technology in the market.[65] For example, in the DNA sequencing technology, a fluorophore/α-azido ether/DNA monomer was incorporated into a polymerase enzymatic reaction. The fluorescence color of the hybridized DNA monomer into DNA template was detected to determine DNA sequence. α-Azido ether was then chemically cleaved by reaction with TCEP at 60 ^{o}C to generate reactive –OH group for the next reacton. This cycle was repeated until the DNA sequence reading was completed.[20] The same α-azido ether chemistry was used for complementary DNA detection by the Kool group.[21] In this case, when a quencher bearing α-azido ether and phosphine functionalized DNA were hybridized with a template DNA, α-azido ether was located proximal to the phosphine group and cleaved to turn-on fluorescence, which resulted in complementary DNA detection.

In contrast to the Staudinger ligation, the cleavage kinetics of the α-azido ether chemistry has not been studied yet. Although its cleavage mechanism is similar to that of the Staudinger ligation,[64] the different chemical structure of α-azido ether, which bears electronegative O adjacent to azido group, could lead to faster reaction rate. Moreover, because its chemistry is bioorthogonal the α-azido ether chemistry can hold a promise for a novel means of degrading materials without changing biological systems and with excellent control by addition of chemical triggers. This thesis will show the chemistry of α-azido ether and its cleavage to find out optimized cleavage conditions. Also, its

integration into a degradable material will be shown using a polyacrylamide hydrogel as the first step toward various *in vitro* and *in vivo* applications.

4.3 Polyacrylamide gel electrophoresis (PAGE)

4.3.1 Basic principles

After the discovery of electrophoresis in biological molecules by Tiselius in 1937,[66] electrophoresis has played essential roles as one of the most ubiquitous, versatile, and powerful tools in biological technology. Historically, the incorporation of starch gel matrix into the electrophoresis initiated a gel electrophoresis by Smithies in 1955.[67] In 1959, Raymond and Weintraub used a commercial gel matrix called Cyanogum 41 that was crosslinked polyacrylamide (PAAm) gel and showed electrophoretic patterns of serum albumin and hemoglobin.[68] After this seminal report, PAAm gel has become one of the ideal matrixes for the electrophoresis and developed many gel electrophoresis methods, such as, DNA/RNA PAGE,[69] IEF PAGE,[70] SDS-PAGE,[71] and 2D-PAGE.[72]

Polyacrylamide (PAAm) gel is synthesized by a free radical polymerization of acrylamide monomers and crosslinker called Bis (*N,N'*-methylene bisacrylamide) using APS/TEMED catalyst system in aqueous solution. PAAm gel has served an ideal matrix in gel electrophoresis because of its inertness to biological samples and stains, stability to pH and a wide range of ionic strengths, charge-free supports, transparency, and strength to be thin gels.[68,73-74] More importantly, PAAm is a synthetic matrix allowing

reproducibility, various pore sizes by changing concentration of monomers and crosslinker, and additional functionality by modification of crosslinkers[5] or copolymerization with chemically modified acrylamide monomers.[75-76]

Biological samples of interests migrate through pores in PAAm gel under applied electric potential based on their charge, size, and shape.[73-74] Varying the concentration of monomers and crosslinkers changes the pore size that determines the degree of the migration retardation. Velocity of the samples is then simply determined by the balance between the electrophoretic migrating force and the retardation caused by molecular sieving effect. As a result, biological molecules are separated based on their own electrophoretic migration velocity. When biological molecules have the same charge-to-mass ratio (*i.e.* nucleic acid, SDS-denatured proteins), the migration distance solely relies on the size (or mass), leaving an arranged band of biological molecules with respect to the size. On the other hand, intact proteins are often separated by electrophoretic migration and show their own band depending on their intrinsic charge, size, and shape. The band is then used to analyze the biological molecules[5,77]; molecular weight, composition, biological function, and so on. After gel electrophoresis is performed, the recovery of biological molecules is frequently employed to obtain more information about the biological system[5]; for example, an intact protein for functional assay,[78] an extremely pure protein sample for protein crystallization,[79] a nucleic acid-protein complex for fundamental study of a biological assembly,[80] and a pure RNA template for protein synthesis.[81]

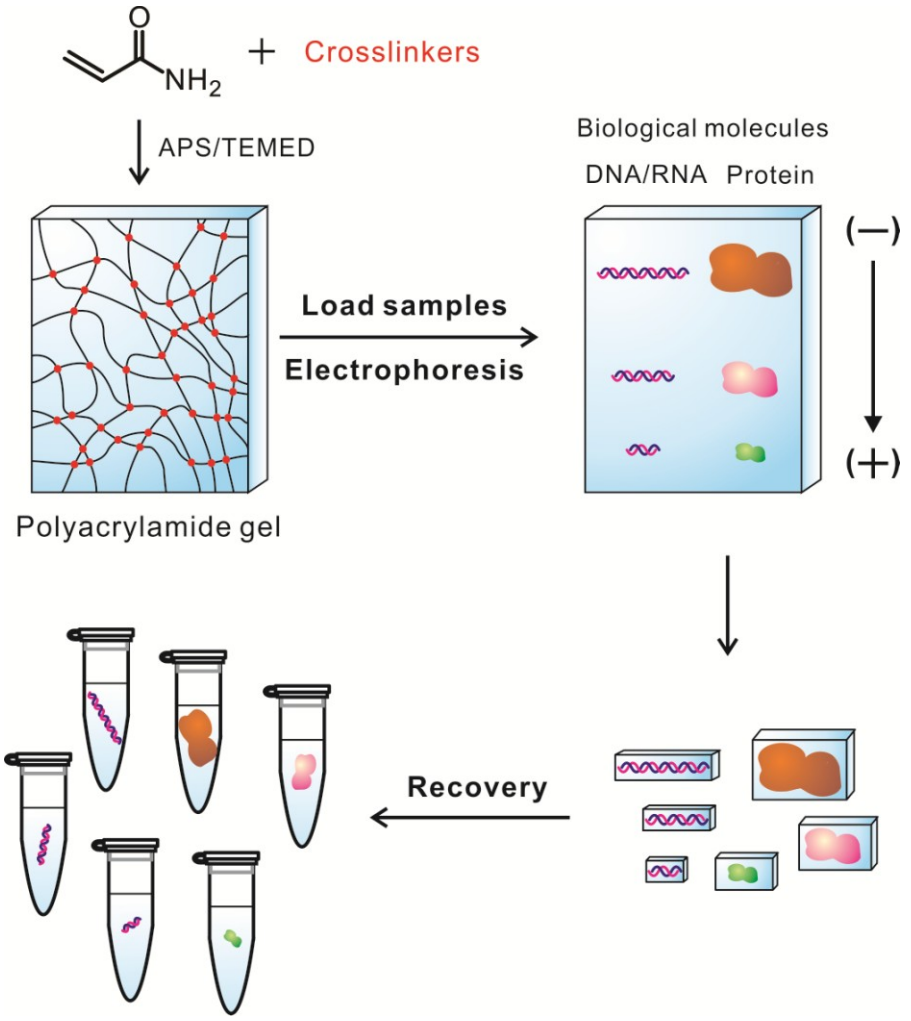

Figure 4-2. Schematic illustration of polyacrylamide (PAAm) gel electrophoresis (PAGE). The PAAm gel is synthesized by a radical polymerization reaction of acrylamides and crosslinkers using APS/TEMED system. The biological molecules are loaded on the top of the gel and electrophoretically migrated by electric potential. The biological molecules are then separated depending on charge, size, and shape. Separated biological molecules in the gel matrix are frequently recovered for further analysis.

4.3.2 Recovery of biological molecules

The recovery of biological interests out of the crosslinked PAAm gel usually includes a passive extraction and an electroelution method.[5] The passive extraction is based on simple diffusion of the interests and can be thus improved by crushing gel or mechanical homogenization.[82] The electroelution method applies electric field to elute the interests electrophoretically using an additional device and a dialysis tubing as a physical barrier to preserve the interests in a reservoir.[83] Each method has advantages and disadvantages. Because the passive extraction only relies on the diffusion of the gigantic molecules through polymeric networks, yield is frequently low and it requires time-consuming process, which often leads to loss of biological activity.[74,84-85] The electroelution may afford better yield; however, it requires a tedious routine work using additional instrumentation.[5]

On the other hand, there is an alternative method in which the gel matrix is solubilized through gel degradation, leading to free biological molecules in the solution. The first attempt based on this idea was to cleave the amide bonds using 30% hydrogen peroxide at 50 ^{o}C.[86] As a consequence, Young could dissolve the gel matrix and measured methionine-^{35}S radioactivity of entrapped proteins. However, this method also dissolves the biological molecules resulting in incurable damage to any kinds of proteins as well as nucleic acids.[87]

Instead, chemical modification can be utilized to solubilize the gel matrix.[5,88-89] Chemical modification of a crosslinker promises gel degradation by proper chemical treatment, which makes biological molecules free in the solution. If the Bis crosslinker is

replaced with a cleavable linker, the gel can be degraded and solubilized under its degradation condition (Figure 4-3). Based on this idea, there were attempts to incorporate a cleavable functional groups into the crosslinker, including 1,2-diol,[89-93] ester,[94-97] acetal,[84-85] and disulfide.[98-101]

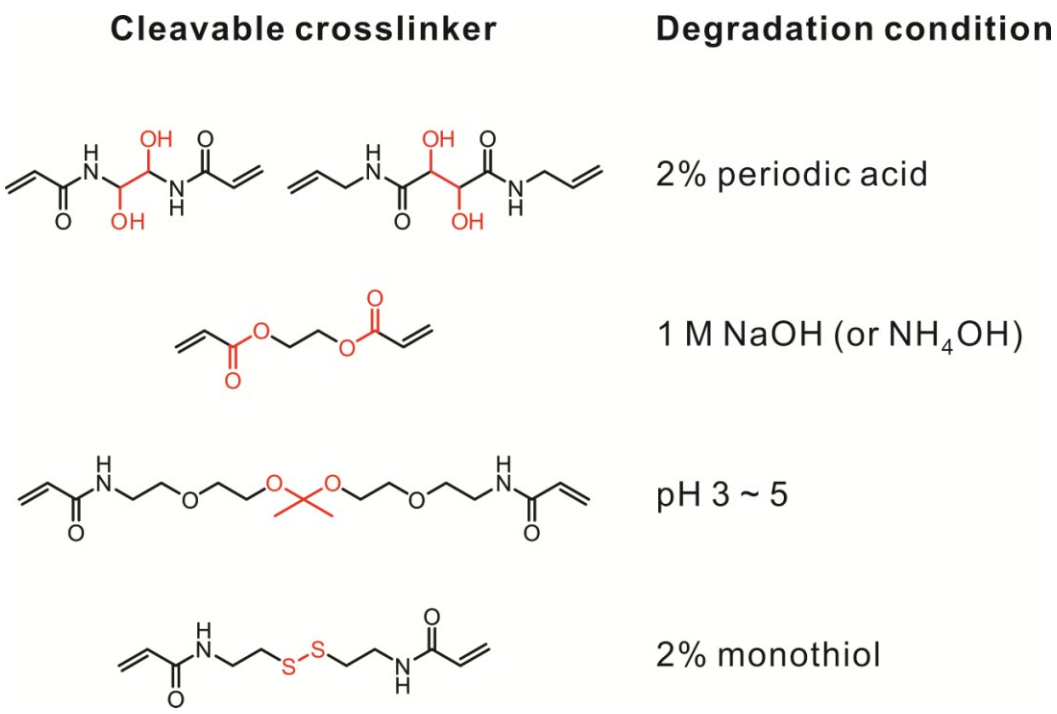

Figure 4-3. Molecular structure of a cleavable crosslinker for a degradable polyacrylamide gel (**Right**) and its degradation condition (**Left**). The cleavage reaction is carried out in the red colored functional groups.

The crosslinker functionalized 1,2-diol had been used to separate various proteins by the degradable PAGE and recovered by oxidative cleavage of the 1,2-diol using 2% periodic acid. However, the cleavage requires harsh conditions that are not compatible with most biological molecules resulting in irreversible loss of bioactivity (i.e. oxidation

of α-hydroxy, -oxo, -amino, and thiol).[102-103] Hydrolysable ester was replaced with the Bis to separate RNA[96] or proteins.[94-95,97] The gel bands containing the biological molecules were then solubilized by addition of strong basic solution like 1 M NaOH or NH_4OH. However, the degradation conditions were so harsh that only quantification of biological molecules in the solubilized gel was achieved without preserving their molecular structures.

Later, Hansen first introduced a disulfide crosslinker (*N,N'*-bisacrylylcystamine, BAC) as a substitute for the Bis. As a result, mild conditions for the gel degradation (1-2% β-mercaptoethanol) can be used to solubilize the gel in physiological environments. Consequently, preparative amounts of intact RNA,[98] DNA fragments,[99] histones,[100] and pyridine nucleotide-linked dehydrogenases[101] were recovered after the gel degradation. However, no more reports have been followed, presumably, because of a tedious, laborious, and non-reproducible preparation.[104] First, BAC is not soluble at room temperature in concentration above 1% because of its hydrophobicity leading to inconsistent gel concentration.[104] Second, it is noted that the BAC needs careful pH control because of its instability under alkaline conditions.[105] Third, the BAC shows a lower reactivity in radical copolymerization reaction being inhomogeneous matrix that might cause insufficient physical and molecular sieving properties.[88] Fourth, the BAC is not applicable to urea denaturating gel, which is one of widely used supports for RNA PAGE, because of the deleterious effect of urea.[104] Next, more importantly, a disulfide may be cleaved by radical species to provide thiyl radical ($S\cdot$)[106] that can react with vinyl groups to form a non-cleavable covalent bond. As a result, Hansen reported that insoluble

BAC gel was prepared due to the undesired crosslinking from reaction between S· and acrylamide monomer.[104] In order to overcome the crosslinking toward a degradable BAC gel, it should increase temperature (40 ^{o}C) and TEMED concentration.[100,104]

Recently, Kwon developed another candidate as a cleavable linker for degradable PAGE. Acidic labile ketal is used to replace the Bis to recover mouse IgG1 protein[85] and nucleic acids[84] without loss of biological activity. It seems that its preparation procedure follows a standard procedure for the Bis gel indicating no detrimental effect on the gelation, which is critical problem in the BAC. However, the applications are limited to acidic stable biological molecules because gel degradation still requires acidic condition (pH 3 - 5), implying that the recovery of biological molecules using degradation gel technique needs improvement that can be achieved by incorporating physiological and biocompatible cleavable linker.

In order to overcome the limitations in the current degradable PAGE system, we incorporated α-azido ether functionality into the degradable PAGE. Because it would be expected that the gel synthesis does not require any specific handling, which is necessary for BAC, as well as its cleavage condition can be conducted in physiological and biocompatible conditions, biological molecules can be electrophoretically separated in the gel matrix and recovered under gel degradation conditions without losing their activity.

4.4 Overview

The rest of this thesis describes the chemistry of α-azido ether linker that could be one of the best candidates as a bioorthogonal, chemically cleavable linker as well as its practical example in a biological technology.

Chapter 5 explores our fundamental study of α-azido ether chemistry as a cleavable linker. It demonstrates how stable α-azido ether functionalized molecules are against hydrolytic degradation depending on the chemical structure. In addition, it provides how fast its cleavage is completed by chemical triggers varying pH of the aqueous solutions, which is then used to propose a cleavage mechanism.

Chapter 6 shows a proof-of-concept study in which α-azido ether plays as an essential linker to develop a degradable material. The α-azido ether linker is incorporated in a degradable hydrogel support in PAGE technology. As a result, biological molecules are electrophoretically separated, recovered by chemical triggers, and isolated without loss of their structure and properties.

Chapter 5. Bioorthogonal, Chemically Cleavable α-Azido Ether; Stability and Cleavage Kinetics Study

5.1 Introduction

A cleavable linker is a covalent chemical bond through which two entities are connected and separated under a specific condition required to trigger the cleavage of the chemical bond.[1] Cleavable linkers have become more indispensible tools in a broad range of applications; a degradable material towards an environment friendly biodegradable plastic[2]; a solubilizable polymeric network to experimentally elucidate the efficiency of crosslinking[3]; solid-phase synthesis in which desired molecules are synthesized via successive reactions and liberated from a solid support[4-6]; proteomics and DNA sequencing to identify specific biological targets incorporated with the cleavable linkers[1,7]; and a microchip in which a cleavable linker produces a specific pattern associated with photolithography.[8-9]

Chemical characteristics of cleavable linkers determine their applications *vice versa*. For example, hydrolytic cleavage of polyester linkers has been developed for making biodegradable plastics that degrade in soil.[10] In photolithography, a light-driven cleavage has been developed as an acid generator for positive and negative photoresists.[11]

The reduction-driven cleavage of a coordination bond between Pt(IV) and ligands inside cells has opened novel drug delivery systems, in which a cisplatin drug is released at a specific target.[12-13]

Recent progress in molecular and medical biology has relied on the chemistry of cleavable linkers. However, not all cleavable linkers have been utilized in molecular and medical biology because a suitable cleavable linker often requires biocompatibility, high efficiency even in a low concentration, facile purification, and a mild cleavage condition.[1] In order to perform a specific function using a cleavable linker, the linker should be compatible with the biological system. As the abundance of biological components is often low, the cleavage reaction should have a high yield to achieve a proper function.[14] Facile and rapid isolation of excess reagents and by-products promise successful results from a complicated biological system. In certain cases, experimental harsh conditions for cleavage has generated nonselective release of biological components and damaged them, causing problems during analysis.[15]

The cleavage of biologically applicable linkers can be initiated by endogenous or exogenous triggers. The ester,[16] peptide,[17-18] acetal,[19] and disulfide linkers,[20] have been developed for *in vitro* and *in vivo* applications in which the cleavage are triggered using endogenous sources, including water,[21] enzyme,[22] pH,[23] and biological entities.[24] For example, *in vitro* applications involve cleavable linkers, such as, a safety-catch-release linker in a solid phase synthesis[4-5] and protein tagging,[25] a crosslinker in a polymeric network for 3D cell culture,[26] and so on. A degradable material[27-28] or targeted cleavage system[29-30] has been adopted those linkers for *in vivo* applications.

On the other hand, cleavable linkers whose cleavage is triggered by exogenous source, including light[31] and a chemical trigger,[15,32] have also been investigated. Those linkers have often advantages over the former linkers in terms of cleavage control. Once the former linkers are incorporated in a cleavable system, frequently, there is little room to control their cleavage, especially in *in vivo* applications. However, post-cleavage control can be achieved using the latter linkers by controlling concentration and duration of exogenous source. For example, a specific pattern of hydrogel was constructed by the spatiotemporal cleavage control using exogenous light.[33]

Among existing linkers cleaved by the exogenous sources, chemically triggered cleavable linkers have more advantages. Although light triggered cleavable linkers have a benefit in terms of spatial control,[34] light may damage biological components[35] and its applications are often limited due to the penetration depth of light.[36] In contrast, chemically cleavable linkers can be developed without damaging biological components and losing cleavage control because of physical obstacles. Moreover, because the chemically cleavable linker should be inert to biological system until triggers approach it, its reaction can be considered as bioorthogonal chemistry, "a chemical reaction that neither interacts with nor interferes with a biological system", which has played an essential role in recent chemical biology.[14,37]

There are only a few systems reported for the bioorthogonal, chemically cleavable linkers; azo-linker,[15,32] Staudinger ligation,[38] and α-azido ether.[39-40] Among them, α-azido ether has gained our attention as a cleavable linker. The azo-linker can be cleaved by a sodium dithionite; however, the chemical trigger is unstable under physiological

conditions being limited to *in vitro* applications so far.[41] Although the Staudinger ligation was successfully utilized to cleave a quencher to provide fluorescent signal for imaging,[38] the relative slow kinetics for the Staudinger ligation restricted its expansion toward a broad range of applications.[42] In contrast, α-azido ether has already been developed as an indispensible chemistry for the next generation DNA sequencing platform in the market,[43] implying it as one of the most promising candidates.

Although the α-azido ether is likely to be an ideal linker for a bioorthogonal, chemically cleavable linker, the chemistry behind its design and function is not fully understood. As a consequence, a certain drawback related to the aqueous stability of α-azido ether has been reported but not addressed.[44] In addition, if we refer that its cleavage affords similar mechanistic steps to those of the Staudinger ligation (azido reduction), its reaction kinetics still needs investigation.[42] As a result, herein, we have explored the stability in aqueous solution and its cleavage kinetics with chemical triggers. The stability was studied using model α-azido ether chemicals to investigate how a chemical structure affects on the stability. The kinetics of reductive cleavage with chemical triggers, such as, a dithiol and a phosphine, were also studied under different experimental conditions. The kinetics was then used to study the cleavage mechanism with which the cleavage system could be improved to be a suitable system for a broad range of applications. Furthermore, the products from the cleavage were examined to understand its biocompatibility through the entire cleavage reaction.

5.2 Experimental Methods

5.2.1 General

TCEP was purchased from Thermo Fisher Scientific, Inc. (Rockford, IL) and deuterated NMR solvents were purchased from Cambridge Isotope Laboratories, Inc. (Andover, MA). DHLA was synthesized from α-lipoic acid.[45] The primary and secondary azide analogs were synthesized using the published procedure[46-47] and their identity and purity were determined using ^{1}H NMR. All other reagents were purchased from Aldrich (St. Louis, MO) unless otherwise noted. Ultrapure water was generated from a Milli-Q water purification system (Millipore Inc.; Billerica, MA, R > 10 MΩ•cm). Visible absorption spectra were obtained on a Hewlett-Packard 8453 UV-Vis spectrophotometer (Palo Alto, CA). ^{1}H NMR spectra were recorded on a Varian Unity (300 MHz or 500 MHz) using solvent peaks for general characterization. High resolution mass spectrometry was performed using an Bruker BioTOF II instrument with PEG (poly(ethylene glycol) as internal standard. Samples were prepared using methanol as the carrier solvent and filtered through a PTFE (0.45 μm) syringe filter before injection. Calibration and analysis was performed using mMass open source mass spectrometry tool.[48]

5.2.2 Synthesis

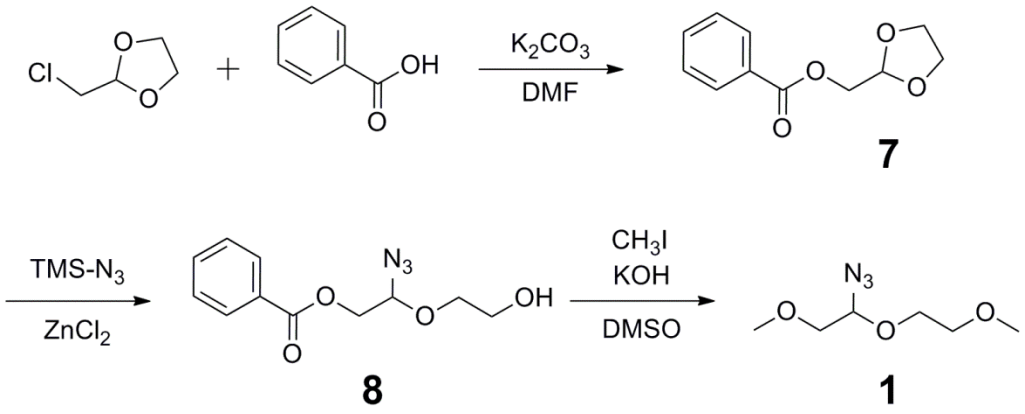

Figure 5-1. Synthetic scheme of α-azido ether **1**, azido-2-methoxy-1-(2-methoxyethoxy)ethane.

(1,3-Dioxolan-2-yl)methyl benzoate synthesis (7). The compound was prepared according to the method similar to that described by Parrish *et al.* with the following modification.[49] Benzoic acid (6 g, 49 mmol), 2-chloromethyl- 1,3-dioxolane (3 g, 24.5 mmol), and potassium carbonate (5 g, 36.75 mmol) were dissolved in 500 mL DMF and stirred at 130 °C for 120 h. The mixture was then cooled and DMF was removed through vacuum distillation. Insoluble precipitates were dissolved in water and the aqueous layer was extracted using ethyl acetate and washed with 5% LiCl solution. Organic layer was dried over Na_2SO_4 and concentrated under reduced pressure to yield 3.6 g (70%). ^{1}H NMR (300 MHz, $CDCl_3$, δ): 8.07 (m, 2H), 7.57 (m, 1H), 7.44 (m, 2H), 5.29 (t, 1H, J = 3.9 Hz), 4.38 (d, 2H, J = 4.0 Hz), 4.00 (m, 4H)

2-Azido-2-(2-hydroxyethoxy)ethyl benzoate synthesis (8). The (1,3-dioxolan-2-yl)methyl benzoate (5 g, 24 mmol) was mixed with $ZnCl_2$ (0.5 g, 3.4 mmol) under

nitrogen atmosphere for 15 min. Trimethyl silyl azide (TMS-N_3) (4.2 g, 36 mmol) was added to the mixture and the reaction was stirred for 24 h. Reaction mixture was neutralized with saturated aq. $NaHCO_3$, stirred overnight, and extracted with dichloromethane (DCM). Organic layer was dried over Na_2SO_4 and concentrated under reduced pressure to yield 5.4 g (90%) of a yellowish liquid product. ^{1}H NMR (500 MHz, $CDCl_3$, δ): 8.06 (d, 2H, *J* = 7.8 Hz), 7.59 (m, 1H), 7.46 (m, 2H), 4.85 (dd, 1H, *J* = 4.88 Hz, 5.37 Hz), 4.48 (t, 2H, *J* = 4.9 Hz), 4.00 (m, 1H), 3.82 (m, 3H), 3.74 (m, 1H), 2.1 (br s, 1H). ^{13}C NMR (125 MHz, $CDCl_3$, δ) 166.22, 133.67, 130.01, 128.73, 89.51, 71.33, 65.04, 61.85. HRMS - ESI (m/z): $[M + Na]^+$ calculated for $C_{11}H_{13}N_3O_4$, 274.0798; observed, 274.0799.

Azido-2-methoxy-1-(2-methoxyethoxy)ethane (1). The compound was prepared according to the method similar to that described by Johnstone *et al.* with the following modification.[50] Powdered potassium hydroxide (85%, 8.5 g, 0.129 mol) was dissolved in 25 mL DMSO for 10 min and 2-azido-2-(2-hydroxyethoxy)ethyl benzoate (3.2 g, 13 mmol) was added to the mixture. Immediately, iodomethane (9.1 g, 64 mmol) was added. The mixture was stirred overnight and was dissolved in water. The aqueous layer was extracted with DCM. The combined organic layers were washed with water and brine. The organic layer was dried over Na_2SO_4 and concentrated under reduced pressure. The product was purified by silica gel column chromatography (ethyl acetate:hexanes = 1:2) to yield 1.59 g (70.6%) of a colorless liquid product. ^{1}H NMR (500 MHz, $CDCl_3$, δ): 4.62 (t, 1H, *J* = 1.07 Hz), 3.91 (m, 1H), 3.73 (m, 1H), 3.59 (m, 3H), 3.53 (m, 1H), 3.41 (s, 3H), 3.37 (s, 3H). ^{13}C NMR (125 MHz, CDCl3, δ) 90.61, 73.60, 71.76, 68.77, 59.67,

59.25. HRMS - ESI (m/z): $[M + Na]^+$ calculated for $C_6H_{13}N_3O_3$, 198.0849; observed, 198.0850.

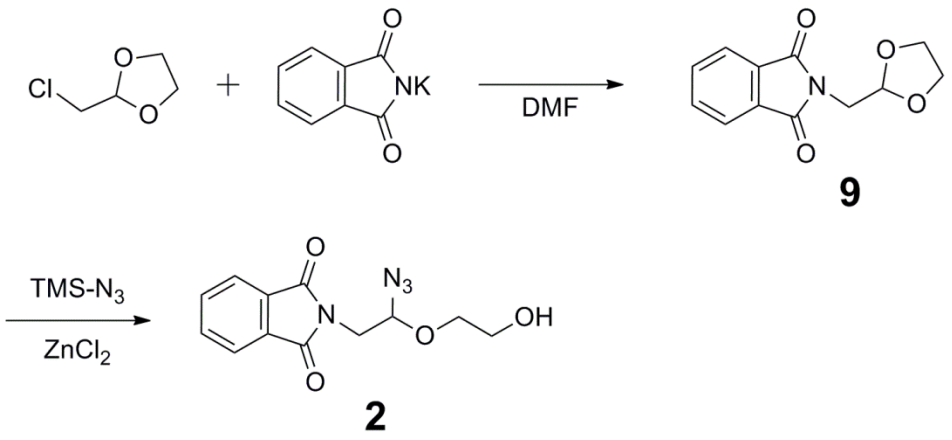

Figure 5-2. Synthetic scheme of α-azido ether **2**, 2-azido-2-(2-hydroxythoxy)ethyl phthalimide.

Phthalimido(1,3-dioxolan-2-yl)methane (9). Potassium phthalimide (50 g, 0.27 mol) was suspended in DMF (400 mL) and 2-chloromethyl-1,3-dioxolane (25 g, 0.2 mol) was added to the mixture under constant stirring. The temperature of the mixture was increased to 140 °C and was stirred for 48 h under nitrogen atmosphere. The mixture was then cooled to room temperature and poured on to 400 mL of cold water. The resulting precipitate was filtered and washed with ethanol. The precipitate was purified by recrystallization from ethanol to yield 43 g of white needle like crystals (92 %). ^{1}H NMR (500 MHz, $CDCl_3$, δ) 7.82 (dd, J = 3.1, 5.4 Hz, 2H), 7.69 (dd, J = 3.1, 5.4 Hz, 2H), 5.21 (t, J = 4.8 Hz, 1H), 3.93 (m, 4H), 3.83 (d, J = 4.7 Hz, 2H). ^{13}C NMR (125 MHz, CDCl3,

δ) 168.11, 134.13, 132.10, 123.50, 100.76, 65.09, 40.22. HRMS - ESI (m/z): $[M + Na]^+$ calcd for $C_{12}H_{11}NO_4$, 256.0580; observed, 256.0572.

2-Azido-2-(2-hydroxythoxy)ethyl phthalimide (2). The compound was synthesized as described above for 2-azido-2-(2-hydroxyethoxy)ethyl benzoate synthesis. To phthalimido(1,3-dioxolan-2-yl)methane (47 g, 0.2 mol), TMS-N_3 (70 g, 0.6 mol) was added anhydrous $ZnCl_2$ (0.04 mol, 5.5 g). The mixture was stirred overnight followed by addition of $NaHCO_3$ solution. After 2 h stirring, the products were extracted with DCM and the organic layer was dried over Na_2SO_4 and concentrated. The product was obtained as a white precipitate with 48 g (89%). ^{1}H NMR (500 MHz, CDCl3, δ) 7.86 (dd, *J* = 3.1, 5.4 Hz, 2H), 7.74 (dd, *J* = 3.0, 5.5 Hz, 2H), 4.81 (t, *J* = 6.0 Hz, 1H), 3.93 (dd, *J* = 1.8, 5.4 Hz, 2H), 3.91 (m, 1H), 3.75 (m, 2H), 3.66 (m, 1H). ^{13}C NMR (125 MHz, $CDCl_3$, δ) 168.13, 134.50, 131.92, 123.78, 89.06, 71.13, 61.72, 40.63. HRMS - ESI (m/z): $[M + Na]^+$ calculated for $C_{12}H_{12}N_4O_4$, 299.0751; observed, 299.0743.

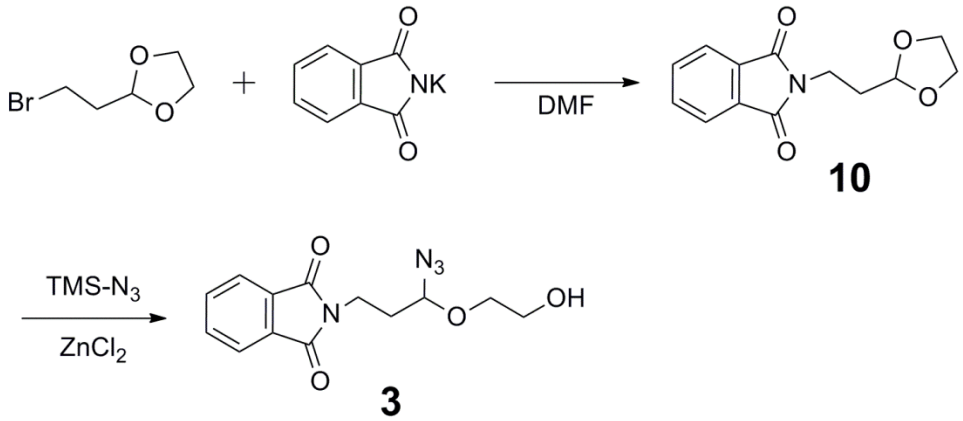

Figure 5-3. Synthetic scheme of *α*-azido ether **3**, 2-(3-phthalimido(1-azidopropoxy))-ethanol.

2-(3-Phthalimido(1-azidopropoxy))ethanol (3). The compound was synthesized as described above for 2-azido-2-(2-hydroxyethoxy)ethyl phthalimide, where the 2-(2-bromoethyl)1,3-dioxolane was used as the starting material. ^{1}H NMR (500 MHz, $CDCl_3$, δ) 7.84 (dd, J = 3.4, 5.4 Hz, 2H), 7.72 (dd, J = 2.9, 5.4 Hz, 2H), 4.50 (dd, J = 5.4, 6.8 Hz, 1H), 3.89 (m, 2H), 3.82 (m, 1H), 3.74 (m, 2H), 3.61 (m, 1H), 2.63 (br s, 1H), 2.13 (m, 2H). ^{13}C NMR (125 MHz, CDCl3, δ) 168.57, 134.36, 132.07, 123.57, 90.71, 71.02, 61.76, 33.97, 33.69. HRMS - ESI (m/z): $[M + Na]^+$ calcd for $C_{13}H_{14}N_4O_4$, 313.0907; observed, 313.0931.

5.2.3 Stability studies against hydrolytic degradation

For the stability studies, 50 mM of each chemicals were dissolved in D_2O (buffered pD 3.59, 7.00 and 10.19) and 1:1 of D_2O:DMF-d_7 for compound **1** and compound **2** and **3**, respectively. DSS (4,4-dimethyl-4-silapentane-1-sulfonic acid, 10 mM) was used as an internal reference.[51] The concentration of the compounds was monitored using ^{1}H NMR, and the plot of ln([concentration]) versus time was fitted to obtain the rate constant of hydrolysis. The area under the methyl proton peaks of DSS at 0 ppm was used as the reference concentration. Integration area under the peaks arising from one of the methylene protons of **1** at 3.839 to 3.776 ppm was used for concentration of compound **1**. For compound **2**, integration area under the peaks of methine proton attached to the carbon bearing the azide, from 5.037 to 4.898 ppm, was used to calculate the concentration. For compound **3**, integration area under the peaks arising from the

methylene protons alpha position to the azide bearing carbon, from 2.206 to 2.030 ppm, was used to calculate the concentration.

5.2.4 Kinetic studies of cleavage using DHLA triggers by UV-Vis spectroscopy

For pH dependent experiments, phosphate (pH 6-8 and 11-13), tris(hydroxymethyl)aminomethane (Tris pH 7-9), borate (pH 8-10), *N*-cyclohexyl-3-aminopropanesulfonic acid (CAPS pH 11), carbonate (pH 9-11) and NaOH (pH 13) were used to prepare buffered solutions. Stock solutions (200 mM) of azide compounds were prepared by dissolving azide chemicals in water, and then the solutions were degassed by blowing N_2 gas. DHLA stock solution (40 mM) was freshly prepared by dissolving DHLA into 40 mM of NaOH solution, and then degassed by blowing N_2 gas. Kinetic studies were initiated by addition of 500 uL azide solution into 1.5 mL mixture of 500 uL DHLA and 1 mL buffer (200 mM) solution in a UV-Vis cuvette. Immediately, the solutions were mixed and UV-Vis spectra were recorded at 25^{o}C. (final concentration : [DHLA] = 10 mM, [azide chemical] = 50 mM and [buffer components] = 100 mM) Absorption values at 350 nm were used to calculate the concentration of lipoic acid (LA) (ε = 102.65 M^{-1} cm^{-1}) using Beer's law. Background correction, presumably, due to the oxidation of DHLA, was done by subtracting the initial concentration of LA at 1.4 s. The concentration versus time curves for appearance of LA were fitted to second order integrated rate law equation having different initial concentration of reactants[52]:

$$log\left[\frac{a(b-x)}{b(a-x)}\right] = \frac{b-a}{2.303} \times kt \quad \ldots(1)$$

where *a* and *b* are initial concentrations of DHLA and azide species, respectively, and *x* is concentration of LA. Linear curves were fitted to obtain slopes that were used to calculate second order kinetic constants (*k*) up to ~50% conversion of DHLA.

For pseudo first order analyses, 2 mM DHLA was mixed with 10, 40, 50, 60, and 90 mM *α*-azido ether **1** at pH 9.90 and the rate constants were calculated under conditions where $b >> a$, $(b - a) = b$ and $(b - x) = b$ in equation 1, resulting in the following equation:

$$log\left[\frac{a}{a-x}\right] = \frac{b}{2.303} \times kt$$

The rate constants were then plotted against the concentration of **1** to identify the order of dependence on [**1**]. To identify the kinetic order of dependence on DHLA, different concentrations of DHLA, from 1 mM to 5 mM, were reacted with 50 mM azide compound **1** at pH 9.90. The initial rates were obtained from the [LA] vs time curves ($\Delta[LA]/\Delta t$) and then plotted against $[DHLA]_o$ to identify the order of dependence on [DHLA].

5.2.5 Kinetic studies of cleavage using TCEP triggers by ^{1}H-NMR

Because TCEP oxide did not show distinct absorption peaks from that of TCEP, ^{1}H-NMR was used to study kinetic of cleavage. Buffer solutions and TCEP stock solutions were prepared in D_2O and lyophilized to minimize the amounts of exchangeable protons content and interference of data analysis from these protons. NMR samples were prepared by mixture of 100 μL of 200 mM TCEP stock solution (with 4 equivalents of NaOD to neutralize TCEP), 500 μL of 200 mM buffer, 100 μL of 100 mM DSS (with one equivalent of NaOD) and 200 μL D_2O in an NMR tube. For cleavage kinetic studies, 100 μL of 200 mM *α*-azido ether compound **1** was added to the NMR tube. (Final concentration: *α*-azido ether compound **1** = 20 mM, TCEP = 20 mM, DSS = 10 mM, and buffer component = 100 mM) Immediately, ^{1}H-NMR spectra were recorded at different time intervals. From NMR, the area under peaks arising from the methylene protons were used to calculate the concentrations of TCEP and TCEP=O. For TCEP=O, area under the peak from 2.19 to 2.06 ppm was used. For mechanistic analysis, NMR peaks arising from intermediates appeared in a region overlapping the peaks from TCEP and TCEP=O. The area of the intermediates was obtained by subtraction entire integration area from the integration area of methylene of TCEP or TCEP=O in isolated peaks. The areas then were used to calculate the concentrations of the intermediates. Two intermediates, **I1** and **I2** were observed. For **I1**, area under the peaks from 2.47 to 2.32 ppm was used to calculate the concentration. For **I2**, area under the peaks from 2.63 to 2.47 ppm was used.

5.2.6 Kinetic studies of cleavage using DHLA triggers by ^{1}H-NMR

A similar protocol of TCEP analysis was used for DHLA analysis. The only difference being the amount of NaOD used was one equivalent instead of four. From NMR, the area under peaks arising from methylene protons alpha to the terminal thiol/thioether from 2.71 to 2.55 ppm and from 3.29 to 3.13 ppm were used to calculate the concentrations of DHLA and LA respectively. For mechanistic analysis, area under the peaks arising from the protons of methoxy group of the α-azido ether from 3.44 to 3.42 ppm and from 3.37 to 3.35 ppm was used to calculate the concentrations of intermediates.

5.2.7 Kinetic analysis

To analyze the data obtained from the kinetic studies, the plot of concentration versus time was fitted to the following equations to obtain second order rate constants for the consumption of reactant and formation of product:

$$\frac{1}{x} = kt + \frac{1}{x_0} \quad \dots (2)$$

$$y = \frac{k{x_0}^2 t}{1 + kx_0 t} \quad \dots (3)$$

where x and x_0 are concentrations of TCEP or DHLA at time t and 0, respectively, and y is concentration of TCEP=O or LA at time t.

5.2.8 pK_a values of DHLA and TCEP

Proton NMR spectra at different pD were recorded to obtain the pK_a value. Chemical shifts of proton as a function of pD were fitted to obtain the pK_a values using nonlinear least-squares equation[53]:

$$\delta(obs) = \delta(P) + \frac{\delta(U) - \delta(P)}{1 + 10^{n(pK-pD)}}$$

where $\delta(obs)$ is experimental chemical shift, $\delta(P)$ and $\delta(U)$ represent the chemical shift corresponding to protonated and unprotonated states, respectively, and n is a Hill constant reflecting the number of proton binding sites – it is fixed as one.

5.3 Results and Discussion

5.3.1 Stability against hydrolysis

For the practical applications of cleavable linkers, especially in biological applications, they need to be stable in their application conditions before cleavage is triggered. For α-azido ether, Jencks et al. reported that the α-azido ether degraded via ionization to form oxocarbenium ions, followed by hydrolysis in aqueous solution (Figure 5-4).[44] Jencks et al. noted that pseudo first order rate constants ranged from 10^{-4} to 10^{-2} s^{-1}corresponding to less than 2 h of half life, indicating impractical use as a cleavable linkers. However, the α-azido ether has been currently involved in several biological technologies, such as, the next generation DNA sequencing technology in the

market (Illumina Genome Analyzer)[39,43] and DNA detection platform,[40,54-56] requiring longer half life. To solve this paradox, we have explored what factors make the stability different based on chemical structure.

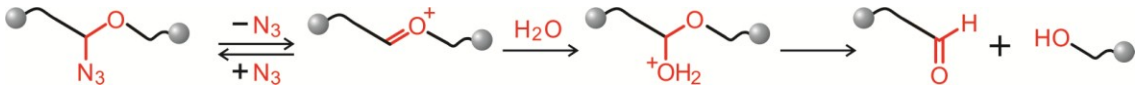

Figure 5-4. Mechanism of α-azido ether degradation via oxocarbenium intermediate in aqueous solution.[44]

The stability of α-azido ether chemicals relies on the stability of oxocarbenium ion intermediates that are governed by the nature of the substituents. For example, if the oxocarbenium ion is destabilized by electronegative atoms like O or N at the gamma position of the azido ether group, the formation of oxocarbenium ion would be forbidden resulting in slower degradation of α-azido ether chemicals. Such substituent effects have also been observed for the hydrolysis of acetals that proceeds through the formation of the same oxocarbenium intermediate.[57] Based on this fact, we synthesized several model chemicals varying atoms at the gamma position and studied their stability using ^{1}H-NMR (Figure 5-5 chemical **1**-**3**). The degradation rate constants of each model chemical were obtained from fitting the plot of ln[α-azido ether] versus time (Figure 5-6). As expected, α-azido ether bearing electronegative atoms (O and N) at the gamma position showed 1.1 x 10^{-8} s^{-1} (**1**) and 2.8 x 10^{-9} s^{-1} (**2**) of first order rate constants, respectively, that had values one or two order lower than that of α-azido ether having C atom at the gamma

position, 1.0 x 10^{-7} s^{-1}(**3**). That means incorporating electronegative atoms instead of C at the gamma position can significantly improve the stability from 76 d to 7.7 yr in terms of half life.

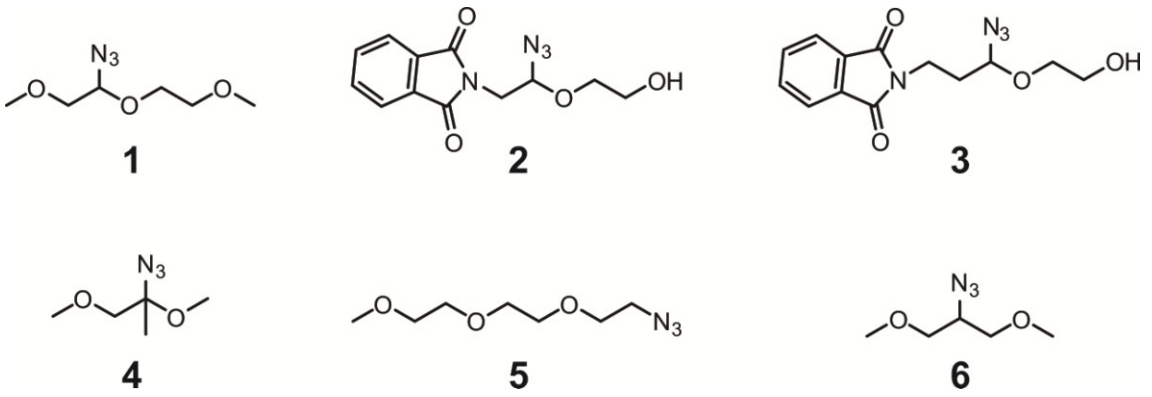

Figure 5-5. Azide chemicals used to study hydrolytic stability (**1-4**) and reductive cleavage of α-azido ether (**1**) and its analogous (**5** and **6**).

In addition, the stability of oxocarbenium ion intermediate is affected by hyperconjugation effects at the alpha position of the azido ether group. When a methyl group was placed in the alpha position instead of a proton, the degradation rate increased dramatically to 5.7 x 10^{-4} s^{-1} (chemical **4** in Figure 5-5) as reported by Jencks et al.[44] because the oxocarbenium ion intermediate was stabilized by hyperconjugation of the methyl group. Similar experimental results were reported from the acetal hydrolysis.[57] In the acetal hydrolysis, hyperconjugation significantly increased the hydrolysis rate of the acetal group due to the stabilization of oxocarbenium ion intermediate.

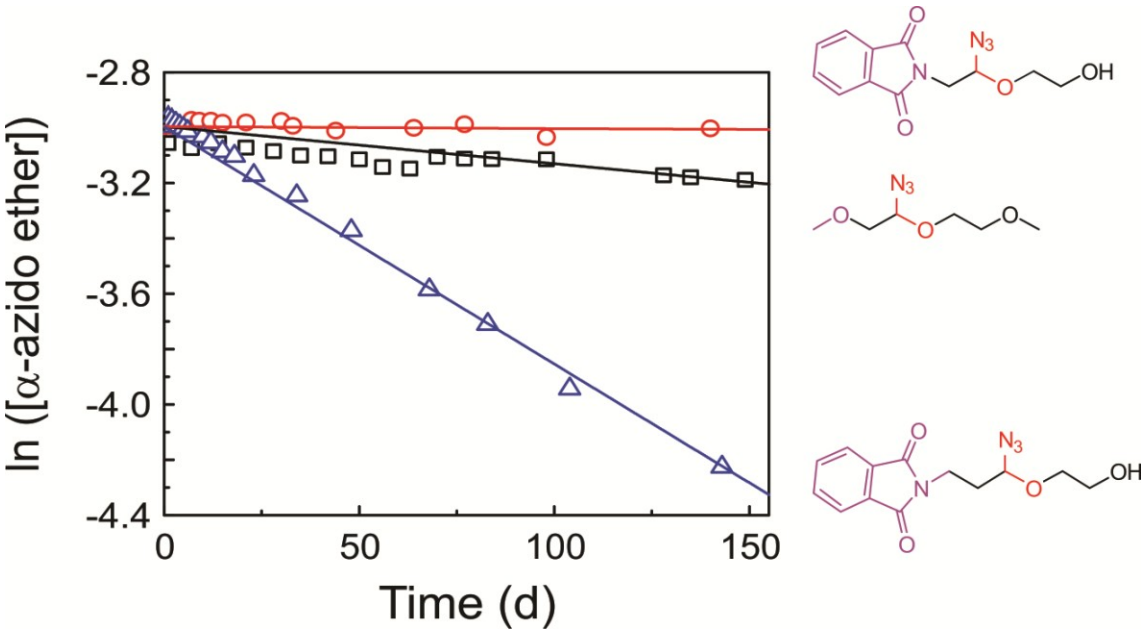

Figure 5-6. Hydrolytic stability of α-azido ether chemicals measured by ^{1}H-NMR. The degradation rate was obtained by fitting the data of ln([α-azido ether]) versus time using the first order rate equation. Chemical **1** was dissolved in several buffered solutions (pD 3.59, 7.00 and 10.19), which showed similar behavior. Here, pH 7.00 data was included. Chemical **2** and **3** were dissolved in 1:1 of D_2O and DMF-d_7 because of solubility.

Therefore, the stability of α-azido ether chemicals is able to be improved through the modification of chemical structure by introducing electronegative atoms at the gamma position as well as a proton at the alpha position. As a result, the degradation without triggers can be minimized up to several years of half life, which allows the α-azido ether chemicals to be suitable for practical applications. Furthermore, any significant difference in degradation was not observed in slightly acidic and basic conditions through the study of pH effect on the stability of α-azido ether chemicals varying the pD of NMR solution to 3.59 and 10.19 containing α-azido ether **1**. It suggests

that the α-azido ether could be used in any buffered solution for storage maintaining its stability and have benefits for applications performed at various pH.

5.3.2 Cleavage of α-azido ether using biocompatible triggers

To cleave the α-azido ether, the azide group should be reduced to amine resulting in rapid hydrolysis as well as cleavage. The reduction of azide has been well-established in the field of synthetic chemistry and recently biological chemistry; for instance, Staudinger reduction to introduce amine[58-59] and Staudinger ligation to chemically link two molecules,[60-61] which has already been incorporated into *in vivo* bioconjugation.[62-63] Particularly, Staudinger ligation has been of great interest because the reactions involving an azide group are considered as bioorthogonal chemistry.[14,37] Thus, incorporating azide into cleavable linkers has advantages in terms of bioorthogonality, which gives rise to controlled cleavage by external chemicals, compared to other cleavable linkers,[1] such as, hydrolytic cleavable ester, enzymatic cleavable peptide linker, and disulfide cleaved by bio-abundant monothiols,[64] which might be limited due to unwanted cleavage in biological systems. The cleavage of α-azido ether can also have an advantage in controlled cleavage for *in vivo* applications, which might be difficult for photocleavable *o*-nitrobenzyl ether[31] because light does not penetrate tissues or skins beyond a couple of hundred micrometers.[36] Moreover, azide reduction has benefits with respect to another bioorthogonal cleavable azo linker[32] because the trigger for the α-azido ether is stable under physiological conditions. It should be noted that α-azido ether can be developed as

a novel and versatile cleavable linker in various biological fields from *in vitro* to *in vivo* applications with controllable and bioorthogonal characteristics.

Although the use of azide reduction would be superior to other cleavable linkers, especially for *in vivo* applications, the reduction has not been widely used nowadays because the slow kinetic of azide reduction has been a challenge to be solved.[42] In contrast, α-azido ether has been getting attention for biological technologies as a cleavable linker as mentioned before.[39-40] However, the reduction conditions in those biological technologies were somehow different from ordinary conditions; in the DNA sequencing technology, the azide reduction was performed at high temperature like 60 ^{o}C,[39] and in the DNA detection assays, the reduction was accelerated owing to rapid DNA hybridization approaching α-azido ether proximal to triggers.[40] These facts prompted us to study the cleavage kinetics to determine the actual rate of cleavage in aqueous solutions. Also, we expected an improved rate compared to typical Staudinger ligation because the electronegative O atom might affect the reduction rate.

Thus, the next step in understanding cleavage kinetics was to study the experimental conditions required for an efficient cleavage in the presence of suitable triggers. It is known that the azide can be reduced by biocompatible triggers including dithiols or phosphines. For instance, dithiothreitol (dithiol) and triarylphosphines were used previously to reduce azides in pharmaceutical compounds[65-66] and reactants of Staudinger ligation,[60-61] respectively. Therefore, in our study, dihydrolipoic acid (DHLA), which is a dithiol chemical, and TCEP, which is a phosphine chemical, were chosen as triggers. We chose DHLA as a trigger because it is a naturally occurring antioxidant, and

is known to be biocompatible.[67] TCEP was studied as well because it is water soluble and biocompatible.[68]

Cleavage of α-azido ether using DHLA triggers

DHLA is oxidized to form lipoic acid (LA) during the azide reduction. Because LA is a cyclic disulfide that absorbs light at 334 nm,[69] and no interference occurs in this absorption peak from azides and cleaved products, the kinetics of the reaction between **1** and DHLA was studied by monitoring the formation of LA using UV-Vis spectroscopy. The hydrolysis of α-amino ether after the reduction of the azide is expected to be spontaneous. Consequently, the formation of LA could be considered as an indication for completion of the reductive cleavage reaction.

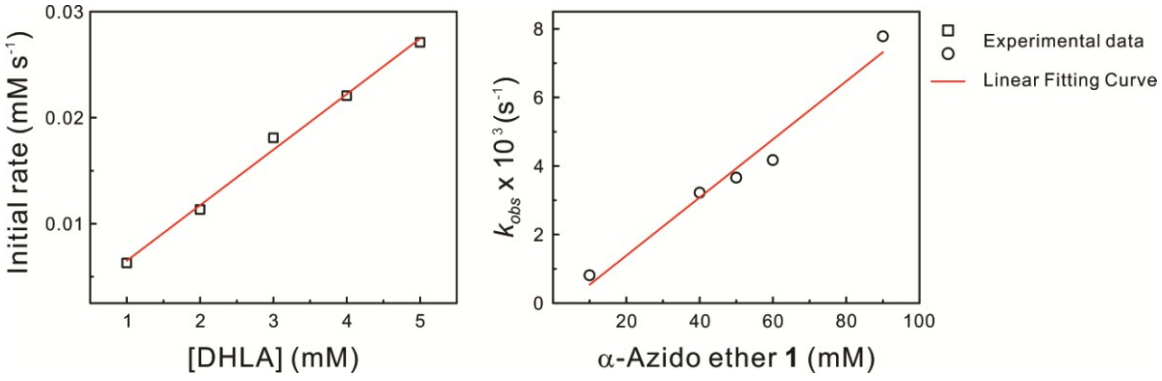

Figure 5-7. Reaction between DHLA and α-azido ether **1** to determine order dependences of DHLA and α-azido ether on cleavage, measured by UV-Vis spectroscopy using LA absorption peak at 334 nm. **Left**: Initial rate (*dx/dt*) of LA formation versus different initial concentration of DHLA with excess α-azido ether **1**. **Right**: Plot of pseudo first order rate constants versus concentration of α-azido ether **1**.

It was reported that azide reduction using dithiols like DTT followed second order kinetics with first order dependences on both the azides and DTT.[66,70] Likewise, DHLA can reduce azide with first order dependences on both the α-azido ether and DHLA. As the concentration of DHLA increased from 1 to 5 mM with constant 50 mM of **1**, the initial rate showed a linear relationship with respect to the concentration of DHLA indicating a first order reaction of DHLA. Under pseudo first order reaction conditions where 2 mM DHLA was reacted with excess concentration of **1** ranging from 10 to 90 mM, a linear curve was obtained indicating a first order reaction of α-azido ether.

For the reduction reaction, we observed that the rate of reduction was changed dependent on pH similar to previous report,[71] *i.e.* the higher the pH, the faster the reduction. The same pH dependence of reaction rate was also reported in several reactions involving thiol or dithiol molecules, such as, thiol exchange reaction,[72] thiol oxidation by hydrogen peroxide,[73] and DHLA and flavin reaction.[74] Thus, we assumed that active reactants using dithiols in the reduction would be deprotonated, thiolated DHLA because the reaction required bases. Next, to study the influence of pH on the reductive cleavage, the reaction between **1** and DHLA was performed in buffered solutions of different pH. The concentration versus time curves for the formation of LA were fitted to second order integrated rate equation and the values of the rate constants (k) were calculated. The variation of the rate constant with pH was plotted as shown in Figure 5-8. The second order kinetic constant relied on the pH of the solutions; $2\sim7 \times 10^{-4}$ at lower pH like 6 or 7, abruptly increased from 0.04 $M^{-1}s^{-1}$ at pH 9 to 0.22 $M^{-1}s^{-1}$ at pH 10.6, leveled off up to pH 12.3, and decreased to 0.06 $M^{-1}s^{-1}$ at pH 13.

To understand the origin of the dependence of *k* on pH, we have obtained the NMR titration curve of DHLA, which has often been used to determine the pK_a value of chemicals.[53] The behavior of the NMR titration curve was similar to that of the *k* curve with respect to pH (or pD) below pH 13 (Figure 5-8). For example, a chemical shift of methylene and methine protons in DHLA next to thiol group was abruptly decreased as pD increased at around pD 9.8, which had a pK_a value of DHLA from NMR titration curves. That clearly indicated the reductive cleavage of α-azido ether involved deprotonated, thiolated DHLA, as we assumed. Although *k* values decrease at high pH (> 13), which is highly basic, the obtained *k* value under slightly basic conditions, for instance 0.1 $M^{-1}s^{-1}$ at pH 9.5, indicates α-azido ether and DHLA can be applied to some bio-materials. In addition, the results suggest that if dithiols would be chemically modified to lower pK_a value, the α-azido ether linkers could play an essential role in degradable bio-materials with relevant cleavage rate.

Furthermore, we compared the reduction rate of α-azido ether with that of typically used azido groups that have hydrocarbon at the alpha position to investigate the effect of electronegative O on the rate. Model compounds **5** and **6** were synthesized and their reduction by DHLA was studied (Figure 5-8). The reduction of all three compounds showed similar pH dependences; the higher the *k* values, the higher the pH (< 13). Primary and secondary azide analogs, **5** and **6**, showed no significant difference in the reduction rates, ranging from 3×10^{-4} $M^{-1}s^{-1}$ to 0.05 $M^{-1}s^{-1}$. The highest observed second order rate constants were 0.059 $M^{-1}s^{-1}$ and 0.046 $M^{-1}s^{-1}$ for **5** and **6,** respectively, that were about four times slower than the *k* value of α-azido ether reduction. We believe that

the increased reactivity of α-azido ethers could be a result of the presence of the electronegative O, making azido more eletrophilic and facilitating the attack of deprotonated DHLA on the azido groups.

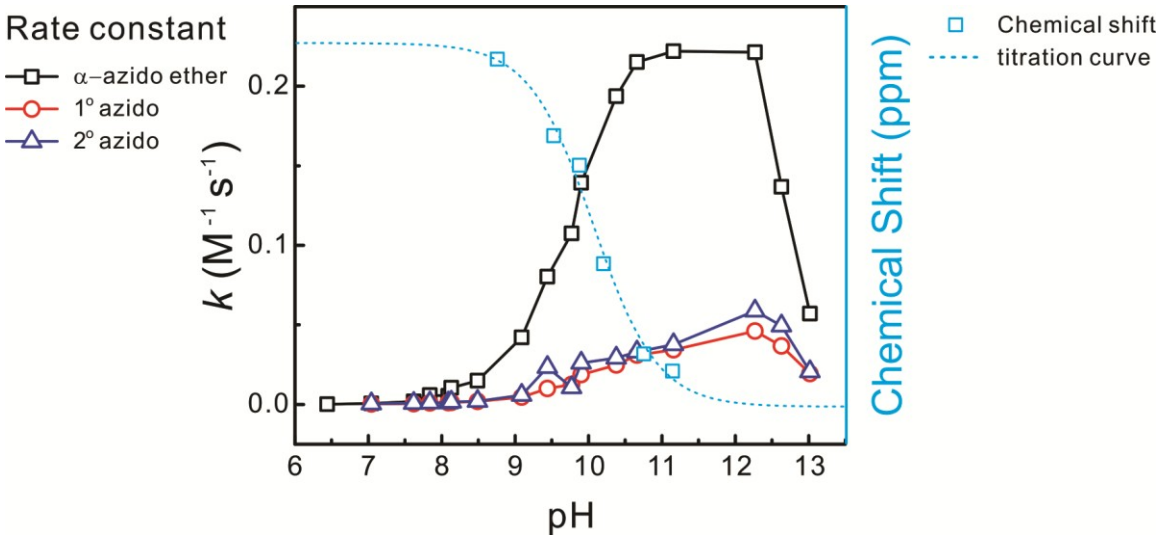

Figure 5-8. Plot of second order rate constant (k) versus pH for the reaction between 50 mM azido compounds (α-azido ether **1**, primary azido **5** and secondary azido **6**) and 10 mM DHLA in buffered aqueous solutions, measured by UV-Vis spectroscopy. Chemical shift of methine proton of DHLA and its NMR titration curve dependent on pD were included.

The reactions were then analyzed using ^{1}H NMR spectroscopy to verify the results obtained from UV-Vis experiments. Kinetic profiles were constructed from an equimolar reaction between **1** and DHLA (Figure 5-9). The concentration of DHLA decreased while the concentration of LA increased exponentially. The sum of both DHLA and LA remained as constant, indicating no other intermediate of dithiol triggers were formed during the reduction. The results were fitted using second order rate

equations to obtain rate constants (k) as 0.22 and 0.32 $M^{-1}s^{-1}$ at pD 9.67 and 10.19, respectively, which were consistent with the results from UV-Vis experiments.

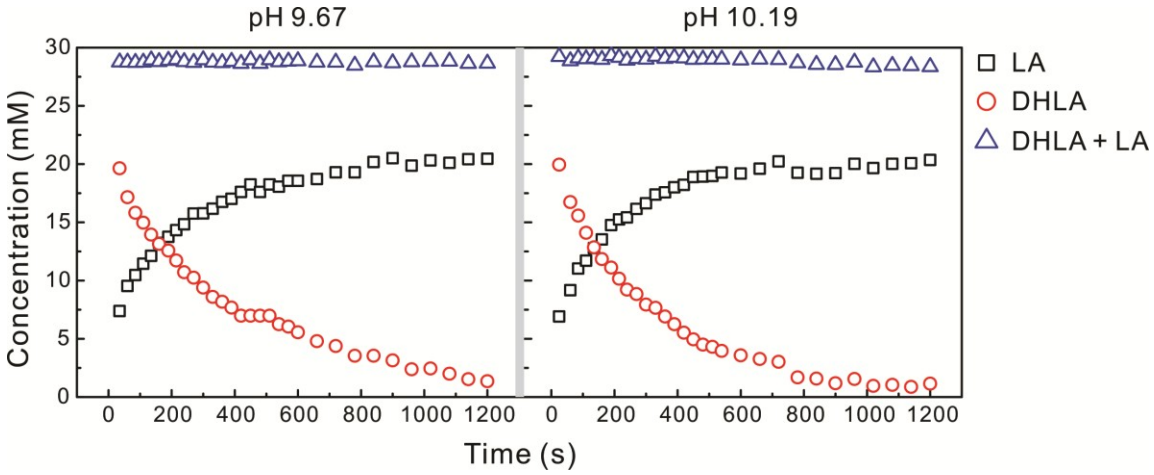

Figure 5-9. Kinetic profiles of DHLA and LA concentration with respect to time for the reaction between α-azido ether **1** and DHLA, measured by ^{1}H-NMR at pH 9.67 (left) and 10.19 (right). The sum of DHLA and LA concentration remained as constant. The plots were converted to 1/concentration and fitted using second order rate equation to obtain kinetic constants (k).

In addition to kinetic studies, mechanistic investigation was conducted for the reaction between **1** and DHLA. Based on earlier reports[70-71] on the reduction of azides by thiols, the hypothesized mechanism for the cleavage of α-azido ethers using DHLA is shown in Figure 5-10. After deprotonated, thiolate DHLA attacks azido, azido is reduced by releasing nitrogen and DHLA is oxidized through the intramolecular cyclization to form disulfide bond. The α-amino ether is then hydrolyzed to cause cleavage. In the NMR analysis, proton peaks arising from the methoxy groups of **1** and the intermediates

arising from its reaction with DHLA were used to follow the formation of intermediates. Only one intermediate, presumably α-amino ether, was observed and there were no indications of any deviations from the suggested mechanism. Moreover, the decrease in the reaction rates at high pH (> 13) could be explained by the suggested mechanism. The formation of α-amino ether should involve the protonation step of N that could become difficult as the pH of the solution increases. It would lead to the observed decrease in reaction rate at higher pH (> 13).

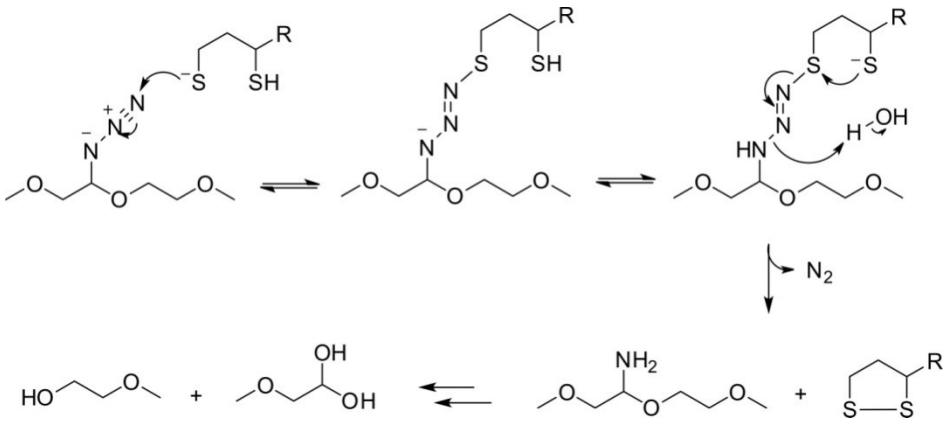

Figure 5-10. Suggested mechanism for the reductive cleavage of α-azido ether using DHLA trigger.

Cleavage of α-azido ether using TCEP triggers

Although DHLA is effective to trigger the reductive cleavage of α-azido ethers, the cleavage might not have practical significance for most biological applications because its rate is slow near neutral pH (k_{DHLA} = ~7 x 10^{-4} $M^{-1}s^{-1}$), likewise, in physiological conditions. It might be improved using chemically tailored dithiol triggers

that have a pK_a value close to neutral or acidic pH.[75-77] However, it requires additional synthesis to investigate. Instead, we have tried to use commercially available reducing reagents, which are better reducing agents for azide than DHLA. As mentioned, phosphines can reduce azide even in neutral pH. Among phosphines, tris(2-carboxyethyl)phosphine (TCEP) is chosen as a trigger because it has been a widely utilized reducing reagent to cleave disulfide bonds in many biological applications as a replacement for dithiols and is highly water soluble as well as resistant to oxidation.[68,78] However, TCEP and TCEP=O, which is a product of the reduction reaction, do not have interpretable absorption bands in the UV-Vis spectrum. As a result, the cleavage kinetics of α-azido ether reduction with TCEP has been studied using ^{1}H NMR analysis rather than UV-Vis spectroscopy, monitored by the consumption of TCEP and formation of TCEP=O in buffered solutions of different pDs.

First, we fitted kinetic profiles of TCEP disappearance during an equimolar reaction between **1** and TCEP using a second order rate equation to obtain the second order rate constant (k_{TCEP}). Similar to DHLA results, the rates relied on the pD; the lower the pD, the lower the kinetic constant value (Figure 5-11). Also, its behavior resembled the NMR titration curve, similar to DHLA results, indicating the pK_a value of TCEP affected the reductive cleavage of α-azido ether. For example, the rate constant (k_{TCEP}) values increased from 0.04 $M^{-1}s^{-1}$ at pD 6.5 to ~0.28 $M^{-1}s^{-1}$ above pD 9, while the chemical shift of the methylene proton in TCEP decreased from 2.4 ppm at pD 6.5 to ~1.7 ppm above pD 9 due to deprotonation of P at its pK_a value (7.7). This fact indicated that the initial step in the reaction mechanism would be the lone pair electrons on P attack

the azide group as well. Most importantly, when the TCEP trigger was used for the azide reduction instead of DHLA, the rate was improved ~200 times from 4 x 10^{-4} $M^{-1}s^{-1}$ to 7 x 10^{-2} $M^{-1}s^{-1}$ at pH ~7 because of the trigger's pK_a shift from 10.0 to 7.7. The rate constant was decreased at high pD (>~11), which might imply a rate determining step shift, observed in the DHLA trigger.

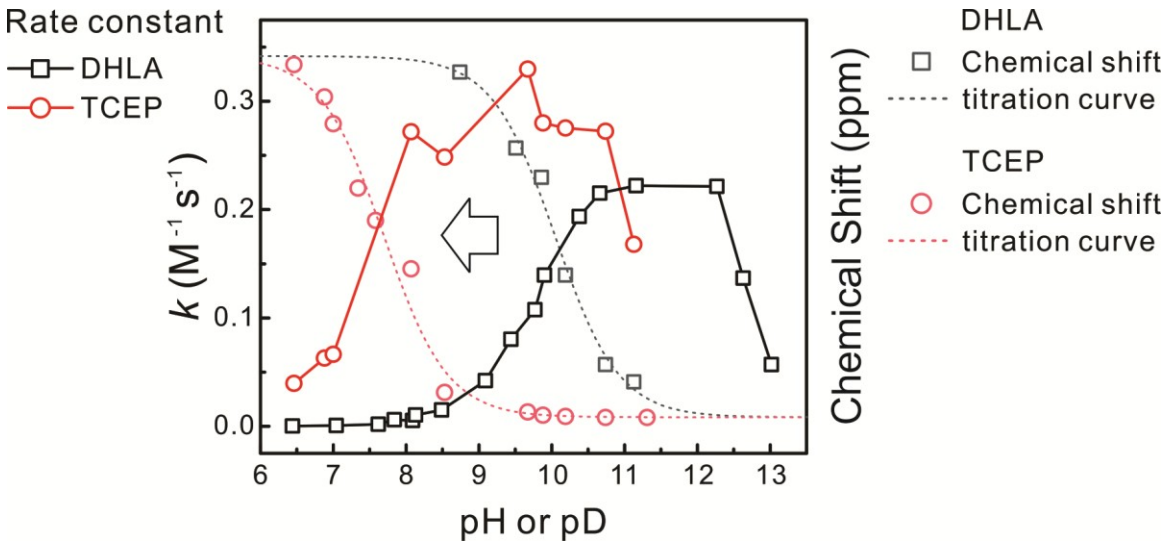

Figure 5-11. Plot of second order rate constant and chemical shift versus pH or pD for the reaction between α-azido ether **1** and TCEP or DHLA. For TCEP, the rate constant was obtained from TCEP consumption, measured by ^{1}H-NMR. For DHLA, the rate constant was obtained from the formation of LA, measured by UV-Vis spectrometry. The NMR titration curve was constructed from the proton chemical shift of methylene protons next to the P atom for TCEP and methine proton for DHLA, measured by ^{1}H-NMR. The arrow indicates that the trigger's pK_a value shifts from 10 to 7.7, which also causes the rate constant curve to shift, improving the rate constant value at neutral pH (or pD).

In contrast to the second order rate of TCEP consumption, TCEP=O formation showed different kinetic profiles as pD increased (Figure 5-12). Its behavior changed from an exponential to a linear relationship between concentration and time, implying a second order reaction and zero order reaction, respectively. For example, exponential dependence was observed when pD was below 9 (Figure 5-12 A and B) while TCEP=O formation became a linear dependence when pD was above 9 (Figure 5-12 C-E). That meant at lower or netural pD α-azido ether and TCEP reactions determined the entire reaction of TCEP=O formation while at higher pD consecutive reactions through intermediate **I1** could occur to form TCEP=O, implying the rate determining step was shifted. As a result, the second order rate constants ($k^2_{TCEP=O}$) at lower pD showed comparative values to k_{TCEP} ranging from 0.15 to 0.50 $M^{-1}s^{-1}$ as well as a similar trend to k_{TCEP}, increasing pD led to higher k values along with pK_a. Above pD 9, zero order rate constants ($k^0_{TCEP=O}$) gradually decreased from 2.1 x 10^{-5} to 1.3 x 10^{-5} M s^{-1} with respect to pD of solutions. Moreover, another parallel reaction pathway was observed even if this pathway did not affect the TCEP=O formation significantly within the measured timescale (1200 s). The parallel pathway went through minor intermediate **I2** because only 7 ~ 23% of **I2** was produced compared to the initial TCEP concentration at ~1200 s or at the time where major intermediate **I1** reached the maximum concentration.

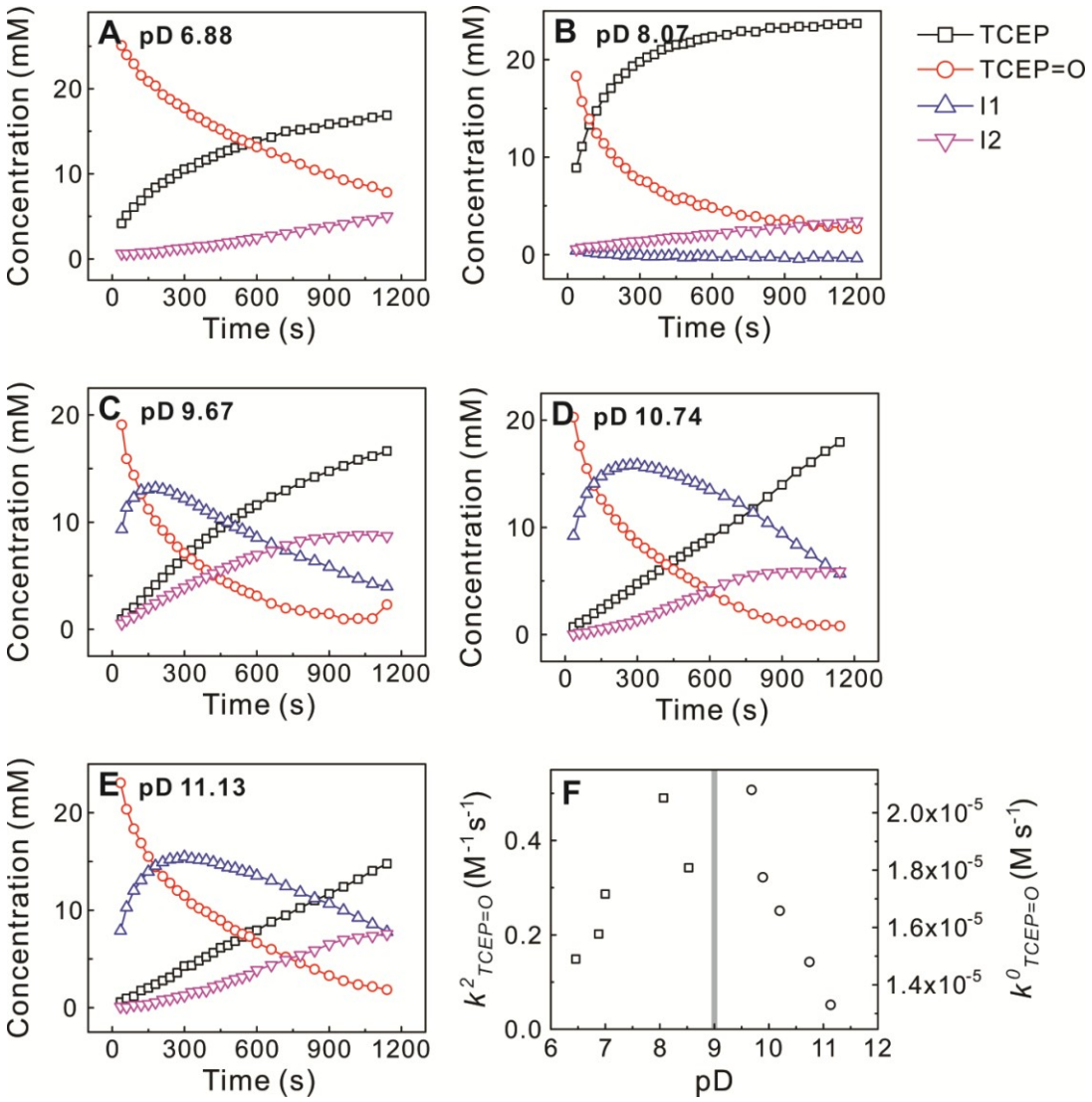

Figure 5-12. (**A-E**) Plot of kinetic profiles of TCEP, TCEP=O, intermediate **I1** and **I2** versus time for and eqimolar reaction between a-azido ether 1 and TCEP in buffered solutions of pD (**A**) 6.88, (**B**) 8.07, (**C**) 9.67, (**D**) 10.74, and (**E**) 11.13, measured by H-NMR spectroscopy. Exponential disappearance of TCEP was observed in every pD solutions. But, the TCEP=O formation followed exponential appearance at lower pD, and shifted then to linear dependence at higher pD with respect to the time. (**F**) Second order rate constants ($k^2_{TCEP=O}$ $M^{-1}s^{-1}$) at lower pD from exponential disappearance of TCEP=O, resulting from **A-B** and zero order rate constants ($k^0_{TCEP=O}$ $M\ s^{-1}$) at higher pD from linear dependence of TCEP=O, resulting from **C-E**.

Although a zero order reaction has not been reported for TCEP=O formation in the azide reduction by phosphines, to the best of our knowledge, we proposed a mechanism to understand these observations as shown in Figure 5-13, based on our results as well as previous reports[79-81] on the reduction of azides by phosphines and hydrolysis of iminophosphoranes in aqueous solutions. Because TCEP consumption showed a second order reaction and pD dependence, deprotonated TCEP should react with azide to form a phosphazide intermediate. After nitrogen was evolved immediately to form iminophosphoranes (**I**), **I** was protonated to provide intermediate **I1**. **I1** was then transformed into **I1'** by reaction with water. Next, after the equilibrium step of protonation of **I1'**, TCEP=O and α-amino ether were produced and α-amino ether would be cleaved via hydrolysis.

Typically, Staudinger reduction[82-83] or ligation[42] followed a second order reaction because the rate determining step (RDS) was phosphines' attack on azides. In α-azido ether reduction, at low pH (or pD, < 9) it would follow the same RDS, providing exponential dependence of TCEP=O formation. However, at high pH (or pD, > 9) the zero order rate of TCEP=O formation indicated that RDS should occur after the reaction between α-azido ether and TCEP.[84] In addition, the zero order behavior was observed above a certain pD, suggesting RDS had to involve protons. Based on these facts, although the provenance of the intermediate was uncertain, we proposed that RDS might be the protonation step of intermediate **I1'** at higher pD. Because the concentration of protons was maintained by the buffered solutions and the concentration of protons was

much less than that of **I1'** above the certain pD, the rate of TCEP=O formation solely relied on the concentration of protons. It provided zero order to both α-azido ether and TCEP as well as decreasing the rate constant with increasing pD. Our results also suggested that the presence of free protons was essential to provide TCEP=O formation and cleavage of α-azido ether.

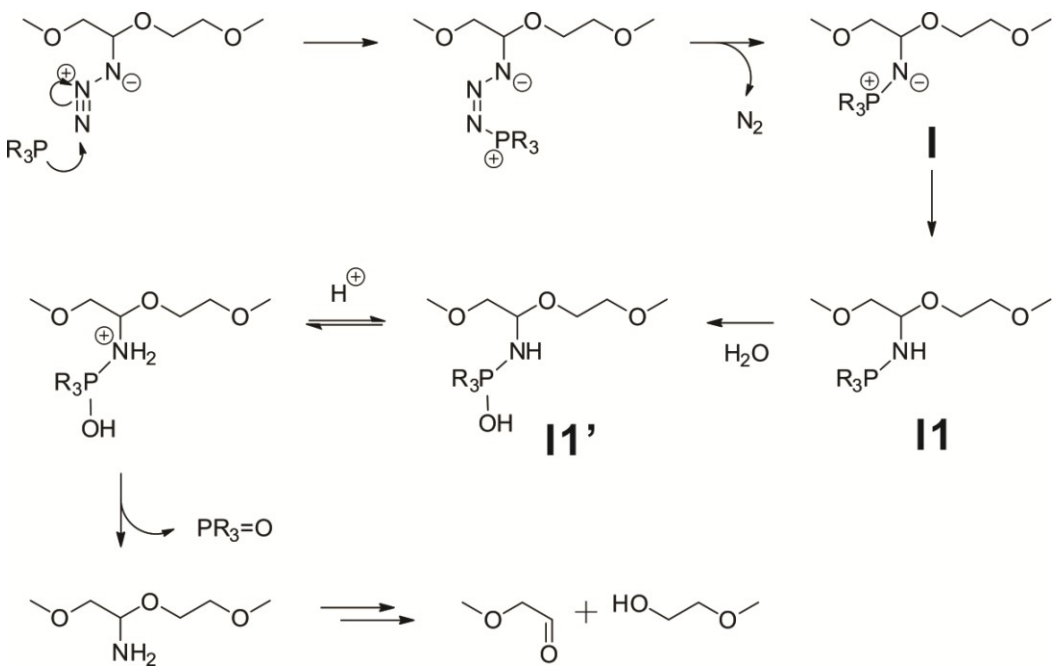

Figure 5-13. Proposed mechanism of the major reaction pathway for the reaction between α-azido ether **1** and phosphines in aqueous solutions.

In addition, a parallel reaction pathway through intermediate **I2** was observed irrespective of the pDs of the reaction even if it was minor (7 – 23 %). The concentration

of **I2** increased without any relationship with **I1**, supported by the fact that concentration of **I2** leveled off while **I1** was converted to TCEP=O when almost all of TCEP was consumed in pD 10.74 at ~1000 s (Figure 5-12D). In addition, **I2** eventually was converted to TCEP=O after 1 d in NMR. The minor pathway did not exist in the reduction of secondary azido chemical **6**, implying electronegative O could play an important role for the minor pathway. Based on these observations, although the identity of intermediate **I2** needs more investigation, we proposed the minor pathway involved the cleavage of C-O bond before TCEP=O formation as shown in Figure 5-14.

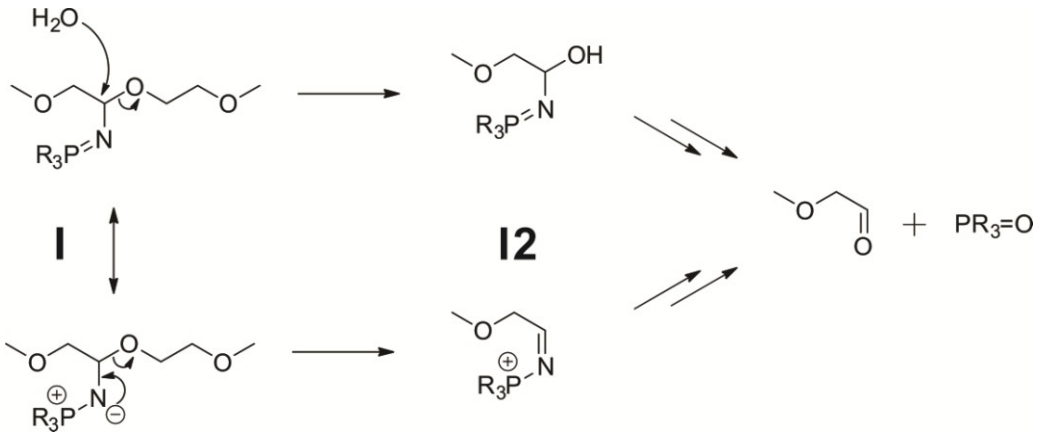

Figure 5-14. Proposed mechanism of minor reaction pathway for the reaction between α-azido ether **1** and phosphines in aqueous solutions. Water (top) or lone pair electrons on N (bottom) might provide intermediate **I2** that was eventually converted to TCEP=O.

5.3.3 Cleavage products of α-azido ether using triggers

The reductive kinetics of α-azido ether has showed that it can be applied to degradable biomaterials with relevant cleavage time scales when appropriate triggers were used depending on the reaction conditions. Along with kinetics, it is also important to study the products of the reductive cleavage because they would determine the biocompatibility of the system. Although reactants are known as biocompatible, the products of α-azido ether have not been investigated but just been hypothesized as alcohols and aldehydes until now.[39-40] Here, we studied the products comparing H-NMR of α-azido ether **1** reduced by TCEP and its model compound.

The azide of **1** is reduced to an amine, followed by alcohol release and imine formation that was hydrolyzed to aldehyde (Figure 5-15A). As a result, in the NMR spectrum of cleavage products 2-methoxy ethanol was observed with two sets of triplet peaks of methylenes (**ii**) at 3.56 and 3.71 ppm and a singlet methoxy peak (**i**) at 3.38 ppm (Figure 5-15B). However, another expected product, aldehyde, was not observed. Instead, 2-methoxyethane-1,1-diol, hydrated form of aldehyde, was observed at neutral pD. The hydrated form of aldehyde is also found in other aldehyde molecules, such as, glutaldehyde[85-86] and aliphatic aldehyde.[87] The hydrated form was verified by comparing the NMR obtained after the reductive cleavage of **1** to that of the model compounds, 2-methoxyethane-1,1-diol, which was generated in the NMR solution after deprotection of commercially available 1,1,2-trimethoxy ethane under acidic condition (Figure 5-15B). In the NMR spectrum, there were peaks corresponding to triplet methine (**a**), doublet

methlyene (**b**), and singlet methyl (**c**) at 5.16, 3.43, and 3.39 ppm, respectively. The adehyde was decomposed into unknown chemicals as pD increased above 9 due to the observations of the disappearance of the triplet methine peak (**a**), which needs further investigation for identification.

Based on the reports using α-azido ether cleavable linkers in biological technologies,[39-40] the cleavage products could be biocompatible. Although aldehyde functional groups can interact with amines to form imines, the imines are generally hydrolyzed in aqueous solution to form carbonyl groups, especially, in aliphatic aldehyde.[37,88] In addition, aldehydes have been believed to be bioorthogonal functional groups.[37] Consequently, aldehydes were used for selective bioconjugation linkers through oximes or hydrazones without significantly changing the functions of biological molecules, suggesting aldehyde is one of the biocompatible functional groups. These facts may imply biocompatibility of cleavage products from α-azido ether reduction.

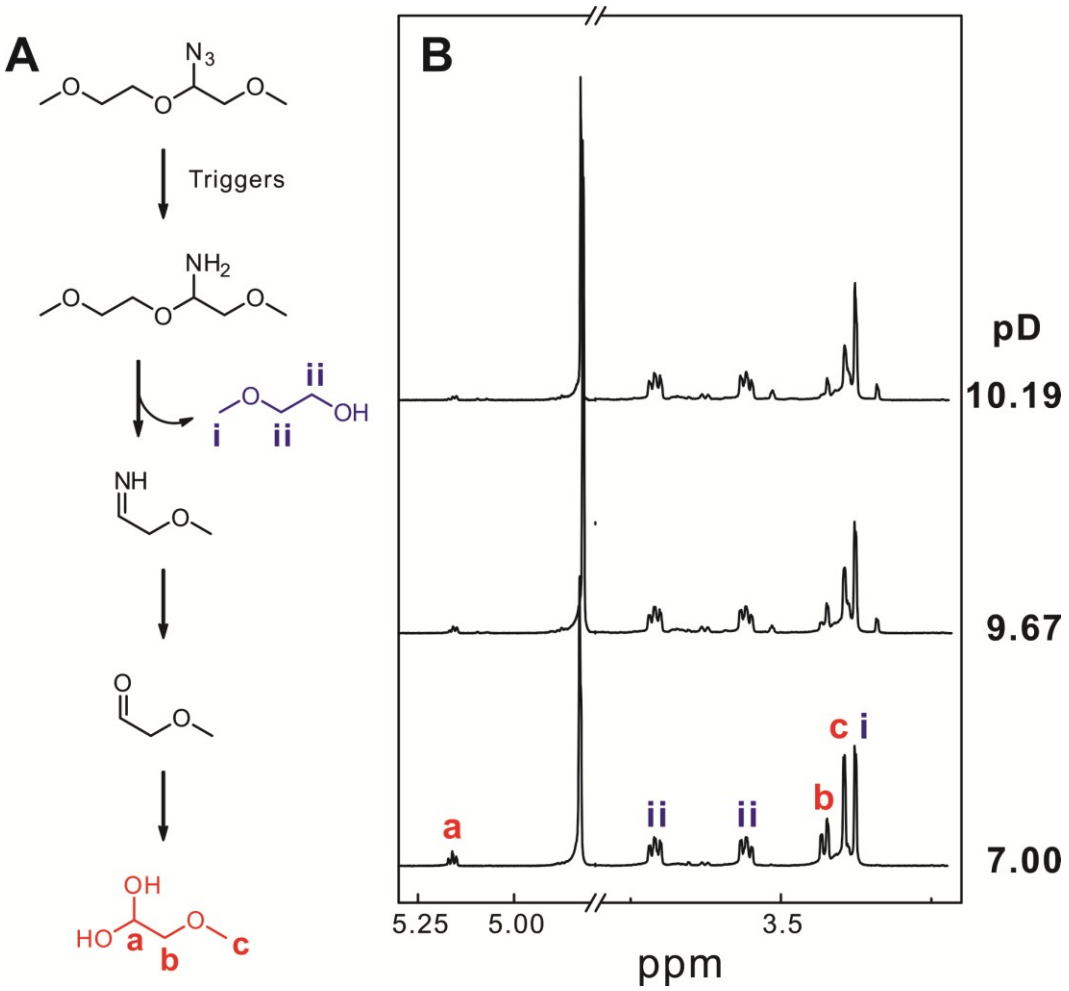

Figure 5-15. (**A**) Expected products from α-azido ether **1** reductive cleavage. (**B**) ^{1}H-NMR spectra of cleavage products from the reaction between α-azido ether **1** and TCEP in different pD (10.19, 9.67, and 7.00) buffered NMR solutions. The alcohol product was supported by the appearance of methoxy (**i**, singlet) protons at 3.38 ppm and methylene (**ii**, triplet) protons at 3.56 and 3.71 ppm. Hydrated aldehyde was formed after the reaction, supported by the peaks corresponding to triplet methine (**a**), doublet methlyene (**b**), and singlet methyl (**c**) at 5.16, 3.43, and 3.39 ppm, respectively, at neutral pD. The hydrated aldehyde was decomposed as the pD of the solution increased, supported by the decrease of those peaks (**a**, **b**, and **c**).

5.4 Summary

We have studied the characteristics of a novel cleavable α-azido ether linker and its reductive cleavage in aqueous solutions using UV-Vis and NMR spectroscopy. The hydrolytic stability of the α-azido ether functionalized molecules can be improved up to several years of half life by introduction of electronegative atoms (O or N) at the gamma position and a proton at the alpha position. Nucleophilic attack of deprotonated dithiol or phosphine triggers can initiate the cleavage of α-azido ether, resulting from pH dependence reaction rate. Although the results of the cleavage rate at neutral pH, which is the most important value for biological applications, were not maximum values when DHLA and TCEP were used as triggers, it could be improved by manipulating the pK_a value of triggers through chemical modifications[75-77] up to ~0.2 $M^{-1}s^{-1}$. That means a pseudo first order half life of α-azido ether would reach to ~ 1 h when 1 mM trigger is used, suggesting α-azido ether can be developed as cleavable linkers for many *in vitro* and *in vivo* biological applications. For example, cleavable linkers can be incorporated into a degradable hydrogel matrix for *in vitro* applications, including cell cuture and gel electrophoresis. Such linkers are also developed in *in vivo* degradable materials, such as, drug delivery systems, tissue regeneration scaffolds, degradable sutures, and degradable bioadhesives. In these applications, it would be anticipated to obtain a unique external control over the cleavage and stability due to bioorthogonal properties of α-azido ether and its triggers. This is unique compared to currently available systems because α-azido

ethers would be devoid of interference from environmental sources as they do not react with endogenous reducing agents.

Chapter 6. Degradable Polyacrylamide Gel Electrophoresis Using Cleavable α-Azido Ether for Efficient and Facile Recovery of Biological Molecules

6.1 Introduction

A crosslinked polymeric network is a structure in which polymers are connected through covalent or physical crosslinking. The polymeric network has been remarkably used in various applications, such as, stimuli-responsive particles or gels,[1] novel hybrid materials,[2-3] and protective outer layers.[4-6] The development of the polymeric networks in aqueous media has brought crosslinked hydrophilic polymeric networks called hydrogels, which contain substantial amounts of water in its network.[7] Many natural[8] and synthetic[9-10] polymers can be used to construct networks and their properties, such as, mechanical strength, viscoelasticity, and pore size, can be manipulated,[11-14] because of which they have become exceptional tools in numerous biological applications; a scaffold to mimic artificial extra-cellular matrix for 3D cell culture and tissue engineering,[15] a cargo to deliver toxic drugs or genes into a cell without side-effects,[16] and an inert matrix for the separation of biological molecules to analyze biological components and functions.[17] The hydrogel has historically been a part of a well-developed and ubiquitous biological

technique, called gel electrophoresis.[18] The hydrogel serves as an inert matrix for the electrophoretic separation of biological molecules depending on their migration length. Based on this technique numerous biological mysteries have been deciphered[19-20]; for example, protein molecular weight, subunit composition, protein-protein interaction and amino acid sequence in conjunction with mass spectrometry have been conducted; size of a nucleic acid and its fragments, its sequence information, and nucleic acid-protein interaction have also been analyzed.

The gel matrix for the electrophoresis can be synthesized using physical or chemical crosslinking in an agarose[21] or a polyacrylamide (PAAm)[22] gel, respectively. In common, the agarose gel has a larger pore size being suitable for larger biological molecules like DNA, while the PAAm gel has been used for mainly proteins due to its smaller pore size. However, nucleic acids are often analyzed using PAAm gels when high resolving power is required, leading to extremely pure molecules.[23] In gel electrophoresis, gigantic biological molecules are separated by charge, size, and shape.[24] The separated biological molecules are then frequently recovered for in-depth analysis,[20] such as, activity study,[25] a protein crystallization,[26] biological assembly study,[27] and a template for a biological reaction.[28]

Current methods for the recovery, including passive extraction and electroelution, often have limitations due to low yield and more effort using additional instrumentation.[20,29-31] Therefore, it is necessary to develop a better solution. There is a chemical solution to improve the recovery without any instrumentation. Chemical modification of a crosslinker promises gel degradation by chemical treatment, which

makes biological molecules free in the solution, leading to a more efficient and facile recovery.[29-30] Based on this idea, there were attempts to incorporate cleavable functional groups into the crosslinker, including 1,2-diol,[32-33] ester,[34-37] acetal,[29-30] and disulfide.[38-41] However, almost all cases require harsh cleavage conditions (*i.e.* 2% periodic acid, 1M NaOH, or pH < 5 acidic solution) that lead to irreversible damage to biological molecules. Although disulfide may be suitable as the cleavable linker because of mild cleavage condition (2% β-mercaptoethanol), the gelation requires careful temperature control to prevent C-S link formation due to a thiyl radical (RS·) in the radical polymerization of PAAm.[39]

We have developed an α-azido ether cleavable linker that is a bioorthogonal, chemically cleavable in mild cleavage conditions as well as having relevant cleavage timescale as described in the previous chapter. As a result, we replaced the Bis with a crosslinker containing α-azido ether (N_3EG_2), synthesized a degradable PAAm gel for gel electrophoresis, and recovered biological molecules by gel degradation after polyacrylamide gel electrophoresis (PAGE) as shown in Figure 6-1. Because our α-azido ether can be cleaved using mild and biocompatible conditions, we believe that the degradable PAGE using the α-azido ether functionality could improve upon the existing methods. Here, we showed a proof-of-concept for the recovery of biological molecules using the degradable PAGE synthesized from acrylamide and α-azido ether crosslinker. The recovery profiles of model biological macromolecules (proteins and DNA) from the PAAm gel matrix were obtained by measuring fluorescence or absorption to investigate how fast biological molecules were recovered. Furthermore, microRNA model molecules

were recovered and isolated through the degradable PAGE, and electrophoresed again to verify the success of the degradable PAGE.

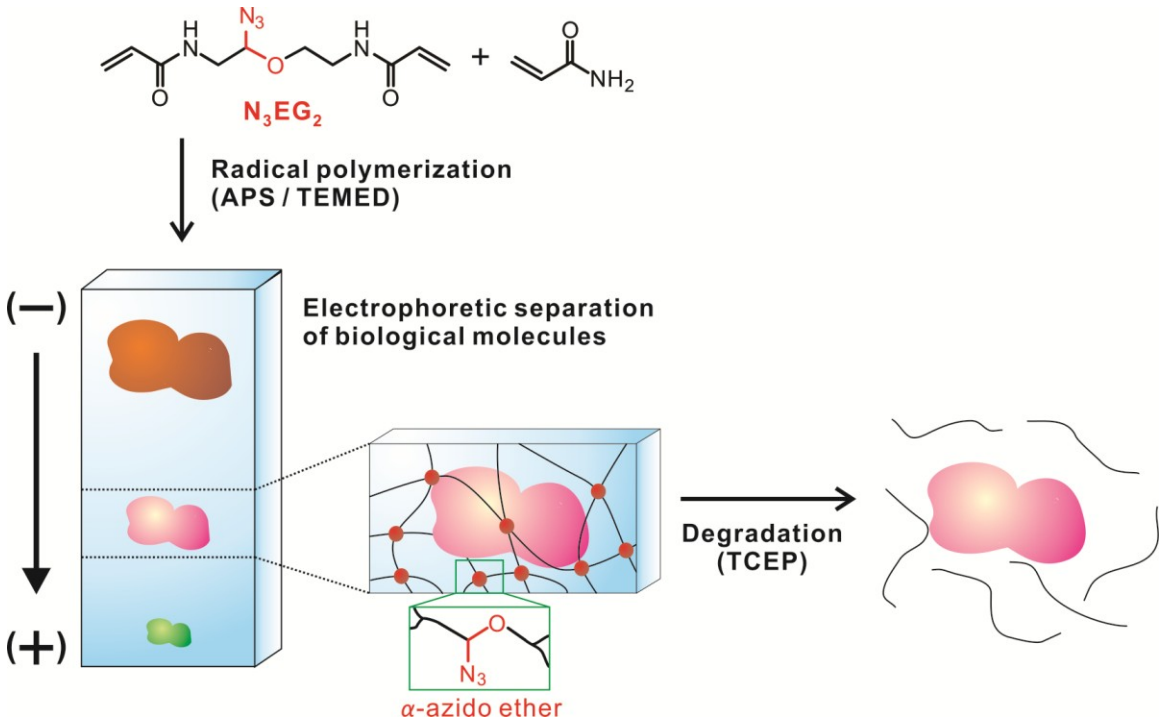

Figure 6-1. A schematic illustration of a degradable polyacrylamide gel electrophoresis (PAGE) using a α-azido ether crosslinker (N_3EG_2). A polyacrylamide gel (PAAm) was synthesized through a radical polymerization of acrylamide monomers and N_3EG_2 crosslinkers using APS/TEMED initiation system in aqueous solution. After biological molecules, such as, proteins, DNA, and RNA, are loaded on the top of the PAAm gel, the biological molecules are separated by gel electrophoresis. The gel containing the biological molecules is excised and embedded molecules are recovered from the gel in mild, biocompatible degradation conditions (TCEP solution).

6.2 Experimental Methods

6.2.1 General

TCEP was purchased from Thermo Fisher Scientific, Inc. (Rockford, IL) and deuterated NMR solvents were purchased from Cambridge Isotope Laboratories, Inc. (Andover, MA). DNA and RNA ladder were purchased from New England BioLabs, Inc. (Ipswich, MA). SYBR Green I and II dyes were purchased from Invitrogen (Carlsbad, CA). B-phycoerythrin fluorescent protein (B-PE, 240 kDa, λ_{ex} 490-560 nm, λ_{em} 575 nm) was purchased from Enzo Life Sciences (Farmingdale, NY). All other reagents were purchased from Aldrich (St. Louis, MO) unless otherwise noted. Tetramethylethylene-diamine (TEMED) was purified using distillation after refluxing in the presence of sodium for 2 h. Ammonium persulfate (APS) was recrystallized from water/EtOH mixture (30 g in 50/60 mL) by chilling the solution in a salt/ice bath. A GFP encoded plasmid was grown with shaking overnight at 37 ^{o}C[42] and the plasmid was purified using a QIAprep spin miniprep kit according to the manufacturer's manual (Qiagen, Germantown, MD). MicroRNA (400 nt) was synthesized according to the procedure similar to that described by Seelig.[28] Acryamide solution (40 %) and ethidium bromide solution were purchased from Bio-rad (Hercules, CA). SequaGel Sequencing system kit for 7.5 M urea denaturated PAGE was purchased from National Diagnostics (Mississauga, ON). Ultrapure water was generated from a Milli-Q water purification system (Millipore Inc.; Billerica, MA, R > 10 MΩ•cm). UV-Visible absorption spectra were obtained on a Hewlett-Packard 8453 UV-Vis spectrophotometer (Palo Alto, CA) or

a Nanodrop 2000C (Thermo Scientific, Wilmington, DE). PD-10 desalting columns were purchased from GE Healthcare (Pittsburgh, PA). ^{1}H NMR spectra were recorded on a Varian Unity (500 MHz) using a solvent peak as an internal standard.

6.2.2 Synthesis

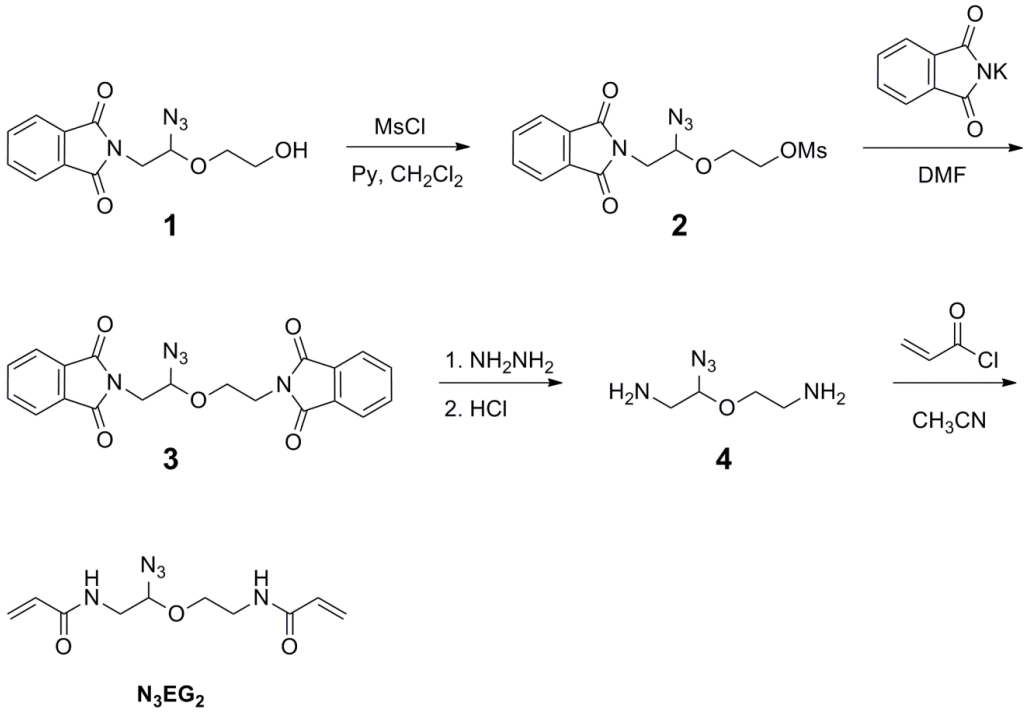

Figure 6-2. Synthetic scheme for α-azido ether crosslinker, N_3EG_2.

***N*-(2-(2-Phthalimido(1-azidoethoxy))ethyl)phthalimide (3).** Phthalimido(1,3-dioxolan-2-yl)methane (**1**, 44 g, 0.16 mol) was dissolved in dichloromethane (500 mL) and placed under nitrogen flow for 15 min on an ice bath. Pyridine (20 mL, 0.25 mol) and methanesulfonyl chloride (20 mL, 0.25 mol) were added slowly under constant stirring.

After stirring for 15 min, a nitrogen balloon was affixed and the mixture was allowed to warm room temperature, and stirring was maintained overnight. After this period, water (500 mL) was added to the reaction mixture and stirred for 2 h to remove any unreacted pyridine. The aqueous layer was removed and the organic layer was washed thrice with saturated aqueous sodium bicarbonate solution (500 mL) and once with brine (500 mL). The organic layer was dried with sodium sulfate and concentrated under reduced pressure to produce yellow oil in quantitative yield. The yellow oil (**2**, 55 g, 0.16 mol) was dissolved in dimethylformamide (500 mL). Potassium phthalimide was added, and the mixture was heated to 75 ^{o}C and stirred overnight under nitrogen atmosphere. The reaction mixture was cooled to room temperature and poured on to cold water resulting in a white precipitate. The precipitate was filtered and washed with ethanol. The product was purified by recrystallization from DMF/water solvent mixture to result in white granular crystals (51 g, 78 % yield). ^{1}H NMR (500 MHz, $CDCl_3$, δ) 7.78 (m, *4*H, Ar-*H*), 7.70 (m, *4*H, Ar-*H*), 4.81 (t, 1H, *J* = 6.2 Hz, C*H*N_3), 4.07 (m, 1H, OCH_2), 3.94 (m, 1H, OCH_2), 3.83-3.92 (m, 4H, OCH_2 and NCH_2)

2-(2-Aminoethoxy)-2-azidoethanamine (4). *N*-(2-(2-Phthalimido(1-azido-ethoxy))ethyl)phthalimide (**3**, 25 g, 62 mmol) was suspended in 0.3 M methanolic hydrazine (150 mL) and refluxed for 2 h. Aqueous hydrochloric acid (5 %, 100 mL) was then added to the solution resulting in the formation of a white precipitate. This suspension was then refluxed for 12 h. Insoluble components were filtered off after acidifying the mixture and the aqueous solution was washed twice with DCM (50 mL). Solid KOH was added to the aqueous solution to make the solution basic (pH > 10). The

basic solution was then extracted with DCM. The organic layers were combined, dried using sodium sulfate and concentrated under vacuum to produce a yellow oil (5.5 g, 61 %). ^{1}H NMR (500 MHz, $CDCl_3$, δ) 4.43 (t, J = 5.3 Hz, 1H, C*H*N_3), 3.86 (m, 1H, OCH_2), 3.59 (m, 1H, OCH_2), 2.94 (m, 4H, NCH_2), 1.37 (s, 4H, NH_2).

***N*-(2-(2-acrylamido-1-azidoethoxy)ethyl)acrylamide – N_3EG_2.** The crosslinker (N_3EG_2) was prepared according to the method similar to that described by Delgado *et al.* with the following modification.[43] 2-(2-Aminoethoxy)-2-azidoethanamine (**4**, 2.23 g, 15.4 mmol) in 60 mL acetonitrile was slowly added dropwise to a solution of acryloyl chloride (1.4 mL, 17.2 mmol) in 90 mL acetonitrile in an ice bath under nitrogen, resulting in the formation of yellow precipitates. The reaction mixture was warmed to room temperature and stirred overnight. The precipitates were filtered and washed with warm acetonitrile. The filtrates were stabilized by addition of 0.1 mL MEHQ (methyl ether hydroquinone, 10 mg / 1 mL methanol). The solution was concentrated to a few mL and remaining salts were removed by short (~2 cm) silica gel filtration using ethyl acetate washing. The solution was concentrated and the product was purified by silica gel column chromatography using ethyl acetate as eluents (R_f = 0.43, 634.5 mg, 29 %). The product N_3EG_2 was dissolved in degassed water with trace amounts of MEHQ and stored at -20 ^{o}C. ^{1}H NMR (500 MHz, $CDCl_3$, δ) 6.33 (m, 2H, CH_2=CH), 6.17 (m, 2H, CH_2=CH), 6.13-6.05 (br, 2H, CON*H*), 5.70 (m, 2H, CH_2=C*H*), 4.64 (t, J = 5.3 Hz, 1H, C*H*N_3), 3.93 (m, 1H, OCH_2), 3.71 (m, 3H, OCH_2CH_2), 3.49 (m, 2H, NCH_2).

6.2.3 Polyacrylamide gel electrophoresis

Degradable polyacrylamide gel using the N_3EG_2 was prepared according to the general protocols for conventionally available non-degradable polyacrylamide gel using the Bis crosslinker The degree of monomers and crosslinkers was regulated by parameters; the percentage of total monomers including crosslinkers (%T) and the crosslinker percentage (%C) according to the equations,

$$\%T = \frac{g\ of\ acrylamide + g\ of\ crosslinker}{total\ volume} \times 100\ (\%)$$

$$\%C = \frac{g\ of\ crosslinker}{g\ of\ acrylamide + g\ of\ crosslinker} \times 100\ (\%)$$

The gelation was initiated by a radical polymerization from TEMED (0.1 %) and APS (1 %) system and continued for about 1 - 2 h. Before samples were loaded, pre-electrophoresis was conducted for 15 – 30 min.

Native protein PAGE. Conventionally developed polyacrylamide gels (37.5:1 gel) were used for native protein PAGE. For comparison to the conventional gel, the mol ratio of a N_3EG_2 crosslinker was adjusted to that of the conventional gel. Gels were prepared from 10/4.3 (%T/%C) of total monomers and N_3EG_2 crosslinkers for the degradable PAGE and 10/2.6 (%T/%C) of total monomers and Bis crosslinkers for a control experiment in Tris·Cl buffers (pH 8.8 for a separating gel and pH 6.8 for a stacking gel). Gel electrophoresis was performed under the Tris-glycine (25 mM Tris and 192 mM glycine, pH 8.3) native running buffer. Samples were prepared by diluting B-PE and ferritin in 1x Tris/glycerol loading buffer (62.5 mM Tris and 10 % glycerol, pH 6.8). After the pre-electrophoresis at 120 V, samples were added to wells (30 μL of 0.8 mg/mL

B-PE or 2 mg/mL ferritin). The electrophoresis was then performed for 2 h at 120 V. Because the proteins had pink (B-PE) and brown (ferritin) colors, without a staining step the migrated protein bands were carefully excised using a razor. The proteins in the excised bands were used for the recovery study.

Native DNA PAGE. The native DNA PAGE was performed using a similar method as described above for the native protein PAGE with modifications. Gels were prepared from 5/5 (%T/%C) of total monomers and N_3EG_2 crosslinkers for the degradable PAGE and 5/3.6 (%T/%C) of total monomers and Bis crosslinkers for the control experiment in 1x TBE buffers (Tris-borate-EDTA pH 8.0, 89 mM Tris, 89 mM borate, and 2 mM EDTA). Gel electrophoresis was performed under 1x TBE buffer. Samples were prepared by diluting 1kb DNA ladder and GFP plasmid in 1x DNA loading buffer (5 % glycerol). After the pre-electrophoresis at 100 V, samples were added to wells (6 μL of 417 μg/mL 1kb DNA ladder or 15 μL of 37.5 μg/mL GFP plasmid). The electrophoresis was then performed for 1 h 40 m at 100 V. Next, the gels were stained using ethidium bromide solution (0.5 μg/mL) or 1x SYBR green I solution. The ethidium bromide stained gel were imaged using a Bio-Rad Molecular Imager FX. The migrated green fluorescent DNA bands from SYBR green I staining were carefully excised using a razor under UV light illumination, which were used for the recovery study.

Denaturating urea RNA PAGE. The denaturating urea PAGE was performed for RNA sample using a similar method as described above for the native DNA PAGE with modifications. Conventional gels were prepared from 4/5 (%T/%C) of total monomers and Bis crosslinker using denaturating 7.5 M urea SequaGel kits in 1x TBE

buffers. Degradable urea gels were prepared from 4/8 (%T/%C) of total monomers and N_3EG_2 crosslinker using denaturating 7.4 M urea gel in 1x TBE buffers. Gel electrophoresis was performed under 1x TBE buffer. RNA sample was prepared by diluting microRNA in 1x loading buffer (1.2 μg/μL, 3 % ficoll). After the pre-electrophoresis at 20 W for 30 m, 4 or 12 μL of microRNA samples were added to wells. The electrophoresis was then performed for 1 h at 150 V. Next, the microRNA bands were visualized by UV-shadowing method[44] and carefully excised using a razor under UV light illumination on a silica plate. The excised gels were stored at -70 ^{o}C.

6.2.4 Recovery of biological molecules

The biological molecules were recovered from the N_3EG_2 gels into the solution by degradation through reductive cleavage of N_3EG_2 crosslinker. The degradation of N_3EG_2 gels was performed using TCEP/TE solution (condition **i**). The recovery profiles of biological molecules were measured by fluorescence (B-PE and DNA) or UV-Vis (ferritin) spectrophotometry. For controls, recovery profiles of degradable N_3EG_2 and non-degradable Bis gels were obtained using TE solution (condition **ii**) and TCEP/TE solution (condition **iii**), respectively.

Proteins recovery. The excised N_3EG_2 band of the B-PE protein were placed in a capped fluorescence cuvette and 3 mL of 10 mM TCEP/TE for the degradation sample (**i**) or 10 mM TE for the control sample (**ii**) were then added to the cuvette (pH 8.0). In addition, the Bis band of the B-PE protein was mixed with 10 mM TCEP/TE for control

sample (**iii**). The samples were then incubated at room temperature. Fluorescence data of solutions, where the gels were settled down on the bottom of the cuvette, were collected by a Quantamaster fluorimeter (PTI, London, Ontario; λ_{ex} = 475 nm) using an excitation optical filter (FF01-492/SP-25, Semrock) to eliminate scattered light. Along with fluorescence data collection, fluorescence images of the gels in a 24-well plate were taken using a digital camera with bench-top UV-lamp illumination. After overnight incubation, the degradable gel (**i**) was not solubilized, leaving swelled gel without B-PE pink color in the gel. The B-PE protein was then isolated physically from the gel matrix and further purified by a PD-10 desalting column, in which each fraction (1 mL) was measured by a fluorimeter.

Ferritin samples were prepared the methods similar to that described in B-PE protein samples. Instead of fluorescence collection, UV-Vis absorption data of solutions, where gels were settled down on the bottom of the cuvette, were collected by HP 8453 UV-Vis spectrophotometer. After 24 h incubation, the brown band was disappeared. The ferritin protein was then isolated physically from the gel matrix and further purified by a PD-10 desalting column, in which each fraction was measured by UV-Vis spectrophotometer.

DNA recovery. The GFP plasmid band was handled similar to the method described in B-PE protein sample handling with modification. The solution contained 1x SYBR green I dye to quantify the DNA using fluorescence intensity of intercalated SYBR green I[45]. The temperatures of the cuvette were controlled in a water bath at 37 ^{o}C and ~50 ^{o}C. Fluorescence data of solutions, where gels were settled down on the bottom

of the cuvette, were collected by the PTI fluorimeter (λ_{ex} = 470 nm) using optical filters (FF01-492/SP-25 and BLP01-488R-25, Semrock) to eliminate scattered light. At each time of fluorescence measurement, the green fluorescence from DNA was imaged by a digital camera with bench-top UV-lamp.

MicroRNA recovery. MicroRNA was recovered by degradation of N_3EG_2 gel using TCEP solution and then isolated from the solution using TRI reagent extraction, followed by Qiagen RNeasy MinElute Cleanup Kit or LiCl precipitation[46]. For the extraction method, a gel was placed in a 1.5 mL tube, crushed using a plastic pipette tip, and then added 400 μL of 10 mM TCEP/TE buffer (pH 7.0). The tube was incubated at 80 ^{o}C for ~ 1 h with occasionally vortex. After completely degradation of the N_3EG_2 gels, 700 μL of TRI reagent and 140 μL of chloroform were added. After vortex, the tube was centrifuged and the top layer was transferred into a new tube. The solution was mixed with 400 μL of ethanol and purified using Qiagen RNeasy MinElute Cleanup Kit according to the manufacturer's manual without addition of RLT buffer. The isolated microRNA was quantified by Nanodrop 2000C (Thermo Scientific, Wilmington, DE).

For the LiCl precipitation, five N_3EG_2 gels were placed in a 1.5 mL tube, crushed using a plastic pipette tip, and then added 500 μL of 20 mM TCEP/TE buffer (pH 7.0). The tube was incubated at 80 ^{o}C for ~ 1 h with occasionally vortex. After completely degradation of the N_3EG_2 gels, 500 μL of 8 M LiCl was added and the solution was then incubated at -20 ^{o}C for 45 m. Next, the solution was centrifuged at 4 ^{o}C for 15 m and supernatant was discarded carefully. MicroRNA was then washed with 400 μL of 70 % EtOH using centrifugation and supernatant removal. After a white pellet of microRNA

was dried for 5 m, the microRNA was dissolved in 20 μL H_2O. The isolated microRNA was quantified by Nanodrop 2000C (Thermo Scientific, Wilmington, DE). The isolated microRNA was further analyzed using conventional Bis PAGE with a RNA ladder. After the electrophoretic separation, microRNA was stained using 1x SYBR green II dye and imaged by C-80 Epi-illumination UV Darkroom (UVP, LLC, Upland, CA).[47]

6.2.5 Expected degradation fraction of N_3EG_2

The degradation fraction of N_3EG_2 can be theoretically calculated using a mixed second order rate equation developed by Micheau *et al.*.[48] When the concentration of reactants (A and B) is different and a second order rate constant (k) is known, the fraction of B, which is lower amounts in reactants, can follow the equation;

$$Y = \frac{B}{B_0} = \frac{a}{(a+b)\exp(at) - b}\,; A_0 > B_0$$

$$a = k(A_0 - B_0), b = kB_0$$

In our experiment, TCEP concentration corresponds to A_0 due to excess amount used. The concentration of N_3EG_2 can be estimated from a gel size and a volume of TCEP solution. The gel size was assumed as 1 x 1 x 0.1 cm, resulting in 0.1 mL of volume.

6.3 Results and Discussion

6.3.1 Synthesis

Acrylamide groups were simply introduced into a crosslinker by reacting between acryloyl chlorides and an amine functionalized α-azido ether. The amine functionalized α-azido ether was initially synthesized through a benzoate protected α-azido ether followed by basic deprotection and Gabriel synthesis using a mesylate as an alternative to a halide[49] (Figure 6-3). However, the chemicals involved in this reaction scheme were a liquid being difficult for purification via recrystallization. Moreover, ring formation occurred during the deprotection of benzoate group lowering yield and purity. In contrast, when a phthalimide protected amine was used instead of a benzoate protected alcohol, developed by Ramasubramanian in Taton group, solid compounds were formed resulting in better yield and facile purification method via recrystallization. In the step of the N_3EG_2 crosslinker synthesis (acrylamide formation), a diamine α-azido ether was used as base, similar to procedure reported previously,[43] rather than use of additional bases like a triethylamine.[50] When the triethylamine was included in the reaction, there were always more unknown byproducts produced, leading to difficult purification and lower yield, compared to the developed procedure. The N_3EG_2 crosslinker was stabilized with BHT or MEHQ radical inhibitor to prevent from air polymerization during storage.

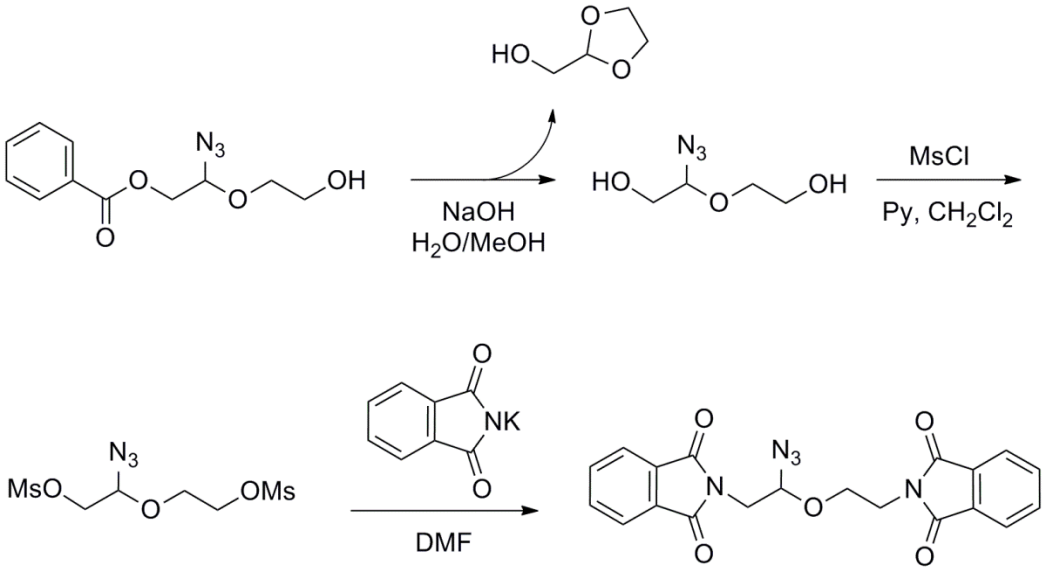

Figure 6-3. Initially designed synthetic scheme for a N_3EG_2 crosslinker through a benzoate protected α-azido ether.

6.3.2 Degradable polyacrylamide (PAAm) gelation

From the literature, it was reported that an azido group could react with an olefin to form a cycloaddition product.[51-52] As a consequence, there were a few reports in which an azide in a controlled radical polymerization reacted with an electron poor olefin, such as, an acrylate or an acrylamide monomer to produce cycloaddition products.[53-55] However, this cycloaddition reaction became negligible when the reaction was performed below 50 ^{o}C.[53,56] The well-controlled polymerization was obtained at 30 ^{o}C or room temperature using azide functionalized methacrylate[53,56] or *N*-isopropylacrylamide[57] monomers without any side reaction. In addition, an acrylamide monomer showed a lower reactivity for the cycloaddition than an acrylate monomer due to more electron

deficient double bond characteristics of the acrylate monomer, indicating that a successful radical polymerization could be achieved using the acrylamide monomers.[55] Moreover, Young in the Taton group has synthesized a degradable hydrogel using α-azido ether functionalized macromers and showed its degradation by chemical triggers.[58]

Therefore, the degradable PAAm gel was prepared by a radical polymerization of acrylamide monomers and the N_3EG_2 crosslinker using a catalyst-redox system of peroxide-amine (APS-TEMED) in aqueous solution, which is one of the widely used systems in PAGE.[24] Tertiary amines like TEMED were frequently used in the radical polymerization to accelerate a free radical formation from peroxides even in room temperature.[59-60] Although it seemed that the efficiency of N_3EG_2 crosslinker in the radical polymerization was little bit lower than that of Bis because the duration of gel casting needed more time than conventional Bis, a transparent N_3EG_2 functionalized PAAm gel was obtained after 1 h or more gelation, having similar appearance to that of the conventional PAAm gel. For the comparison to the conventional Bis gel, the molar ratio of a monomer to a crosslinker (N_3EG_2 or Bis) was adjusted. It should be noted that the gel can be casted without any detrimental effect, which was reported in the gel casted from a disulfide crosslinker due to the formation of RS· radical.[39]

6.3.3 Degradable native protein PAGE

The degradable native PAGE for protein recovery was performed to investigate how efficient and fast gigantic proteins were recovered from the gel into solution. The gel

concentration was adjusted to that of conventionally developed materials, 2.6 %C of Bis crosslinker (16.9 mM). For the comparison of recovered proteins out of the degradable gel, the same molarity of N_3EG_2 crosslinker was used to cast the degradable gel, leading to 4.3 %C of N_3EG_2. B-phycoerythrin fluorescent protein (240 kDa, pI ~4.2–4.4)[61-62] and ferritin (440 kDa, pI ~4.5)[63-64] were chosen as model proteins because they are commercially developed as biomarkers in a native protein ladder, more importantly, and have a color band giving facile visualization and tracking. During the native protein PAGE, B-PE bands were moved further than ferritin, mainly due to larger size of ferritin. After the electrophoretic separation, each protein was recovered out of the gel matrix by reductive cleavage of α-azido ether using 10 mM TCEP solution and the amounts of recovered protein were monitored.

The recovery profile of B-PE from the degradable N_3EG_2 gel with TCEP (**i**) was measured using fluorescence intensity in the solution. For control samples, the degradable N_3EG_2 gel and the conventional, non-degradable Bis gel were prepared and incubated in non-degradable (without TCEP, **ii**) and degradable (with TCEP, **iii**) solution, respectively. The B-PE was recovered from the gel gradually in all conditions, **i - iii**. But, the recovery of B-PE was faster in the degradable N_3EG_2 gel with the TCEP trigger (**i**), compared to control samples (**ii** and **iii**) as shown in Figure 6-4A. For example, the recovery amounts of B-PE using condition **i** was 1.5 and 1.7 times higher than that of condition **ii** and **iii**, respectively. The recovery profile of B-PE in the condition **i** was almost leveled off at 5 h and reached to maximum at 8 h, suggesting quantitative recovery of B-PE.

Consistent results were obtained from fluorescence images although these did not give quantitative results (Figure 6-4C). As incubation time increased, the fluorescence intensity became fainted and disappeared at 8 h in the degradable N_3EG_2 gel with the TCEP trigger (**i**), similar to the results from the recovery profile. For the N_3EG_2 gel without the TCEP (**ii**), although the fluorescence intensity became weaker with increasing incubation time, the fluorescence intensity was always relatively stronger than that of condition **i** as well as the fluorescence band was observed even at 17 h. On the other hand, the fluorescence intensity of **iii** was always the most intense over the entire experimental timescale.

We believed that the cleavage of N_3EG_2 led to degradation of the gel, leading to larger pores in the matrix through which more proteins diffused out. It caused the most increase fluorescence of the recovery profile (Figure 6-4A) and the most fainted pink band in the gel (Figure 6-4C) in the condition **i**. The result from the condition **ii** showed faster recovery compared to **iii**, presumably, due to longer and hydrophilic N_3EG_2 that absorbed more water. It caused the extended matrix to have larger pore sizes than that of the Bis gel. The observations indicated that when the degradable gel in the presence of the trigger (**i**) was used, faster and quantitative recovery of protein could be obtained, although the gel was not solublized within the experimental timescale.

In fact, non-solubilization resulted in efficient and facile isolation of B-PE from the gel matrix physically. Furthermore, small molecules like TCEP=O (oxidized TCEP by-products) were excluded using a desalting column in 1 - 3 mL elution volume (Figure 6-4D). It should be noted that the results might show that the degradable condition (**i**)

would be biocompatible because the fluorescence of B-PE did not change during the entire experiments.

Next, ferritin, which is a bigger protein, was used for recovery because it was expected to have slower diffusion and lower recovery yield. Similar to the results of B-PE, the recovery rate of ferritin in condition **i** was 1.7 and 3.0 times faster than that of the condition **ii** and **iii**, respectively (Figure 6-4B). After 24 h incubation, ferritin was still embedded in the gel in both of **ii** and **iii** while all ferritin was recovered in condition **i** because no more color band was left in the gel. Ferritin was further isolated from the gel matrix and small molecules using a desalting column with quantitative recovery yield (Figure 6-4D). The results show that if the N_3EG_2 gel and degradation condition (**i**) are applied in PAGE any gigantic proteins can be electrophoretically separated, recovered, and purified with improved yield that could not be obtained using the conventional PAGE.

It is possible to expect theoretical fraction of α-azido ether remaining in the gel with respect to time under the degradation condition using a mixed second order rate equation. Because a general excised gel size was 0.1 x 1 x 1 cm and 2 mL of 10 mM TCEP solution was added, the concentration of N_3EG_2 became 8 μM. The second order rate constant was obtained from the previous chapter as ~0.2 $M^{-1}s^{-1}$ at pH 8 in TCEP case. From the calculation, 31 % and 3.4 % of N_3EG_2 were left in the gel at 10 and 30 m, respectively. That might promise solubilization of the N_3EG_2 gel within 1 h under experimental conditions. However, the N_3EG_2 gel was not solubilized within the experimental condition (~24 h). It suggests that because the expected calculation was

based on the homogeneous reaction between α-azido ether molecule and TCEP in aqueous solution, its exertion to heterogeneous system was not applicable. In order to be more accurate expectation, heterogeneous reaction conditions need to be considered.

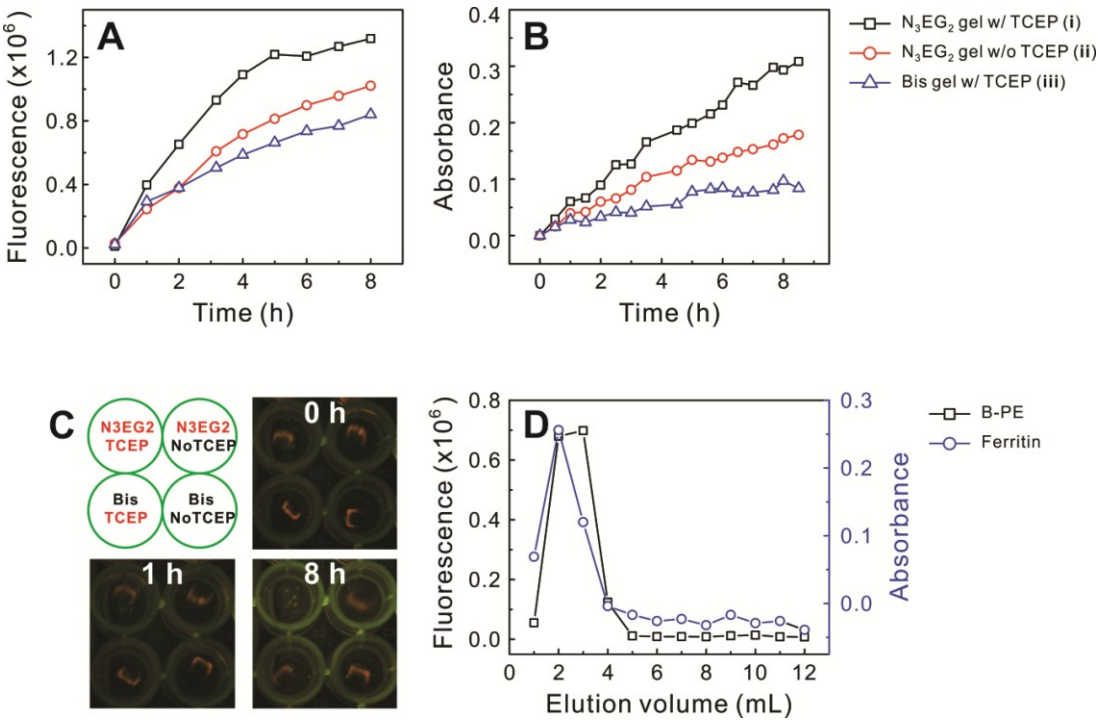

Figure 6-4. Protein recovery after PAGE. (**A**) Recovery profiles of a B-PE protein and (**B**) a ferritin from a degradable N_3EG_2 gel with a TCEP trigger solution (black square, **i**), a degradable N_3EG_2 gel without a TCEP trigger (red circle, **ii**), and a non-degradable Bis gel with a TCEP trigger (blue triangle, **iii**), measured by a fluorescence spectrophotometer (λ_{ex} 475 nm and λ_{em} 570 nm) and a UV-Vis spectrophotometer (absorbance at 400 nm), respectively. (**C**) Fluorescent images during B-PE recovery. A pink band indicated the embedded B-PE in the gel matrix. (**D**) Isolation of the recovered proteins from the degradable N_3EG_2 gel matrix and small molecules like TCEP and TCEP=O using a PD-10 desalting column. The concentration of isolated proteins, B-PE and ferritin, at each fraction (1 mL) were measured by a fluorescence (λ_{ex} 475 nm and λ_{em} 570 nm) and a UV-Vis spectrophotometer (absorbance at 400 nm), respectively.

6.3.4 Degradable PAGE for a nucleic acid

Next, a nucleic acid was separated and recovered from the degradable N_3EG_2 gel. Although a nucleic acid is commonly separated by the electrophoresis of an agarose gel that has larger pore size than a PAAm gel, a PAAm gel is often utilized to obtain an extremely pure nucleic acid using its better resolution and more sensitive detection methods[23,30]. In addition, using a larger biological molecule than a protein allows us to study the efficiency of the biocompatible, degradable N_3EG_2 gel for the recovery. As a result, nucleic acids, such as, a plasmid (4343 bp, 2638 kDa) and microRNA (400 nt, 128 kDa), were electrophoretically separated and recovered.

Because the plasmid had a larger size than the previous proteins, it was required that the gel concentration decreased to 5 %T. After the plasmid and DNA ladder were loaded into either of 5 %C (N_3EG_2) or 3.6 %C (Bis) gel, the DNA was separated electrophoretically. When the DNA bands were visualized using ethdium bromide fluorescence, separated DNA bands were observed for both N_3EG_2 and Bis gels according to a basepair (or size) in Figure 6-5A because DNA separation in the gel electrophoresis relied on the basepair (or size). In addition, another gel was prepared and stained with SYBR green I dye that has green fluorescence by intercalating into double strand DNA[45]. The green fluorescence band of plasmid was then cut and the plasmid DNA embedded in the gel matrix was recovered using the same method as above in the protein recovery except incubation temperature. Because DNA is relatively stable at a higher temperature, the gels were incubated at 37 and 50 ^{o}C to investigate temperature

effect on the recovery rate. The recovery rate was then measured by monitoring green fluorescence intensity with respect to the time.

From the recovery profiles (Figure 6-5C and D), it was observed that no plasmid DNA was liberated from the gel matrix under the non-degradable conditions, **ii** (degradable N_3EG_2 gel without TCEP trigger) and **iii** (non-degradable Bis gel with TCEP trigger) at both 37 and 55 ^oC. However, when the degradation of N_3EG_2 gel was triggered using TCEP at 37 ^oC, recovery of the plasmid DNA began at 3 h, followed by abrupt increase after 4 h, and completed at 6 h in which the gel was solubilized and quantitative recovery was obtained. The recovery rate was improved at elevated temperature 50 ^oC, based on the fact that recovery completion and gel solubilization were achieved at ~2.5 h. The results were also verified by fluorescence images of the embedded plasmid DNA (Figure 6-5B). In the images, the recovery of the plasmid DNA led to the disappearance of the green fluorescence band at 6.5 h at 37 ^oC in the degradation condition **i** only while the green fluorescence band was persisted in other non-degradation conditions (**ii** and **iii**). The results suggested that the recovery of large biological molecules like the plasmid DNA was completely restricted using the conventional Bis gel. But, when the degradable N_3EG_2 gel was replaced for the Bis gel any size of gigantic biological molecules could be recovered from the gel matrix using TCEP trigger. Moreover, the recovery time could be significantly reduced by increasing the temperature.

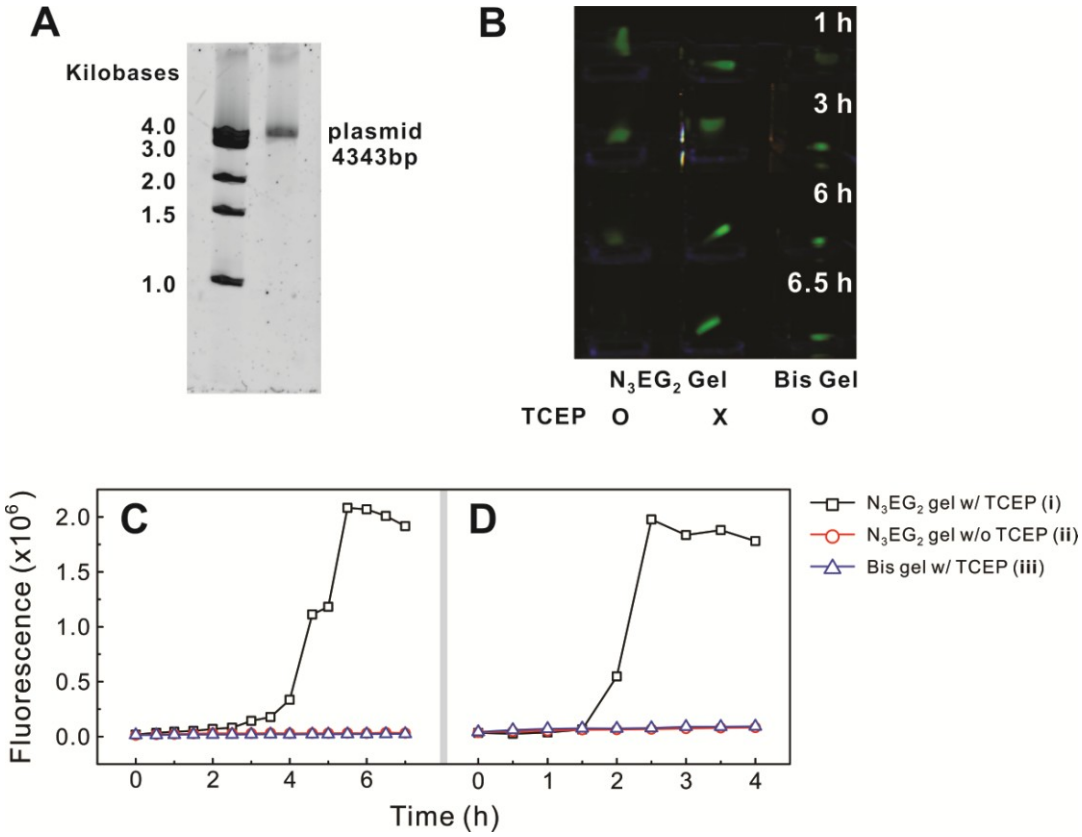

Figure 6-5. (**A**) Gel electrophoresis (5 %T / 5 %C N_3EG_2 polyacrylamide gel, 1x TBE) of a 1 kb DNA ladder and a plasmid DNA. After electrophoresis, the DNA bands were stained with ethidium bromide solution and then scanned to provide the image. (**B**) Green fluorescence images of intercalated SYBR green I into DNA under UV light illumination with respect to the time. Green fluorescence indicated an embedded plasmid DNA band in the gels. Recovery profiles of a plasmid DNA out of the gels incubated at 37 ^{o}C (**C**) and 50 ^{o}C (**C**), measured by a fluorescence intensity of the intercalated SYBR green I dye of dsDNA in the recovery solution. Only the degradation condition (**i**) could liberate the plasmid DNA from the gel matrix completely leading to the green band disappearance (**B**) and max fluorescence intensity (**C** and **D**), as a result of gel solubilization, while other non-degradable conditions (**ii** and **iii**) showed no change.

Micro RNA (microRNA) was also recovered using a similar method. Because RNA is single strand which might cause secondary structures leading to false separation[65], denaturating gel electrophoresis was performed using concentrated urea (~7.5 M). In addition, pre-electrophoresis was conducted to warm electrophoresis system to aid denaturation of RNA. After microRNA (400 nt) was electrophoretically separated, the microRNA band was simply excised using UV-shadowing method[44] (Figure 6-6A), followed by gel degradation using TCEP in pH 7.0 buffer to prevent hydrolysis of RNA. In order to reduce the recovery time, the gel was crushed and temperature was elevated to 80 ^{o}C which is frequently conducted in crush-and-soak method for recovery of small RNA[46]. As a result, the gel was solubilized within ~1 h that was faster than what was observed previously when the recovery was performed at 50 ^{o}C. Next, the microRNA was isolated from the solubilized gel and other small components using either of TRI reagent extraction (guanidine thiocyanate/phenol/ chloroform), followed by a Qiagen purification kit or LiCl precipitation method, which is frequently used in microRNA purification[46], to afford 21-47 % yield.

The isolated microRNA was further analyzed by a secondary PAGE to verify compatibility of degradation condition to microRNA. After the secondary gel electrophoresis, the same migration bands of microRNA before and after gel degradation were obtained as shown in Figure 6-6B. It indicated that the microRNA was inert under the degradation condition (10 mM TCEP, pH 7.0, 80 ^{o}C) being no structural change and hydrolysis even if the RNA is chemically unstable relative to DNA.

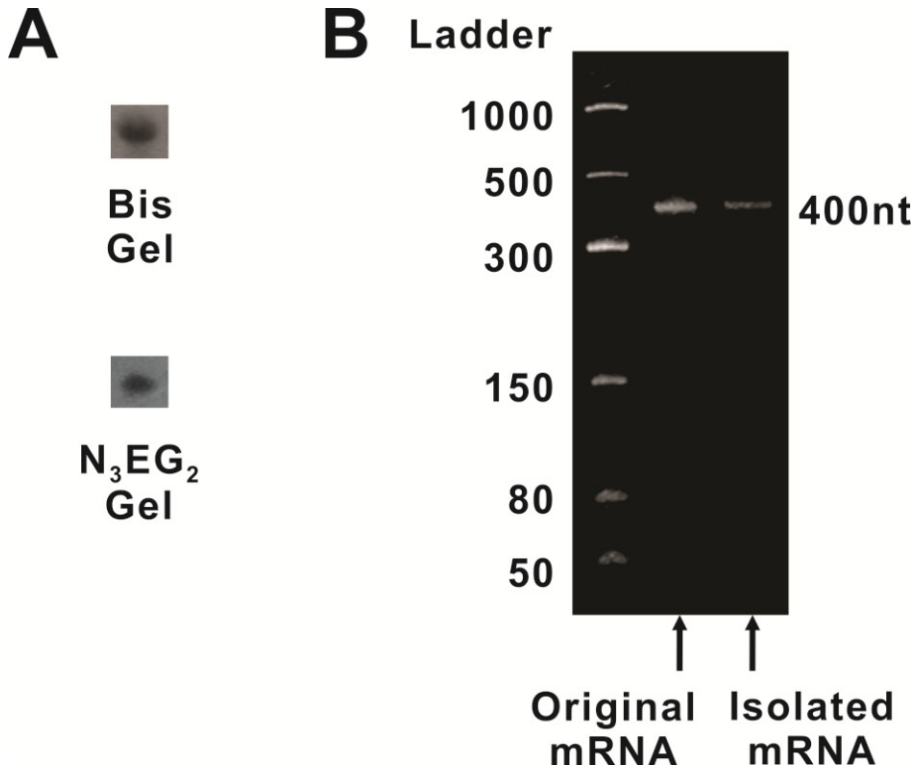

Figure 6-6. RNA denaturating urea gel electrophoresis. (**A**) Gel electrophoresis (4 %T polyacrylamide gel, 1x TBE, ~7.5 M urea) of 400nt microRNA. After electrophoresis, the RNA bands were visualized by UV-shadowing method to provide the image. (top) RNA band using a conventional 5 %C Bis polyacrylamide gel. (bottom) RNA band using a degradable 8 %C N_3EG_2 polyacrylamide gel. (**B**) Secondary denaturating urea gel electrophoresis of ssRNA ladder, original and isolated microRNA (400nt). After gel electrophoresis using a Bis gel, the gel was stained with SYBR green II solution and fluorescence image was taken under UV illumination. The isolated microRNA had the same migration as that of original microRNA, maintaining their size after degradation. The result indicated the degradation condition was compatible with RNA even in high temperature resulting in no effect on the RNA band migration.

6.4 Summary

We have demonstrated that the degradable PAGE using a bioorthogonal, chemically cleavable α-azido ether crosslinker (N_3EG_2) replaced for a Bis crosslinker is a chemical alternative to current methods for recovery of biological molecules, such as, protein, DNA, and RNA. Under the mild and biocompatible degradation conditions using TCEP trigger, the N_3EG_2 was cleaved making bigger pore size or solubilizing the entire gel matrix. As a result, the biological macromolecules were recovered rapidly and efficiently through simple diffusion compared to conventional methods. The degradation can be manipulated by elevating temperature to reduce degradation time. Although more optimization would be performed to improve the system, we anticipate that the degradable PAGE could be a versatile and universal tool for an efficient and facile recovery of biological molecules. In addition, the result has verified the proof-of-concept of incorporation of the bioorthogonal, chemically cleavable α-azido ether into a degradable hydrogel. As a result, we believe that the α-azido ether can be expanded to novel degradable biomaterials for *in vivo* applications, such as, drug delivery, bio-adhesive, and tissue regeneration scaffolds.

Chapter 7. Concluding Remarks

This thesis describes our efforts to develop novel nano/bio-materials and their biological applications. It demonstrates how chemistry can improve properties of nano/bio-materials that have been incorporated into biological technologies. As a result, the improved properties give benefits to the biological technologies. We anticipate that the developed chemistry in this thesis would provide tools for technological advance in biological applications.

Particularly, oligothiol stabilized AuNPs were prepared using the advantages of graft copolymer with thermally and chemically resistant AuNPs. The graft copolymer stabilized AuNPs were then integrated into a biological technology, SP-PCR, for rapid colorimetric post-PCR analysis to improve the current analytical method by excluding instrumental needs and removing subsequent analysis for target DNA detection. Although this thesis deals with only colorimetric target DNA detection, the graft copolymer stabilized AuNPs with SP-PCR would be further expanded into advanced PCR technologies; SNP detection using a sequence-specific restriction enzyme[1]; multiplex SP-PCR using AuNP-primer libraries composed of various sizes and shapes[2] that lead to simultaneous, automated target DNA detection through various methods[3]; and mobilized gene colonies that can be sequenced by a hybridization sequencing method or a currently being developed nanopore method.[4]

The bioorthgonal, chemically cleavable α-azido ether has also been studied as a essential part of degradable materials. The fundamental studies of the α-azido ether were

performed to elucidate its stability and cleavage kinetics, which gave the ways to improve its performance in degradable materials. A representative example of chemically degradable materials was also demonstrated by incorporating the α-azido ether into a polyacrylamide gel, which is an essential matrix in a biological technology, PAGE. Although the degradable gel showed the efficient and facile recovery of biological molecules through the chemical cleavage of the α-azido ether, it would become improved by further investigations: a simple preparation that can be achieved using a radical reaction of azide with benzyl ether,[5] development of triggers bearing low pK_a,[6-7] and catalytic cleavage of azide through visible-light-induced azide reduction.[8] Afterwards, the α-azido ether would hold a promise for novel cleavable linkers in degradable materials by chemical and/or light triggered degradation. Furthermore, it would be possible to use the α-azido ether as dual-functional groups in which ligation and cleavage reactions occur through Staudinger ligation and azide reduction, respectively.[9-10]

In conclusion, we anticipate that these efforts on surface functionalization of AuNPs with graft copolymers bearing oligothiols and the novel α-azido ether functionality with controllable chemical cleavage open a broad range of biological applications. As a consequence, we hope that these approaches would play an important role in advanced biomaterials as well as biotechnologies.

Bibliography

CHAPTER 1

(1) Drexler, E. "There's Plenty of Room at the Bottom" (Richard Feynman, Pasadena, 29 December 1959) 2009. http://metamodern.com/2009/12/29/theres-plenty-of-room-at-the-bottom%E2%80%9D-feynman-1959/.

(2) Feynman, R. P. There's Plenty of Room at the Bottom. http://media.wiley.com/product_data/excerpt/53/07803108/0780310853.pdf.

(3) Giljohann, D. A.; Mirkin, C. A., *Nature* **2009,** *462*, 461-464.

(4) Rosi, N. L.; Mirkin, C. A., *Chemical Reviews* **2005,** *105*, 1547-1562.

(5) Shirasaki, Y.; Supran, G. J.; Bawendi, M. G.; Bulovic, V., *Nature Photonics* **2013,** *7*, 13-23.

(6) Medintz, I. L.; Uyeda, H. T.; Goldman, E. R.; Mattoussi, H., *Nature Materials* **2005,** *4*, 435-446.

(7) Pankhurst, Q. A.; Connolly, J.; Jones, S. K.; Dobson, J., *Journal of Physics D: Applied Physics* **2003,** *36*, R167.

(8) Yoo, D.; Lee, J.-H.; Shin, T.-H.; Cheon, J., *Accounts of Chemical Research* **2011,** *44*, 863-874.

(9) Ajayan, P. M.; Tour, J. M., *Nature* **2007,** *447*, 1066-1068.

(10) Hu, L.; Hecht, D. S.; Grüner, G., *Chemical Reviews* **2010,** *110*, 5790-5844.

(11) Bell, A. T., *Science* **2003,** *299*, 1688-1691.

(12) Mahmoud, M. A.; Narayanan, R.; El-Sayed, M. A., *Accounts of Chemical Research* **2013**.

(13) Alkilany, A. M.; Lohse, S. E.; Murphy, C. J., *Accounts of Chemical Research* **2012,** *46*, 650-661.

(14) Rotello, V., *Nanoparticles Buliding Blocks for Nanotechnology*. Kluwer Academic/Plenum Publishers: New York, **2004**.

(15) Higby, G. J., *Gold Bulletin* **1982,** *15*, 130-140.

(16) Faraday, M., *Philosophical Transactions of the Royal Society of London* **1857,** *147*, 145-181.

(17) Turkevich, J.; Stevenson, P. C.; Hillier, J., *Discussions of the Faraday Society* **1951,** *11*, 55-75.

(18) Frens, G., *Nature Physical Science* **1973,** *241*, 20-22.

(19) Hayat, M. A., *Colloidal Gold: Principles, Methods, and Applications*. Academic Press, Inc.: San Diego, **1989**; Vol. 1.

(20) Nuzzo, R. G.; Allara, D. L., *Journal of the American Chemical Society* **1983,** *105*, 4481-4483.

(21) Mirkin, C. A.; Letsinger, R. L.; Mucic, R. C.; Storhoff, J. J., *Nature* **1996,** *382*, 607-609.

(22) Alivisatos, A. P.; Johnsson, K. P.; Peng, X.; Wilson, T. E.; Loweth, C. J.; Bruchez, M. P.; Schultz, P. G., *Nature* **1996,** *382*, 609-611.

(23) Taton, T. A.; Mirkin, C. A.; Letsinger, R. L., *Science* **2000,** *289*, 1757-1760.

(24) Nam, J.-M.; Park, S.-J.; Mirkin, C. A., *Journal of the American Chemical Society* **2002,** *124*, 3820-3821.

(25) Cao, Y. W. C.; Jin, R. C.; Mirkin, C. A., *Science* **2002,** *297*, 1536-1540.

(26) Park, S. Y.; Lytton-Jean, A. K. R.; Lee, B.; Weigand, S.; Schatz, G. C.; Mirkin, C. A., *Nature* **2008,** *451*, 553-556.

(27) Jain, S.; Hirst, D. G.; O'Sullivan, J. M., *British Journal of Radiology* **2012,** *85*, 101-113.

(28) Weintraub, K., *Nature* **2013,** *495*, S14-S16.

(29) Cretu, C.; Lingen, E., *Gold Bulletin* **1999,** *32*, 115-126.

(30) Jain, P. K.; Lee, K. S.; El-Sayed, I. H.; El-Sayed, M. A., *The Journal of Physical Chemistry B* **2006,** *110*, 7238-7248.

(31) Yguerabide, J.; Yguerabide, E. E., *Analytical Biochemistry* **1998,** *262*, 137-156.

(32) Mie, G., *Annalen der Physik* **1908,** *330*, 377-445.

(33) Haiss, W.; Thanh, N. T. K.; Aveyard, J.; Fernig, D. G., *Analytical Chemistry* **2007,** *79*, 4215-4221.

(34) Liu, X.; Atwater, M.; Wang, J.; Huo, Q., *Colloids and Surfaces B: Biointerfaces* **2007,** *58*, 3-7.

(35) Sonnichsen, C.; Reinhard, B. M.; Liphardt, J.; Alivisatos, A. P., *Nature Biotechnology* **2005,** *23*, 741-745.

(36) Yguerabide, J.; Yguerabide, E. E., *Analytical Biochemistry* **1998,** *262*, 157-176.

(37) Jain, P. K.; Huang, X.; El-Sayed, I. H.; El-Sayed, M. A., *Accounts of Chemical Research* **2008,** *41*, 1578-1586.

(38) Murphy, C. J.; Gole, A. M.; Stone, J. W.; Sisco, P. N.; Alkilany, A. M.; Goldsmith, E. C.; Baxter, S. C., *Accounts of Chemical Research* **2008,** *41*, 1721-1730.

(39) Hunter, R. J., *Foundations of colloid science*. 2nd ed.; Oxford University Press: **2001**.

(40) Love, J. C.; Estroff, L. A.; Kriebel, J. K.; Nuzzo, R. G.; Whitesides, G. M., *Chemical Reviews* **2005,** *105*, 1103-1170.

(41) Hiemenz, P. C.; Rajagopalan, R., *Principles of Colloid and Surface Chemistry*. 3rd ed.; CRC Press: **1997**.

(42) Sperling, R. A.; Parak, W. J., *Philosophical Transactions of the Royal Society A: Mathematical, Physical and Engineering Sciences* **2010,** *368*, 1333-1383.

(43) Ghosh, S. K.; Pal, T., *Chemical Reviews* **2007,** *107*, 4797-4862.

(44) Katz, E.; Willner, I., *Angewandte Chemie, International Edition* **2004,** *43*, 6042-6108.

(45) Shan, J.; Tenhu, H., *Chemical Communications* **2007**, 4580-4598.

(46) Kang, Y.; Taton, T. A., *Angewandte Chemie International Edition* **2005,** *44*, 409-412.

(47) Daniel, M.-C.; Astruc, D., *Chemical Reviews* **2003,** *104*, 293-346.

(48) Tkachenko, A. G.; Xie, H.; Coleman, D.; Glomm, W.; Ryan, J.; Anderson, M. F.; Franzen, S.; Feldheim, D. L., *Journal of the American Chemical Society* **2003,** *125*, 4700-4701.

(49) Chah, S.; Hammond, M. R.; Zare, R. N., *Chemistry & Biology* **2005,** *12*, 323-328.

(50) Lowe, A. B.; Sumerlin, B. S.; Donovan, M. S.; McCormick, C. L., *Journal of the American Chemical Society* **2002,** *124*, 11562-11563.

(51) Wuelfing, W. P.; Gross, S. M.; Miles, D. T.; Murray, R. W., *Journal of the American Chemical Society* **1998,** *120*, 12696-12697.

(52) Corbierre, M. K.; Cameron, N. S.; Sutton, M.; Mochrie, S. G. J.; Lurio, L. B.; Rühm, A.; Lennox, R. B., *Journal of the American Chemical Society* **2001,** *123*, 10411-10412.

(53) Zhu, M.-Q.; Wang, L.-Q.; Exarhos, G. J.; Li, A. D. Q., *Journal of the American Chemical Society* **2004,** *126*, 2656-2657.

(54) Wang, B.; Li, B.; Zhao, B.; Li, C. Y., *Journal of the American Chemical Society* **2008,** *130*, 11594-11595.

(55) Shan, J.; Nuopponen, M.; Jiang, H.; Kauppinen, E.; Tenhu, H., *Macromolecules* **2003,** *36*, 4526-4533.

(56) Gentilini, C.; Evangelista, F.; Rudolf, P.; Franchi, P.; Lucarini, M.; Pasquato, L., *Journal of the American Chemical Society* **2008,** *130*, 15678-15682.

(57) Nishi, H.; Kobatake, S., *Macromolecules* **2008,** *41*, 3995-4002.

(58) Hilf, S.; Kilbinger, A. F. M., *Macromolecules* **2009,** *42*, 4127-4133.

(59) Kruger, C.; Agarwal, S.; Greiner, A., *Journal of the American Chemical Society* **2008,** *130*, 2710-2711.

(60) Wilson, R.; Chen, Y.; Aveyard, J., *Chemical Communications* **2004**, 1156-1157.

(61) Jana, N. R.; Erathodiyil, N.; Jiang, J.; Ying, J. Y., *Langmuir* **2010,** *26*, 6503-6507.

(62) Huang, H.-M.; Chang, C.-Y.; Liu, I.-C.; Tsai, H.-C.; Lai, M.-K.; Tsiang, R. C.-C., *Journal of Polymer Science, Part A: Polymer Chemistry* **2005,** *43*, 4710-4720.

(63) Mangeney, C., et al., *Journal of the American Chemical Society* **2002,** *124*, 5811-5821.

(64) Teranishi, T.; Kiyokawa, I.; Miyake, M., *Advanced Materials* **1998,** *10*, 596-599.

(65) Wu, S.-H.; Huang, H.-M.; Chen, K.-C.; Hu, C.-W.; Hsu, C.-C.; Tsiang, R. C.-C., *Advanced Functional Materials* **2006,** *16*, 1959-1966.

(66) Han, D.-H.; Pan, C.-Y., *Journal of Polymer Science Part A: Polymer Chemistry* **2008,** *46*, 341-352.

(67) Wen, Y.; Jiang, X.; Yin, G.; Yin, J., *Chemical Communications* **2009**, 6595-6597.

(68) Abraham, S.; Kim, I.; Batt, Carl A., *Angewandte Chemie International Edition* **2007,** *46*, 5720-5723.

(69) Luo, S.; Xu, J.; Zhang, Y.; Liu, S.; Wu, C., *Journal of Physical Chemistry B* **2005,** *109*, 22159-22166.

(70) Costanzo, P. J.; Demaree, J. D.; Beyer, F. L., *Langmuir* **2006,** *22*, 10251-10257.

(71) Javakhishvili, I.; Hvilsted, S., *Biomacromolecules* **2008,** *10*, 74-81.

(72) Herdt, A. R.; Drawz, S. M.; Kang, Y.; Taton, T. A., *Colloids and Surfaces B: Biointerfaces* **2006,** *51*, 130-139.

(73) Klajn, R.; Gray, T. P.; Wesson, P. J.; Myers, B. D.; Dravid, V. P.; Smoukov, S. K.; Grzybowski, B. A., *Advanced Functional Materials* **2008,** *18*, 2763-2769.

(74) Wong, J. K. F.; Yip, S. P.; Lee, T. M. H., *Small* **2012,** *8*, 214-219.

(75) Hostetler, M. J.; Templeton, A. C.; Murray, R. W., *Langmuir* **1999,** *15*, 3782-3789.

(76) Guo, R.; Song, Y.; Wang, G.; Murray, R. W., *Journal of the American Chemical Society* **2005,** *127*, 2752-2757.

(77) Kassam, A.; Bremner, G.; Clark, B.; Ulibarri, G.; Lennox, R. B., *Journal of the American Chemical Society* **2006,** *128*, 3476-3477.

(78) Hong, R.; Han, G.; Fernández, J. M.; Kim, B.-J.; Forbes, N. S.; Rotello, V. M., *Journal of the American Chemical Society* **2006,** *128*, 1078-1079.

(79) Schoenfisch, M. H.; Pemberton, J. E., *Journal of the American Chemical Society* **1998,** *120*, 4502-4513.

(80) Song, Y.; Huang, T.; Murray, R. W., *Journal of the American Chemical Society* **2003,** *125*, 11694-11701.

(81) Coutts, M. J.; Cortie, M. B.; Ford, M. J.; McDonagh, A. M., *Journal of Physical Chemistry C* **2009,** *113*, 1325-1328.

(82) Nuzzo, R. G.; Zegarski, B. R.; Dubois, L. H., *Journal of the American Chemical Society* **1987,** *109*, 733-740.

(83) Schlenoff, J. B.; Li, M.; Ly, H., *Journal of the American Chemical Society* **1995,** *117*, 12528-12536.

(84) Schessler, H. M.; Karpovich, D. S.; Blanchard, G. J., *Journal of the American Chemical Society* **1996,** *118*, 9645-9651.

(85) Olson, M. A.; Coskun, A.; Klajn, R.; Fang, L.; Dey, S. K.; Browne, K. P.; Grzybowski, B. A.; Stoddart, J. F., *Nano Letters* **2009,** *9*, 3185-3190.

(86) Kang, J. S.; Taton, T. A., *Langmuir* **2012,** *28*, 16751-16760.

(87) Wojczykowski, K.; Mei; Jutzi, P.; Ennen, I.; Hutten, A.; Fricke, M.; Volkmer, D., *Chemical Communications* **2006**, 3693-3695.

(88) Li, Z.; Jin, R.; Mirkin, C. A.; Letsinger, R. L., *Nucleic Acids Research* **2002,** *30*, 1558-1562.

(89) Zhang, S.; Leem, G.; Srisombat, L.; Lee, T. R., *Journal of the American Chemical Society* **2008,** *130*, 113-120.

(90) Perumal, S.; Hofmann, A.; Scholz, N.; Rühl, E.; Graf, C., *Langmuir* **2011,** *27*, 4456-4464.

(91) Srisombat, L.; Zhang, S.; Lee, T. R., *Langmuir* **2010,** *26*, 41-46.

(92) van Pelt-Verkuil, E.; van Belkum, A.; Hays, J. P., *Principles and technical aspects of PCR amplification*. Springer: **2008**.

(93) Saiki, R.; Gelfand, D.; Stoffel, S.; Scharf, S.; Higuchi, R.; Horn, G.; Mullis, K.; Erlich, H., *Science* **1988,** *239*, 487-491.

(94) Saiki, R. K.; Scharf, S.; Faloona, F.; Mullis, K. B.; Horn, G. T.; Erlich, H. A.; Arnheim, N., *Science* **1985,** *230*, 1350-1354.

(95) Steitz, T. A., *Journal of Biological Chemistry* **1999,** *274*, 17395-17398.

(96) Wong, C.; Dowling, C. E.; Saiki, R. K.; Higuchi, R. G.; Erlich, H. A.; Kazazian, H. H., *Nature* **1987,** *330*, 384-386.

(97) Chien, A.; Edgar, D. B.; Trela, J. M., *Journal of Bacteriology* **1976,** *127*, 1550-1557.

(98) Chamberlain, J. S.; Gibbs, R. A.; Rainer, J. E.; Nguyen, P. N.; Thomas, C., *Nucleic Acids Research* **1988,** *16*, 11141-11156.

(99) Sanchez, J. A.; Pierce, K. E.; Rice, J. E.; Wangh, L. J., *Proceedings of the National Academy of Sciences of the United States of America* **2004,** *101*, 1933-1938.

(100) Heid, C. A.; Stevens, J.; Livak, K. J.; Williams, P. M., *Genome Research* **1996,** *6*, 986-994.

(101) Yang, M.; Kong, R. Y. C.; Kazmi, N.; Leung, A. K. C., *Chemistry Letters* **1998,** *27*, 257-258.

(102) Adessi, C.; Matton, G.; Ayala, G.; Turcatti, G.; Mermod, J.-J.; Mayer, P.; Kawashima, E., *Nucleic Acids Research* **2000,** *28*, e87.

(103) Fedurco, M.; Romieu, A.; Williams, S.; Lawrence, I.; Turcatti, G., *Nucleic Acids Research* **2006,** *34*, e22.

(104) Kohsaka, H.; Carson, D. A., *Journal of Clinical Laboratory Analysis* **1994,** *8*, 452-455.

(105) Rasmussen, S. R.; Rasmussen, H. B.; Larsen, M. R.; Hoff-Jørgensen, R.; Cano, R. J., *Clinical Chemistry* **1994,** *40*, 200-5.

(106) Oroskar, A. A.; Rasmussen, S. E.; Rasmussen, H. N.; Rasmussen, S. R.; Sullivan, B. M.; Johansson, A., *Clinical Chemistry* **1996,** *42*, 1547-55.

(107) Bentley, D. R., et al., *Nature* **2008,** *456*, 53-59.

(108) Hoffmann, J.; Hin, S.; Stetten, F. v.; Zengerle, R.; Roth, G., *RSC Advances* **2012**.

(109) Margulies, M., et al., *Nature* **2005,** *437*, 376-380.

(110) Shapero, M. H.; Leuther, K. K.; Nguyen, A.; Scott, M.; Jones, K. W., *Genome Research* **2001,** *11*, 1926-1934.

(111) Diehl, F.; Li, M.; He, Y.; Kinzler, K. W.; Vogelstein, B.; Dressman, D., *Nature Methods* **2006,** *3*, 551-559.

(112) Liu, H.; Li, S.; Wang, Z.; Ji, M.; Nie, L.; He, N., *Journal of Biotechnology* **2007,** *131*, 217-222.

(113) Palanisamy, R.; Connolly, A. R.; Trau, M., *Bioconjugate Chemistry* **2010,** *21*, 690-695.

(114) Chen, W.; Bian, A.; Agarwal, A.; Liu, L.; Shen, H.; Wang, L.; Xu, C.; Kotov, N. A., *Nano Letters* **2009,** *9*, 2153-2159.

(115) Pollet, J.; Janssen, K. P. F.; Knez, K.; Lammertyn, J., *Small* **2011,** *7*, 1003-1006.

(116) Wilson, T.; Carson, J.; Bowman, J., *Journal of Microbiological Methods* **2002,** *51*, 163-170.

(117) Shendure, J., et al., *Science* **2005,** *309*, 1728-1732.

(118) Kim, J. B.; Porreca, G. J.; Song, L.; Greenway, S. C.; Gorham, J. M.; Church, G. M.; Seidman, C. E.; Seidman, J. G., *Science* **2007,** *316*, 1481-1484.
(119) Mercier, J.-F.; Slater, G. W., *Biophysical Journal* **2005,** *89*, 32-42.
(120) Carmon, A.; Vision, T. J.; Mitchell, S. E.; Thannhauser, T. W.; Müller, U.; Kresovich, S., *BioTechniques* **2002,** *32*, 410-420.
(121) Tiemann-Boege, I.; Curtis, C.; Shinde, D. N.; Goodman, D. B.; Tavaré, S.; Arnheim, N., *Analytical Chemistry* **2009,** *81*, 5770-5776.
(122) Hoffmann, J.; Trotter, M.; Stetten, F. v.; Zengerle, R.; Roth, G., *Lab on a Chip* **2012,** *12*, 3049-3054.
(123) Rasmussen, S. E., *Annales de Biologie Clinique* **1990,** *48*, 647-650.
(124) Dressman, D.; Yan, H.; Traverso, G.; Kinzler, K. W.; Vogelstein, B., *Proceedings of the National Academy of Sciences* **2003,** *100*, 8817-8822.

CHAPTER 2

(1) Kang, J. S.; Taton, T. A., *Langmuir* **2012,** *28*, 16751-16760.
(2) Sperling, R. A.; Parak, W. J., *Philosophical Transactions of the Royal Society A: Mathematical, Physical and Engineering Sciences* **2010,** *368*, 1333-1383.
(3) Baraton, M.-I., *Synthesis, Functionalization and Surface Treatment of Nanoparticles*. American Scientific Publishers: Stevenson Ranch, California, **2003**.
(4) Love, J. C.; Estroff, L. A.; Kriebel, J. K.; Nuzzo, R. G.; Whitesides, G. M., *Chemical Reviews (Washington, DC, United States)* **2005,** *105*, 1103-1170.
(5) Katz, E.; Willner, I., *Angewandte Chemie, International Edition* **2004,** *43*, 6042-6108.
(6) Alivisatos, A. P.; Johnsson, K. P.; Peng, X.; Wilson, T. E.; Loweth, C. J.; Bruchez, M. P.; Schultz, P. G., *Nature* **1996,** *382*, 609-611.
(7) Mirkin, C. A.; Letsinger, R. L.; Mucic, R. C.; Storhoff, J. J., *Nature* **1996,** *382*, 607-609.
(8) Giljohann, D. A.; Seferos, D. S.; Prigodich, A. E.; Patel, P. C.; Mirkin, C. A., *Journal of the American Chemical Society* **2009,** *131*, 2072-2073.

(9) Tkachenko, A. G.; Xie, H.; Coleman, D.; Glomm, W.; Ryan, J.; Anderson, M. F.; Franzen, S.; Feldheim, D. L., *Journal of the American Chemical Society* **2003,** *125*, 4700-4701.

(10) Aubin-Tam, M.-E.; Hamad-Schifferli, K., *Langmuir* **2005,** *21*, 12080-12084.

(11) de la Fuente, J. M.; Barrientos, A. G.; Rojas, T. C.; Rojo, J.; Cañada, J.; Fernández, A.; Penadés, S., *Angewandte Chemie, International Edition* **2001,** *40*, 2257-2261.

(12) Wuelfing, W. P.; Gross, S. M.; Miles, D. T.; Murray, R. W., *Journal of the American Chemical Society* **1998,** *120*, 12696-12697.

(13) Corbierre, M. K.; Cameron, N. S.; Sutton, M.; Mochrie, S. G. J.; Lurio, L. B.; Rühm, A.; Lennox, R. B., *Journal of the American Chemical Society* **2001,** *123*, 10411-10412.

(14) Wilson, R.; Chen, Y.; Aveyard, J., *Chemical Communications* **2004**, 1156-1157.

(15) Jana, N. R.; Erathodiyil, N.; Jiang, J.; Ying, J. Y., *Langmuir* **2010,** *26*, 6503-6507.

(16) Huang, H.-M.; Chang, C.-Y.; Liu, I.-C.; Tsai, H.-C.; Lai, M.-K.; Tsiang, R. C.-C., *Journal of Polymer Science, Part A: Polymer Chemistry* **2005,** *43*, 4710-4720.

(17) Teranishi, T.; Kiyokawa, I.; Miyake, M., *Advanced Materials* **1998,** *10*, 596-599.

(18) Wu, S.-H.; Huang, H.-M.; Chen, K.-C.; Hu, C.-W.; Hsu, C.-C.; Tsiang, R. C.-C., *Advanced Functional Materials* **2006,** *16*, 1959-1966.

(19) Han, D.-H.; Pan, C.-Y., *Journal of Polymer Science Part A: Polymer Chemistry* **2008,** *46*, 341-352.

(20) Abraham, S.; Kim, I.; Batt, Carl A., *Angewandte Chemie International Edition* **2007,** *46*, 5720-5723.

(21) Luo, S.; Xu, J.; Zhang, Y.; Liu, S.; Wu, C., *Journal of Physical Chemistry B* **2005,** *109*, 22159-22166.

(22) Zalipsky, S., *Bioconjugate Chemistry* **1995,** *6*, 150-165.

(23) Otsuka, H.; Nagasaki, Y.; Kataoka, K., *Advanced Drug Delivery Reviews* **2003,** *55*, 403-419.

(24) Herdt, A. R.; Drawz, S. M.; Kang, Y.; Taton, T. A., *Colloids and Surfaces B: Biointerfaces* **2006,** *51*, 130-139.

(25) Klajn, R.; Bishop, K. J. M.; Fialkowski, M.; Paszewski, M.; Campbell, C. J.; Gray, T. P.; Grzybowski, B. A., *Science* **2007,** *316*, 261-264.
(26) Bhatt, N.; Huang, P.-J. J.; Dave, N.; Liu, J., *Langmuir* **2011,** *27*, 6132-6137.
(27) Kassam, A.; Bremner, G.; Clark, B.; Ulibarri, G.; Lennox, R. B., *Journal of the American Chemical Society* **2006,** *128*, 3476-3477.
(28) Hong, R.; Han, G.; Fernández, J. M.; Kim, B.-J.; Forbes, N. S.; Rotello, V. M., *Journal of the American Chemical Society* **2006,** *128*, 1078-1079.
(29) Song, Y.; Murray, R. W., *Journal of the American Chemical Society* **2002,** *124*, 7096-7102.
(30) Chompoosor, A.; Han, G.; Rotello, V. M., *Bioconjugate Chemistry* **2008,** *19*, 1342-1345.
(31) Song, Y.; Huang, T.; Murray, R. W., *Journal of the American Chemical Society* **2003,** *125*, 11694-11701.
(32) Nuzzo, R. G.; Zegarski, B. R.; Dubois, L. H., *Journal of the American Chemical Society* **1987,** *109*, 733-740.
(33) Schessler, H. M.; Karpovich, D. S.; Blanchard, G. J., *Journal of the American Chemical Society* **1996,** *118*, 9645-9651.
(34) Bain, C. D.; Troughton, E. B.; Tao, Y. T.; Evall, J.; Whitesides, G. M.; Nuzzo, R. G., *Journal of the American Chemical Society* **1989,** *111*, 321-335.
(35) Guo, R.; Song, Y.; Wang, G.; Murray, R. W., *Journal of the American Chemical Society* **2005,** *127*, 2752-2757.
(36) Ingram, R. S.; Hostetler, M. J.; Murray, R. W., *Journal of the American Chemical Society* **1997,** *119*, 9175-9178.
(37) Flynn, N. T.; Tran, T. N. T.; Cima, M. J.; Langer, R., *Langmuir* **2003,** *19*, 10909-10915.
(38) Schoenfisch, M. H.; Pemberton, J. E., *Journal of the American Chemical Society* **1998,** *120*, 4502-4513.
(39) Shon, Y.-S.; Lee, T. R., *Journal of Physical Chemistry B* **2000,** *104*, 8192-8200.
(40) Zhang, S.; Leem, G.; Srisombat, L.; Lee, T. R., *Journal of the American Chemical Society* **2008,** *130*, 113-120.

(41) Srisombat, L.; Zhang, S.; Lee, T. R., *Langmuir* **2010,** *26*, 41-46.
(42) Wojczykowski, K.; Mei; Jutzi, P.; Ennen, I.; Hutten, A.; Fricke, M.; Volkmer, D., *Chemical Communications* **2006**, 3693-3695.
(43) Perumal, S.; Hofmann, A.; Scholz, N.; Rühl, E.; Graf, C., *Langmuir* **2011,** *27*, 4456-4464.
(44) Li, Z.; Jin, R.; Mirkin, C. A.; Letsinger, R. L., *Nucleic Acids Research* **2002,** *30*, 1558-1562.
(45) Inglis, A. J.; Sinnwell, S.; Davis, T. P.; Barner-Kowollik, C.; Stenzel, M. H., *Macromolecules* **2008,** *41*, 4120-4126.
(46) Frens, G., *Nature Physical Science* **1973,** *241*, 20-22.
(47) Liu, X.; Atwater, M.; Wang, J.; Huo, Q., *Colloids and Surfaces B: Biointerfaces* **2007,** *58*, 3-7.
(48) Pasche, S.; De Paul, S. M.; Vörös, J.; Spencer, N. D.; Textor, M., *Langmuir* **2003,** *19*, 9216-9225.
(49) Lee, S.; Spencer, N. D., *Langmuir* **2008,** *24*, 9479-9488.
(50) Park, J. W.; Mok, H.; Park, T. G., *Journal of Controlled Release* **2010,** *142*, 238-244.
(51) Wattendorf, U.; Koch, M. C.; Walter, E.; Voros, J.; Textor, M.; Merkle, H. P., *Biointerphases* **2006,** *1*, 123-133.
(52) Feuz, L.; Leermakers, F. A. M.; Textor, M.; Borisov, O., *Langmuir* **2008,** *24*, 7232-7244.
(53) Gon, S.; Santore, M. M., *Langmuir* **2011,** *27*, 1487-1493.
(54) Jeon, S. I.; Lee, J. H.; Andrade, J. D.; De Gennes, P. G., *Journal of Colloid and Interface Science* **1991,** *142*, 149-158.
(55) Szleifer, I., *Biophysical Journal* **1997,** *72*, 595-612.
(56) Mok, H.; Park, J. W.; Park, T. G., *Bioconjugate Chemistry* **2008,** *19*, 797-801.
(57) Miyamoto, D.; Oishi, M.; Kojima, K.; Yoshimoto, K.; Nagasaki, Y., *Langmuir* **2008,** *24*, 5010-5017.
(58) Miyata, K.; Kakizawa, Y.; Nishiyama, N.; Harada, A.; Yamasaki, Y.; Koyama, H.; Kataoka, K., *Journal of the American Chemical Society* **2004,** *126*, 2355-2361.

(59) Maurizi, L.; Bisht, H.; Bouyer, F.; Millot, N., *Langmuir* **2009,** *25*, 8857-8859.
(60) Kelly, K. L.; Coronado, E.; Zhao, L. L.; Schatz, G. C., *Journal of Physical Chemistry B* **2002,** *107*, 668-677.
(61) Liu, Y.; Shipton, M. K.; Ryan, J.; Kaufman, E. D.; Franzen, S.; Feldheim, D. L., *Analytical Chemistry* **2007,** *79*, 2221-2229.
(62) Takae, S.; Akiyama, Y.; Otsuka, H.; Nakamura, T.; Nagasaki, Y.; Kataoka, K., *Biomacromolecules* **2005,** *6*, 818-824.
(63) Xia, X.; Yang, M.; Wang, Y.; Zheng, Y.; Li, Q.; Chen, J.; Xia, Y., *ACS Nano* **2011,** *6*, 512-522.
(64) Hurst, S. J.; Lytton-Jean, A. K. R.; Mirkin, C. A., *Analytical Chemistry* **2006,** *78*, 8313-8318.
(65) Zareie, H. M.; Boyer, C.; Bulmus, V.; Nateghi, E.; Davis, T. P., *ACS Nano* **2008,** *2*, 757-765.
(66) Ghosh, S. K.; Pal, T., *Chemical Reviews (Washington, DC, United States)* **2007,** *107*, 4797-4862.
(67) Dulkeith, E., et al., *Physical Review Letters* **2002,** *89*, 203002.
(68) Stewart, M. H.; Susumu, K.; Mei, B. C.; Medintz, I. L.; Delehanty, J. B.; Blanco-Canosa, J. B.; Dawson, P. E.; Mattoussi, H., *Journal of the American Chemical Society* **2010,** *132*, 9804-9813.
(69) Hou, W.; Dasog, M.; Scott, R. W. J., *Langmuir* **2009,** *25*, 12954-12961.
(70) Agasti, S. S.; You, C.-C.; Arumugam, P.; Rotello, V. M., *Journal of Materials Chemistry* **2008,** *18*, 70-73.
(71) VandeVondele, S.; Vörös, J.; Hubbell, J. A., *Biotechnology and Bioengineering* **2003,** *82*, 784-790.
(72) Zhen, G.; Falconnet, D.; Kuennemann, E.; Vörös, J.; Spencer, N. D.; Textor, M.; Zürcher, S., *Advanced Functional Materials* **2006,** *16*, 243-251.

CHAPTER 3

(1) Saiki, R.; Gelfand, D.; Stoffel, S.; Scharf, S.; Higuchi, R.; Horn, G.; Mullis, K.; Erlich, H., *Science* **1988,** *239*, 487-491.

(2) Heid, C. A.; Stevens, J.; Livak, K. J.; Williams, P. M., *Genome Research* **1996,** *6*, 986-994.

(3) Leslie, D. C., et al., *Journal of the American Chemical Society* **2012,** *134*, 5689-5696.

(4) Ho, H.-A.; Boissinot, M.; Bergeron, M. G.; Corbeil, G.; Doré, K.; Boudreau, D.; Leclerc, M., *Angewandte Chemie International Edition* **2002,** *41*, 1548-1551.

(5) Lou, X.; Lewis, M. S.; Gorman, C. B.; He, L., *Analytical Chemistry* **2005,** *77*, 4698-4705.

(6) Kelly, K. L.; Coronado, E.; Zhao, L. L.; Schatz, G. C., *Journal of Physical Chemistry B* **2002,** *107*, 668-677.

(7) Elghanian, R.; Storhoff, J. J.; Mucic, R. C.; Letsinger, R. L.; Mirkin, C. A., *Science* **1997,** *277*, 1078-1081.

(8) Taton, T. A.; Mirkin, C. A.; Letsinger, R. L., *Science* **2000,** *289*, 1757-1760.

(9) Alivisatos, A. P.; Johnsson, K. P.; Peng, X.; Wilson, T. E.; Loweth, C. J.; Bruchez, M. P.; Schultz, P. G., *Nature* **1996,** *382*, 609-611.

(10) Mirkin, C. A.; Letsinger, R. L.; Mucic, R. C.; Storhoff, J. J., *Nature* **1996,** *382*, 607-609.

(11) Li; Rothberg, L. J., *Journal of the American Chemical Society* **2004,** *126*, 10958-10961.

(12) Jung, Y. L.; Jung, C.; Parab, H.; Cho, D.-Y.; Park, H. G., *Chembiochem* **2011,** *12*, 1387-1390.

(13) Deng, H., et al., *Analytical Chemistry* **2012,** *84*, 1253-1258.

(14) Wong, J. K. F.; Yip, S. P.; Lee, T. M. H., *Small* **2012,** *8*, 214-219.

(15) Zhao, Y.; Xu, L.; Kuang, H.; Wang, L.; Xu, C., *Journal of Materials Chemistry* **2012,** *22*, 5574-5580.

(16) Kuang, H.; Zhao, S.; Chen, W.; Ma, W.; Yong, Q.; Xu, L.; Wang, L.; Xu, C., *Biosensors and Bioelectronics* **2011,** *26*, 2495-2499.

(17) Cai, M.; Li, F.; Zhang, Y.; Wang, Q., *Nano Research* **2010,** *3*, 557-563.

(18) Chen, W.; Bian, A.; Agarwal, A.; Liu, L.; Shen, H.; Wang, L.; Xu, C.; Kotov, N. A., *Nano Letters* **2009,** *9*, 2153-2159.

(19) Shen, H. B.; Hu, M.; Wang, Y. B.; Zhou, H. Q., *Biophysical Chemistry* **2005,** *115*, 63-66.

(20) Storhoff, J. J.; Fritz, B. M.; Herrmann, M. Real-Time Monitoring of PCR Amplification Using Nanoparticle Probes. WO/2003/048769, **2003**.

(21) Klajn, R.; Gray, T. P.; Wesson, P. J.; Myers, B. D.; Dravid, V. P.; Smoukov, S. K.; Grzybowski, B. A., *Advanced Functional Materials* **2008,** *18*, 2763-2769.

(22) Klajn, R.; Bishop, K. J. M.; Fialkowski, M.; Paszewski, M.; Campbell, C. J.; Gray, T. P.; Grzybowski, B. A., *Science* **2007,** *316*, 261-264.

(23) Herdt, A. R.; Drawz, S. M.; Kang, Y.; Taton, T. A., *Colloids and Surfaces B: Biointerfaces* **2006,** *51*, 130-139.

(24) Guo, R.; Song, Y.; Wang, G.; Murray, R. W., *Journal of the American Chemical Society* **2005,** *127*, 2752-2757.

(25) Song, Y.; Murray, R. W., *Journal of the American Chemical Society* **2002,** *124*, 7096-7102.

(26) Hill, H. D.; Mirkin, C. A., *Nature Protocols* **2006,** *1*, 324-336.

(27) Li, Z.; Jin, R.; Mirkin, C. A.; Letsinger, R. L., *Nucleic Acids Research* **2002,** *30*, 1558-1562.

(28) Hong, R.; Han, G.; Fernández, J. M.; Kim, B.-J.; Forbes, N. S.; Rotello, V. M., *Journal of the American Chemical Society* **2006,** *128*, 1078-1079.

(29) Bhatt, N.; Huang, P.-J. J.; Dave, N.; Liu, J., *Langmuir* **2011,** *27*, 6132-6137.

(30) Mittal, S.; Bushman, F.; Orgel, L. E., *Journal of Chemical Technology & Biotechnology* **2003,** *78*, 471-473.

(31) Wan, W.; Yeow, J. T. W., *Nanotechnology* **2009,** *20*, 325702.

(32) Wong, J. F.; Yip, S.; Lee, T. H., *Nano Research* **2012,** *5*, 585-594.

(33) Schwabacher, A. W.; Lane, J. W.; Schiesher, M. W.; Leigh, K. M.; Johnson, C. W., *The Journal of Organic Chemistry* **1998,** *63*, 1727-1729.

(34) Kang, J. S.; Taton, T. A., *Langmuir* **2012,** *28*, 16751-16760.

(35) Marks, I. S.; Kang, J. S.; Jones, B. T.; Landmark, K. J.; Cleland, A. J.; Taton, T. A., *Bioconjugate Chemistry* **2011,** *22*, 1259-1263.

(36) Liu, X.; Atwater, M.; Wang, J.; Huo, Q., *Colloids and Surfaces B: Biointerfaces* **2007,** *58*, 3-7.

(37) Zhang, S.; Leem, G.; Srisombat, L.; Lee, T. R., *Journal of the American Chemical Society* **2008,** *130*, 113-120.

(38) Dougan, J. A.; Karlsson, C.; Smith, W. E.; Graham, D., *Nucleic Acids Research* **2007,** *35*, 3668-3675.

(39) Parak, W. J.; Pellegrino, T.; Micheel, C. M.; Gerion, D.; Williams, S. C.; Alivisatos, A. P., *Nano Letters* **2002,** *3*, 33-36.

(40) Zanchet, D.; Micheel, C. M.; Parak, W. J.; Gerion, D.; Alivisatos, A. P., *Nano Letters* **2000,** *1*, 32-35.

(41) Özdemir, C.; Güner, A., *Journal of Applied Polymer Science* **2006,** *101*, 203-216.

(42) Li, H.; Huang, J.; Lv, J.; An, H.; Zhang, X.; Zhang, Z.; Fan, C.; Hu, J., *Angewandte Chemie International Edition* **2005,** *44*, 5100-5103.

(43) Chen, P., et al., *Nature Nanotechnology* **2011,** *6*, 639-644.

(44) Margulies, M., et al., *Nature* **2005,** *437*, 376-380.

(45) Shendure, J., et al., *Science* **2005,** *309*, 1728-1732.

(46) Diehl, F.; Li, M.; He, Y.; Kinzler, K. W.; Vogelstein, B.; Dressman, D., *Nature Methods* **2006,** *3*, 551-559.

(47) Kojima, T.; Takei, Y.; Ohtsuka, M.; Kawarasaki, Y.; Yamane, T.; Nakano, H., *Nucleic Acids Research* **2005,** *33*, e150.

(48) Shendure, J.; Ji, H., *Nature Biotechnology* **2008,** *26*, 1135-1145.

(49) Fedurco, M.; Romieu, A.; Williams, S.; Lawrence, I.; Turcatti, G., *Nucleic Acids Research* **2006,** *34*, e22.

(50) Sjöroos, M.; Ilonen, J.; Lövgren, T., *Clinical Chemistry* **2001,** *47*, 498-504.

(51) Reinhard, B. M.; Sheikholeslami, S.; Mastroianni, A.; Alivisatos, A. P.; Liphardt, J., *Proceedings of the National Academy of Sciences* **2007,** *104*, 2667-2672.

(52) Liu, G. L., et al., *Nature Nanotechnology* **2006,** *1*, 47-52.

(53) Hill, H. D.; Millstone, J. E.; Banholzer, M. J.; Mirkin, C. A., *ACS Nano* **2009,** *3*, 418-424.

(54) Tiemann-Boege, I.; Curtis, C.; Shinde, D. N.; Goodman, D. B.; Tavaré, S.; Arnheim, N., *Analytical Chemistry* **2009,** *81*, 5770-5776.

(55) Palanisamy, R.; Connolly, A. R.; Trau, M., *Bioconjugate Chemistry* **2010,** *21*, 690-695.

(56) Nicewarner Peña, S. R.; Raina, S.; Goodrich, G. P.; Fedoroff, N. V.; Keating, C. D., *Journal of the American Chemical Society* **2002,** *124*, 7314-7323.

(57) Gijs, M. A. M.; Lacharme, F. d. r.; Lehmann, U., *Chemical Reviews* **2009,** *110*, 1518-1563.

(58) Adessi, C.; Matton, G.; Ayala, G.; Turcatti, G.; Mermod, J.-J.; Mayer, P.; Kawashima, E., *Nucleic Acids Research* **2000,** *28*, e87.

(59) Huber, M.; Losert, D.; Hiller, R.; Harwanegg, C.; Mueller, M. W.; Schmidt, W. M., *Analytical Biochemistry* **2001,** *299*, 24-30.

(60) Dai, Q.; Liu, X.; Coutts, J.; Austin, L.; Huo, Q., *Journal of the American Chemical Society* **2008,** *130*, 8138-8139.

(61) Falabella, J. B.; Cho, T. J.; Ripple, D. C.; Hackley, V. A.; Tarlov, M. J., *Langmuir* **2010,** *26*, 12740-12747.

(62) Zipper, H.; Brunner, H.; Bernhagen, J.; Vitzthum, F., *Nucleic Acids Research* **2004,** *32*, e103.

(63) Kramer, M. F.; Coen, D. M., Enzymatic Amplification of DNA by PCR: Standard Procedures and Optimization. In *Current Protocols in Toxicology*, John Wiley & Sons, Inc.: **2001**.

(64) Chi, C.; Vargas-Lara, F.; Tkachenko, A. V.; Starr, F. W.; Gang, O., *ACS Nano* **2012,** *6*, 6793-6802.

(65) Srisa-Art, M.; Dyson, E. C.; deMello, A. J.; Edel, J. B., *Analytical Chemistry* **2008,** *80*, 7063-7067.

(66) Henry, M. R.; Wilkins Stevens, P.; Sun, J.; Kelso, D. M., *Analytical Biochemistry* **1999,** *276*, 204-214.

(67) Fan, Z. H.; Mangru, S.; Granzow, R.; Heaney, P.; Ho, W.; Dong, Q.; Kumar, R., *Analytical Chemistry* **1999,** *71*, 4851-4859.

CHAPTER 4

(1) Barenberg, S. A.; Brash, J. L.; Narayan, R.; Redpath, A. E., *Degradable materials : perspectives, issues and opportunities : the first international scientific consensus workshop proceedings*. CRC Press: **1990**.

(2) Gross, R. A.; Kalra, B., *Science* **2002,** *297*, 803-807.

(3) Seliktar, D., *Science* **2012,** *336*, 1124-1128.

(4) D. Nicodemus, G.; J. Bryant, S., *Tissue Engineering: Part B* **2008,** *14*, 149-165.

(5) Seelert, H.; Krause, F., *Electophoresis* **2008,** *29*, 2617-2636.

(6) Kloxin, A. M.; Kasko, A. M.; Salinas, C. N.; Anseth, K. S., *Science* **2009,** *324*, 59-63.

(7) Lasprilla, A. J. R.; Martinez, G. A. R.; Lunelli, B. H.; Jardini, A. L.; Filho, R. M., *Biotechnology Advances* **2012,** *30*, 321-328.

(8) LeGeros, R. Z., *Clinical Materials* **1993,** *14*, 65-88.

(9) Ehrlich, H.; Demadis, K. D.; Pokrovsky, O. S.; Koutsoukos, P. G., *Chemical Reviews* **2010,** *110*, 4656-4689.

(10) Horcajada, P.; Gref, R.; Baati, T.; Allan, P. K.; Maurin, G.; Couvreur, P.; Férey, G.; Morris, R. E.; Serre, C., *Chemical Reviews* **2011,** *112*, 1232-1268.

(11) Van Vlierberghe, S.; Dubruel, P.; Schacht, E., *Biomacromolecules* **2011,** *12*, 1387-1408.

(12) Leriche, G.; Chisholm, L.; Wagner, A., *Bioorganic & Medicinal Chemistry* **2012,** *20*, 571-582.

(13) van Nostrum, C. F.; Veldhuis, T. F. J.; Bos, G. W.; Hennink, W. E., *Polymer* **2004,** *45*, 6779-6787.

(14) Hisano, N.; Morikawa, N.; Iwata, H.; Ikada, Y., *Journal of Biomedical Materials Research* **1998,** *40*, 115-123.

(15) Hu, J.; Zhang, G.; Liu, S., *Chemical Society Reviews* **2012,** *41*, 5933-5949.

(16) Zhao, H.; Sterner, E. S.; Coughlin, E. B.; Theato, P., *Macromolecules* **2012,** *45*, 1723-1736.

(17) Smith, R. J.; Capaldi, R. A.; Muchmore, D.; Dahlquist, F., *Biochemistry* **1978,** *17*, 3719-3723.

(18) Verhelst, S. H. L.; Fonović, M.; Bogyo, M., *Angewandte Chemie International Edition* **2007,** *46*, 1284-1286.

(19) Hangauer, M. J.; Bertozzi, C. R., *Angewandte Chemie* **2008,** *120*, 2428-2431.

(20) Guo, J., et al., *Proceedings of the National Academy of Sciences* **2008,** *105*, 9145-9150.

(21) Franzini, R. M.; Kool, E. T., *Journal of the American Chemical Society* **2009,** *131*, 16021-16023.

(22) Luo, Y.; hoichet, M. S., *Nature Materials* **2004,** *3*, 1476-1122.

(23) Kloxin, A. M.; Tibbitt, M. W.; Anseth, K. S., *Nature Protocols* **2010,** *5*, 1867-87.

(24) Vesterberg, O., *Electophoresis* **1993,** *14*, 1243-1249.

(25) Merrifield, R. B., *Journal of the American Chemical Society* **1963,** *85*, 2149-2154.

(26) Matteucci, M. D.; Caruthers, M. H., *Journal of the American Chemical Society* **1981,** *103*, 3185-3191.

(27) Wang, S.-S., *Journal of the American Chemical Society* **1973,** *95*, 1328-1333.

(28) Parrott, M. C.; Luft, J. C.; Byrne, J. D.; Fain, J. H.; Napier, M. E.; DeSimone, J., *Journal of the American Chemical Society* **2010,** *132*, 17928-17932.

(29) Bruyère, H.; Westwell, A. D.; Jones, A. T., *Bioorganic & Medicinal Chemistry Letters* **2010,** *20*, 2200-2203.

(30) Cui, L.; Cohen, J. L.; Chu, C. K.; Wich, P. R.; Kierstead, P. H.; Fréchet, J. M. J., *Journal of the American Chemical Society* **2012,** *134*, 15840-15848.

(31) Griset, A. P.; Walpole, J.; Liu, R.; Gaffey, A.; Colson, Y. L.; Grinstaff, M. W., *Journal of the American Chemical Society* **2009,** *131*, 2469-2471.

(32) Murthy, N.; Xu, M.; Schuck, S.; Kunisawa, J.; Shastri, N.; Fréchet, J. M. J., *Proceedings of the National Academy of Sciences* **2003,** *100*, 4995-5000.

(33) Aryal, S.; Hu, C.-M. J.; Zhang, L., *ACS Nano* **2009,** *4*, 251-258.

(34) Gao, W.; Chan, J. M.; Farokhzad, O. C., *Molecular Pharmaceutics* **2010,** *7*, 1913-1920.

(35) Speers, A. E.; Cravatt, B. F., *Journal of the American Chemical Society* **2005,** *127*, 10018-10019.

(36) Dieterich, D. C.; Link, A. J.; Graumann, J.; Tirrell, D. A.; Schuman, E. M., *Proceedings of the National Academy of Sciences of the United States of America* **2006,** *103*, 9482-9487.

(37) Phelps, E. A.; Landázuri, N.; Thulé, P. M.; Taylor, W. R.; García, A. J., *Proceedings of the National Academy of Sciences* **2010,** *107*, 3323-3328.

(38) Olson, E. S.; Jiang, T.; Aguilera, T. A.; Nguyen, Q. T.; Ellies, L. G.; Scadeng, M.; Tsien, R. Y., *Proceedings of the National Academy of Sciences of the United States of America* **2010,** *107*, 4311-4316.

(39) Pullela, P. K.; Chiku, T.; Carvan, M. J.; Sem, D. S., *Analytical Biochemistry* **2006,** *352*, 265-273.

(40) Gao, W.; Langer, R.; Farokhzad, O. C., *Angewandte Chemie-International Edition* **2010,** *49*, 6567-6571.

(41) Zhang, W.; Song, J.; Mu, L.; Zhang, B.; Liu, L.; Xing, Y.; Wang, K.; Li, Z.; Wang, R., *Bioorganic & Medicinal Chemistry Letters* **2011,** *21*, 1452-1455.

(42) Yokoshima, S.; Abe, Y.; Watanabe, N.; Kita, Y.; Kan, T.; Iwatsubo, T.; Tomita, T.; Fukuyama, T., *Bioorganic & Medicinal Chemistry Letters* **2009,** *19*, 6869-6871.

(43) Long, L.; Lin, W.; Chen, B.; Gao, W.; Yuan, L., *Chemical Communications* **2011,** *47*, 893-895.

(44) Whitesides, G. M.; Lilburn, J. E.; Szajewski, R. P., *The Journal of Organic Chemistry* **1977,** *42*, 332-338.

(45) Gartner, C. A.; Elias, J. E.; Bakalarski, C. E.; Gygi, S. P., *Journal of Proteome Research* **2007,** *6*, 1482-1491.

(46) Chen, Q., et al., *Journal of Controlled Release* **2010,** *144*, 227-232.

(47) Lee, H.-M.; Larson, D. R.; Lawrence, D. S., *ACS Chemical Biology* **2009,** *4*, 409-427.

(48) Vivero-Escoto, J. L.; Slowing, I. I.; Wu, C.-W.; Lin, V. S. Y., *Journal of the American Chemical Society* **2009,** *131*, 3462-+.

(49) Fedorovich, N. E.; Oudshoorn, M. H.; van Geemen, D.; Hennink, W. E.; Alblas, J.; Dhert, W. J. A., *Biomaterials* **2009,** *30*, 344-353.

(50) Meinhardt, M.; Krebs, R.; Anders, A.; Heinrich, U.; Tronnier, H., *Journal of Biomedical Optics* **2008,** *13*, 044030-044030.

(51) Yang, Y., et al., *Angewandte Chemie International Edition* **2012,** *51*, 3125-3129.

(52) Sinha, D. K., et al., *Chembiochem* **2010,** *11*, 653-663.

(53) Neveu, P.; Aujard, I.; Benbrahim, C.; Le Saux, T.; Allemand, J.-F.; Vriz, S.; Bensimon, D.; Jullien, L., *Angewandte Chemie International Edition* **2008,** *47*, 3744-3746.

(54) Leriche, G.; Budin, G.; Brino, L.; Wagner, A., *European Journal of Organic Chemistry* **2010**, 4360-4364.

(55) Li, H.; Franzini, R. M.; Bruner, C.; Kool, E. T., *Chembiochem* **2010,** *11*, 2132-2137.

(56) Franzini, R. M.; Kool, E. T., *Chemistry – A European Journal* **2011,** *17*, 2168-2175.

(57) Franzini, R. M.; Kool, E. T., *Bioconjugate Chemistry* **2011,** *22*, 1869-1877.

(58) Harcourt, E. M.; Kool, E. T., *Nucleic Acids Research* **2012,** *40*, e65.

(59) Proudnikov, D.; Mirzabekov, A., *Nucleic Acids Research* **1996,** *24*, 4535-4542.

(60) Cera, C.; Egbertson, M.; Teng, S. P.; Crothers, D. M.; Danishefsky, S. J., *Biochemistry* **1989,** *28*, 5665-5669.

(61) Sletten, E. M.; Bertozzi, C. R., *Accounts of Chemical Research* **2011,** *44*, 666-676.

(62) Sletten, E. M.; Bertozzi, C. R., *Angewandte Chemie International Edition* **2009,** *48*, 6974-6998.

(63) Saxon, E.; Bertozzi, C. R., *Science* **2000,** *287*, 2007-2010.

(64) Lin, F. L.; Hoyt, H. M.; van Halbeek, H.; Bergman, R. G.; Bertozzi, C. R., *Journal of the American Chemical Society* **2005,** *127*, 2686-2695.

(65) Bentley, D. R., et al., *Nature* **2008,** *456*, 53-59.

(66) Tiselius, A., *Transactions of the Faraday Society* **1937,** *33*, 524-531.

(67) Smithies, O., *Biochemical Journal* **1955,** *61*, 629-641.

(68) Raymond, S.; Weintraub, L., *Science* **1959,** *130*, 711.

(69) Stellwagen, N. C., *Electophoresis* **2009,** *30*, S188-S195.

(70) Gianazza, E.; Righetti, P. G., *Electophoresis* **2009,** *30*, S112-S121.

(71) Rabilloud, T., *Journal of Proteomics* **2010,** *73*, 1562-1572.

(72) Klose, J., *Electophoresis* **2009,** *30*, S142-S149.

(73) Allen, R. C.; Budowle, B., *Gel electrophoresis of proteins and nucleic acids*. Walter de Gruyter: New York, **1994**.

(74) Hawcroft, D. M., *Electrophoresis*. Oxford University Press: **1997**.

(75) Heegaard, N. H. H., *Electophoresis* **2009,** *30*, S229-S239.

(76) Kinoshita, E.; Kinoshita-Kikuta, E.; Matsubara, M.; Aoki, Y.; Ohie, S.; Mouri, Y.; Koike, T., *Electophoresis* **2009,** *30*, 550-559.

(77) Alberts, B.; Johnson, A.; Lewis, J.; Raff, M.; Roberts, K.; Walter, P., *Molecular Biology of the Cell*. 5th ed.; Garland Science: **2007**.

(78) Krause, F., *Electrophoresis* **2006,** *27*, 2759-2781.

(79) Poetsch, A.; Neff, D.; Seelert, H.; Schägger, H.; Dencher, N. A., *Biochimica et Biophysica Acta (BBA) - Biomembranes* **2000,** *1466*, 339-349.

(80) Coppola, J. A.; Luse, D. S., *Journal of Molecular Biology* **1984,** *178*, 415-437.

(81) Seelig, B., *Nature Protocols* **2011,** *6*, 540-552.

(82) Scheer, J. M.; Ryan, C. A., *Analytical Biochemistry* **2001,** *298*, 130-132.

(83) Antal, J.; Banyasz, B.; Buzas, Z., *Electrophoresis* **2007,** *28*, 508-511.

(84) Kim, Y. K.; Kwon, Y. J., *Electophoresis* **2010,** *31*, 1656-1661.

(85) Kim, Y. K.; Kwon, Y. J., *Proteomics* **2009,** *9*, 3765-3771.

(86) Young, R. W.; Fulhorst, H. W., *Analytical Biochemistry* **1965,** *11*, 389-391.

(87) Armitage, B., *Chemical Reviews* **1998,** *98*, 1171-1200.

(88) Gelfi, C.; Righetti, P. G., *Electophoresis* **1981,** *2*, 213-219.

(89) Righetti, P. G.; Brost, B. C. W.; Snyder, R. S., *Journal of Biochemical and Biophysical Methods* **1981,** *4*, 347-363.

(90) Anker, H. S., *FEBS Letters* **1970,** *7*, 293.

(91) Tas, J.; de Vries, A. C. J.; Berndsen, R., *Analytical Biochemistry* **1979,** *100*, 264-270.

(92) Hahn, E. C.; Hahn, P. S., *Journal of Virological Methods* **1987,** *15*, 41-52.

(93) Baumann, G.; Chrambach, A., *Analytical Biochemistry* **1976,** *70*, 32-38.
(94) Cain, D. F.; Pitney, R. E., *Analytical Biochemistry* **1968,** *22*, 11-20.
(95) Choules, G. L.; Zimm, B. H., *Analytical Biochemistry* **1965,** *13*, 336-344.
(96) Peacock, A. C.; Dingman, C. W., *Biochemistry* **1967,** *6*, 1818-1827.
(97) Alpers, D. H.; Glickman, R., *Analytical Biochemistry* **1970,** *35*, 314-320.
(98) Hansen, J. N., *Analytical Biochemistry* **1976,** *76*, 37-44.
(99) Hansen, J. N., *Analytical Biochemistry* **1981,** *116*, 146-151.
(100) Faulkner, R. D.; Carraway, R.; Bhatnagar, Y. M., *Biochimica et Biophysica Acta (BBA) - Protein Structure and Molecular Enzymology* **1982,** *708*, 245-252.
(101) Seymour, J. L.; Lazarus, R. A., *Analytical Biochemistry* **1989,** *178*, 243-247.
(102) Späth, P. J.; Koblet, H., *Analytical Biochemistry* **1979,** *93*, 275-285.
(103) Maros, L.; Molnar-Perl, I.; Kover, L., *Journal of the Chemical Society, Perkin Transactions 2* **1976,** *0*, 1337-1342.
(104) Hansen, J. N.; Pheiffer, B. H.; Boehnert, J. A., *Analytical Biochemistry* **1980,** *105*, 192-201.
(105) Galvani, M.; Hamdan, M.; Righetti, P. G., *Electophoresis* **2000,** *21*, 3684-3692.
(106) Haenen, G. R. M. M.; Bast, A., *Biochemical Pharmacology* **1991,** *42*, 2244-2246.

CHAPTER 5

(1) Leriche, G.; Chisholm, L.; Wagner, A., *Bioorganic & Medicinal Chemistry* **2012,** *20*, 571-582.
(2) Chen, G.-Q.; Patel, M. K., *Chemical Reviews* **2011,** *112*, 2082-2099.
(3) Zhou, H.; Woo, J.; Cok, A. M.; Wang, M.; Olsen, B. D.; Johnson, J. A., *Proceedings of the National Academy of Sciences* **2012**.
(4) Merrifield, R. B., *Journal of the American Chemical Society* **1963,** *85*, 2149-2154.
(5) Wang, S.-S., *Journal of the American Chemical Society* **1973,** *95*, 1328-1333.
(6) Scott, P. J. H., *Linker strategies in solid-phase organic synthesis*. 1st ed.; John Wiley & Sons Ltd: **2009**.
(7) Guo, J.; Yu, L.; Turro, N. J.; Ju, J., *Accounts of Chemical Research* **2010,** *43*, 551-563.

(8) Sassolas, A.; Leca-Bouvier, B. D.; Blum, L. J., *Chemical Reviews* **2007,** *108*, 109-139.

(9) Montague, M. F.; Hawker, C. J., *Chemistry of Materials* **2007,** *19*, 526-534.

(10) Gross, R. A.; Kalra, B., *Science* **2002,** *297*, 803-807.

(11) MacDonald, S. A.; Willson, C. G.; Frechet, J. M. J., *Accounts of Chemical Research* **1994,** *27*, 151-158.

(12) Dhar, S.; Kolishetti, N.; Lippard, S. J.; Farokhzad, O. C., *Proceedings of the National Academy of Sciences* **2011,** *108*, 1850-1855.

(13) Dhar, S.; Liu, Z.; Thomale, J. r.; Dai, H.; Lippard, S. J., *Journal of the American Chemical Society* **2008,** *130*, 11467-11476.

(14) Sletten, E. M.; Bertozzi, C. R., *Accounts of Chemical Research* **2011,** *44*, 666-676.

(15) Verhelst, S. H. L.; Fonović, M.; Bogyo, M., *Angewandte Chemie International Edition* **2007,** *46*, 1284-1286.

(16) Lasprilla, A. J. R.; Martinez, G. A. R.; Lunelli, B. H.; Jardini, A. L.; Filho, R. M., *Biotechnology Advances* **2012,** *30*, 321-328.

(17) Bremer, C.; Tung, C. H.; Weissleder, R., *Nature Medicine* **2001,** *7*, 743-748.

(18) Cravatt, B. F.; Wright, A. T.; Kozarich, J. W., Activity-based protein profiling: From enzyme chemistry. *Annual Review of Biochemistry*, **2008**; Vol. 77, pp 383-414.

(19) Cui, L.; Cohen, J. L.; Chu, C. K.; Wich, P. R.; Kierstead, P. H.; Fréchet, J. M. J., *Journal of the American Chemical Society* **2012,** *134*, 15840-15848.

(20) Traut, R. R.; Bollen, A.; Sun, T.-T.; Hershey, J. W. B.; Sundberg, J.; Pierce, L. R., *Biochemistry* **1973,** *12*, 3266-3273.

(21) van Nostrum, C. F.; Veldhuis, T. F. J.; Bos, G. W.; Hennink, W. E., *Polymer* **2004,** *45*, 6779-6787.

(22) Hu, J.; Zhang, G.; Liu, S., *Chemical Society Reviews* **2012,** *41*, 5933-5949.

(23) Murthy, N.; Xu, M.; Schuck, S.; Kunisawa, J.; Shastri, N.; Fréchet, J. M. J., *Proceedings of the National Academy of Sciences* **2003,** *100*, 4995-5000.

(24) Pullela, P. K.; Chiku, T.; Carvan, M. J.; Sem, D. S., *Analytical Biochemistry* **2006,** *352*, 265-273.

(25) Gartner, C. A.; Elias, J. E.; Bakalarski, C. E.; Gygi, S. P., *Journal of Proteome Research* **2007,** *6*, 1482-1491.

(26) D. Nicodemus, G.; J. Bryant, S., *Tissue Engineering: Part B* **2008,** *14*, 149-165.

(27) Patterson, J.; Siew, R.; Herring, S. W.; Lin, A. S. P.; Guldberg, R.; Stayton, P. S., *Biomaterials* **2010,** *31*, 6772-6781.

(28) Phelps, E. A.; Landázuri, N.; Thulé, P. M.; Taylor, W. R.; García, A. J., *Proceedings of the National Academy of Sciences* **2010,** *107*, 3323-3328.

(29) Griset, A. P.; Walpole, J.; Liu, R.; Gaffey, A.; Colson, Y. L.; Grinstaff, M. W., *Journal of the American Chemical Society* **2009,** *131*, 2469-2471.

(30) Nguyen, Q. T.; Olson, E. S.; Aguilera, T. A.; Jiang, T.; Scadeng, M.; Ellies, L. G.; Tsien, R. Y., *Proceedings of the National Academy of Sciences of the United States of America* **2010,** *107*, 4317-4322.

(31) Kloxin, A. M.; Kasko, A. M.; Salinas, C. N.; Anseth, K. S., *Science* **2009,** *324*, 59-63.

(32) Leriche, G.; Budin, G.; Brino, L.; Wagner, A., *European Journal of Organic Chemistry* **2010**, 4360-4364.

(33) Luo, Y.; hoichet, M. S., *Nature Materials* **2004,** *3*, 1476-1122.

(34) Kloxin, A. M.; Tibbitt, M. W.; Anseth, K. S., *Nature Protocols* **2010,** *5*, 1867-87.

(35) Fedorovich, N. E.; Oudshoorn, M. H.; van Geemen, D.; Hennink, W. E.; Alblas, J.; Dhert, W. J. A., *Biomaterials* **2009,** *30*, 344-353.

(36) Meinhardt, M.; Krebs, R.; Anders, A.; Heinrich, U.; Tronnier, H., *Journal of Biomedical Optics* **2008,** *13*, 044030-044030.

(37) Sletten, E. M.; Bertozzi, C. R., *Angewandte Chemie International Edition* **2009,** *48*, 6974-6998.

(38) Hangauer, M. J.; Bertozzi, C. R., *Angewandte Chemie* **2008,** *120*, 2428-2431.

(39) Guo, J., et al., *Proceedings of the National Academy of Sciences* **2008,** *105*, 9145-9150.

(40) Franzini, R. M.; Kool, E. T., *Journal of the American Chemical Society* **2009,** *131*, 16021-16023.

(41) Cera, C.; Egbertson, M.; Teng, S. P.; Crothers, D. M.; Danishefsky, S. J., *Biochemistry* **1989,** *28*, 5665-5669.
(42) Lin, F. L.; Hoyt, H. M.; van Halbeek, H.; Bergman, R. G.; Bertozzi, C. R., *Journal of the American Chemical Society* **2005,** *127*, 2686-2695.
(43) Bentley, D. R., et al., *Nature* **2008,** *456*, 53-59.
(44) Amyes, T. L.; Jencks, W. P., *Journal of the American Chemical Society* **1989,** *111*, 7888-7900.
(45) Gunsalus, I. C.; Barton, L. S.; Gruber, W., *Journal of the American Chemical Society* **1956,** *78*, 1763-1766.
(46) Daun, J.; Fields, S.; Kobayashi, S. *US patent application* US20040186127 A1 **2004**
(47) Pötzsch, R.; Fleischmann, S.; Tock, C.; Komber, H.; Voit, B. I., *Macromolecules* **2011,** *44*, 3260-3269.
(48) Strohalm, M.; Kavan, D.; Novák, P.; Volný, M.; Havlíček, V. r., *Analytical Chemistry* **2010,** *82*, 4648-4651.
(49) Parrish, J. P.; Dueno, E. E.; Kim, S. I.; Jung, K. W., *Synthetic Communications* **2000,** *30*, 2687-2700.
(50) Johnstone, R. A. W.; Rose, M. E., *Tetrahedron* **1979,** *35*, 2169-2173.
(51) Nowick, J. S.; Brower, J. O., *Journal of the American Chemical Society* **2003,** *125*, 876-877.
(52) Upadhyay, S. K., *Chemical Kinetics and Reaction Dynamics*. Springer: **2006**.
(53) Moody, E. M.; Brown, T. S.; Bevilacqua, P. C., *Journal of the American Chemical Society* **2004,** *126*, 10200-10201.
(54) Li, H.; Franzini, R. M.; Bruner, C.; Kool, E. T., *Chembiochem* **2010,** *11*, 2132-2137.
(55) Franzini, R. M.; Kool, E. T., *Chemistry – A European Journal* **2011,** *17*, 2168-2175.
(56) Franzini, R. M.; Kool, E. T., *Bioconjugate Chemistry* **2011,** *22*, 1869-1877.
(57) Kreevoy, M. M.; Taft, R. W., *Journal of the American Chemical Society* **1955,** *77*, 5590-5595.
(58) Staudinger, H.; Meyer, J., *Helvetica Chimica Acta* **1919,** *2*, 635-646.
(59) Scriven, E. F. V.; Turnbull, K., *Chemical Reviews* **1988,** *88*, 297-368.
(60) Saxon, E.; Bertozzi, C. R., *Science* **2000,** *287*, 2007-2010.

(61) van Berkel, S. S.; van Eldijk, M. B.; van Hest, J. C. M., *Angewandte Chemie International Edition* **2011,** *50*, 8806-8827.

(62) Prescher, J. A.; Dube, D. H.; Bertozzi, C. R., *Nature* **2004,** *430*, 873-877.

(63) Saxon, E.; Luchansky, S. J.; Hang, H. C.; Yu, C.; Lee, S. C.; Bertozzi, C. R., *Journal of the American Chemical Society* **2002,** *124*, 14893-14902.

(64) Whitesides, G. M.; Lilburn, J. E.; Szajewski, R. P., *The Journal of Organic Chemistry* **1977,** *42*, 332-338.

(65) Baker, N. D.; Griffin, R. J.; Irwin, W. J.; Slack, J. A., *International Journal of Pharmaceutics* **1989,** *52*, 231-238.

(66) Handlon, A.; Oppenheimer, N., *Pharmaceutical Research* **1988,** *5*, 297-299.

(67) Shay, K. P.; Moreau, R. F.; Smith, E. J.; Smith, A. R.; Hagen, T. M., *Biochimica et Biophysica Acta (BBA) - General Subjects* **2009,** *1790*, 1149-1160.

(68) Han, J. C.; Han, G. Y., *Analytical Biochemistry* **1994,** *220*, 5-10.

(69) Matsugo, S.; Han, D.; Tritschler, H. J.; Packer, L., *Biochemistry & Molecular Biology International* **1996,** *38*, 51-59.

(70) Naik, A.; Irwin, W. J.; Griffin, R. J., *International Journal of Pharmaceutics* **1993,** *89*, 51-63.

(71) Cartwright, I. L.; Hutchinson, D. W.; Armstrong, V. W., *Nucleic Acids Research* **1976,** *3*, 2331-2339.

(72) Shaked, Z. e.; Szajewski, R. P.; Whitesides, G. M., *Biochemistry* **1980,** *19*, 4156-4166.

(73) Luo, D.; Smith, S. W.; Anderson, B. D., *Journal of Pharmaceutical Sciences* **2005,** *94*, 304-316.

(74) Gascoigne, I. M.; Radda, G. K., *Biochimica et Biophysica Acta* **1967,** *131*, 498-507.

(75) Lamoureux, G. V.; Whitesides, G. M., *The Journal of Organic Chemistry* **1993,** *58*, 633-641.

(76) Singh, R.; Whitesides, G. M., *The Journal of Organic Chemistry* **1991,** *56*, 2332-2337.

(77) Lukesh, J. C.; Palte, M. J.; Raines, R. T., *Journal of the American Chemical Society* **2012,** *134*, 4057-4059.

(78) Getz, E. B.; Xiao, M.; Chakrabarty, T.; Cooke, R.; Selvin, P. R., *Analytical Biochemistry* **1999,** *273*, 73-80.

(79) Tam, A.; Soellner, M. B.; Raines, R. T., *Journal of the American Chemical Society* **2007,** *129*, 11421-11430.

(80) Pyun, S. Y.; Lee, Y. H.; Kim, T. R., *Kinetics and Catalysis* **2005,** *46*, 21-28.

(81) Shalev, D. E.; Chiacchiera, S. M.; Radkowsky, A. E.; Kosower, E. M., *The Journal of Organic Chemistry* **1996,** *61*, 1689-1701.

(82) Leffler, J. E.; Tsuno, Y., *The Journal of Organic Chemistry* **1963,** *28*, 902-906.

(83) Leffler, J. E.; Temple, R. D., *Journal of the American Chemical Society* **1967,** *89*, 5235-5246.

(84) Mathew, J. S.; Klussmann, M.; Iwamura, H.; Valera, F.; Futran, A.; Emanuelsson, E. A. C.; Blackmond, D. G., *The Journal of Organic Chemistry* **2006,** *71*, 4711-4722.

(85) Whipple, E. B.; Ruta, M., *The Journal of Organic Chemistry* **1974,** *39*, 1666-1668.

(86) Migneault, I.; Dartiguenave, C.; Bertrand, M. J.; Waldron, K. C., *BioTechniques* **2004,** *37*, 790-802.

(87) Gruen, L. C.; McTigue, P. T., *Journal of the Chemical Society* **1963**, 5217-5223.

(88) Jencks, W. P., *Journal of the American Chemical Society* **1959,** *81*, 475-481.

CHAPTER 6

(1) Stuart, M. A. C., et al., *Nature Materials* **2010,** *9*, 101-113.

(2) Ugelstad, J.; Soderberg, L.; Berge, A.; Bergstrom, J., *Nature* **1983,** *303*, 95-96.

(3) Zhang, J.; Xu, S.; Kumacheva, E., *Journal of the American Chemical Society* **2004,** *126*, 7908-7914.

(4) Kang, Y.; Taton, T. A., *Angewandte Chemie International Edition* **2005,** *44*, 409-412.

(5) Gan, D.; Mueller, A.; Wooley, K. L., *Journal of Polymer Science Part A: Polymer Chemistry* **2003,** *41*, 3531-3540.

(6) Dong, B.; Manolache, S.; Somers, E. B.; Lee Wong, A. C.; Denes, F. S., *Journal of Applied Polymer Science* **2005,** *97*, 485-497.

(7) Kopecek, J., *Journal of Polymer Science Part A: Polymer Chemistry* **2009,** *47*, 5929-5946.

(8) Van Vlierberghe, S.; Dubruel, P.; Schacht, E., *Biomacromolecules* **2011,** *12*, 1387-1408.

(9) Wichterle, O.; Lim, D., *Nature* **1960,** *185*, 117-118.

(10) Lee, K. Y.; Mooney, D. J., *Chemical Reviews* **2001,** *101*, 1869-1880.

(11) Hoffman, A. S., *Advanced Drug Delivery Reviews* **2002,** *54*, 3-12.

(12) Li, P., et al., *Nature Materials* **2011,** *10*, 149-156.

(13) Gilbert, P. M., et al., *Science* **2010,** *329*, 1078-1081.

(14) Rabilloud, T., *Journal of Proteomics* **2010,** *73*, 1562-1572.

(15) D. Nicodemus, G.; J. Bryant, S., *Tissue Engineering: Part B* **2008,** *14*, 149-165.

(16) Lin, C.-C.; Metters, A. T., *Advanced Drug Delivery Reviews* **2006,** *58*, 1379-1408.

(17) Raymond, S.; Weintraub, L., *Science* **1959,** *130*, 711.

(18) Vesterberg, O., *Electophoresis* **1993,** *14*, 1243-1249.

(19) Alberts, B.; Johnson, A.; Lewis, J.; Raff, M.; Roberts, K.; Walter, P., *Molecular Biology of the Cell*. 5th ed.; Garland Science: **2007**.

(20) Seelert, H.; Krause, F., *Electophoresis* **2008,** *29*, 2617-2636.

(21) Aaij, C.; Borst, P., *Biochimica et Biophysica Acta (BBA) - Nucleic Acids and Protein Synthesis* **1972,** *269*, 192-200.

(22) Raymond, S.; Nakamichi, M., *Analytical Biochemistry* **1962,** *3*, 23-30.

(23) Stellwagen, N. C., *Electophoresis* **2009,** *30*, S188-S195.

(24) Hawcroft, D. M., *Electrophoresis*. Oxford University Press: **1997**.

(25) Krause, F., *Electrophoresis* **2006,** *27*, 2759-2781.

(26) Poetsch, A.; Neff, D.; Seelert, H.; Schägger, H.; Dencher, N. A., *Biochimica et Biophysica Acta (BBA) - Biomembranes* **2000,** *1466*, 339-349.

(27) Coppola, J. A.; Luse, D. S., *Journal of Molecular Biology* **1984,** *178*, 415-437.

(28) Seelig, B., *Nature Protocols* **2011,** *6*, 540-552.

(29) Kim, Y. K.; Kwon, Y. J., *Proteomics* **2009,** *9*, 3765-3771.

(30) Kim, Y. K.; Kwon, Y. J., *Electophoresis* **2010,** *31*, 1656-1661.

(31) Antal, J.; Banyasz, B.; Buzas, Z., *Electrophoresis* **2007,** *28*, 508-511.

(32) Anker, H. S., *FEBS Letters* **1970,** *7*, 293.

(33) Tas, J.; de Vries, A. C. J.; Berndsen, R., *Analytical Biochemistry* **1979,** *100*, 264-270.

(34) Cain, D. F.; Pitney, R. E., *Analytical Biochemistry* **1968,** *22*, 11-20.

(35) Choules, G. L.; Zimm, B. H., *Analytical Biochemistry* **1965,** *13*, 336-344.

(36) Peacock, A. C.; Dingman, C. W., *Biochemistry* **1967,** *6*, 1818-1827.

(37) Alpers, D. H.; Glickman, R., *Analytical Biochemistry* **1970,** *35*, 314-320.

(38) Hansen, J. N., *Analytical Biochemistry* **1976,** *76*, 37-44.

(39) Hansen, J. N., *Analytical Biochemistry* **1981,** *116*, 146-151.

(40) Faulkner, R. D.; Carraway, R.; Bhatnagar, Y. M., *Biochimica et Biophysica Acta (BBA) - Protein Structure and Molecular Enzymology* **1982,** *708*, 245-252.

(41) Seymour, J. L.; Lazarus, R. A., *Analytical Biochemistry* **1989,** *178*, 243-247.

(42) Duckworth, B. P.; Xu, J.; Taton, T. A.; Guo, A.; Distefano, M. D., *Bioconjugate Chemistry* **2006,** *17*, 967-974.

(43) Delgado, M.; Spanka, C.; Kerwin, L. D.; Wentworth, P.; Janda, K. D., *Biomacromolecules* **2001,** *3*, 262-271.

(44) Hassur, S. M.; Whitlock Jr, H. W., *Analytical Biochemistry* **1974,** *59*, 162-164.

(45) Zipper, H.; Brunner, H.; Bernhagen, J.; Vitzthum, F., *Nucleic Acids Research* **2004,** *32*, e103.

(46) Sambrook, J.; Russell, D. W., *Molecular Cloning: a Laboratory Manual*. 3rd ed.; Cold Spring Harb. Lab. Press: **2001**; Vol. 3.

(47) Ortí, G.; Pearse, D. E.; Avise, J. C., *Proceedings of the National Academy of Sciences* **1997,** *94*, 10745-10749.

(48) Lavabre, D.; Pimienta, V.; Levy, G.; Micheau, J. C., *The Journal of Physical Chemistry* **1993,** *97*, 5321-5326.

(49) Gibson, M. S.; Bradshaw, R. W., *Angewandte Chemie International Edition in English* **1968,** *7*, 919-930.

(50) Kwon, Y. J.; Standley, S. M.; Goodwin, A. P.; Gillies, E. R.; Fréchet, J. M. J., *Molecular Pharmaceutics* **2005,** *2*, 83-91.

(51) Broeckx, W.; Overbergh, N.; Samyn, C.; Smets, G.; L'Abbé, G., *Tetrahedron* **1971,** *27*, 3527-3534.

(52) Anderson, G. T.; Henry, J. R.; Weinreb, S. M., *The Journal of Organic Chemistry* **1991,** *56*, 6946-6948.

(53) Li, Y.; Yang, J.; Benicewicz, B. C., *Journal of Polymer Science Part A: Polymer Chemistry* **2007,** *45*, 4300-4308.

(54) Sumerlin, B. S.; Tsarevsky, N. V.; Louche, G.; Lee, R. Y.; Matyjaszewski, K., *Macromolecules* **2005,** *38*, 7540-7545.

(55) Ladmiral, V.; Legge, T. M.; Zhao, Y.; Perrier, S. b., *Macromolecules* **2008,** *41*, 6728-6732.

(56) Li, G.; Zheng, H.; Bai, R., *Macromolecular Rapid Communications* **2009,** *30*, 442-447.

(57) Li, C.; Hu, J.; Yin, J.; Liu, S., *Macromolecules* **2009,** *42*, 5007-5016.

(58) Young, A. J. Tailored Biomaterials for T Cell-Directed Applications. University of Minnesota, **2011**.

(59) Brauer G, M.; Argentar, H., Initiator-Accelerator Systems for Dental Resins. In *Initiation of Polymerization*, American Chemical Society: **1983**; Vol. 212, pp 359-371.

(60) Oldfield, F. F.; Yasuda, H. K., *Journal of Biomedical Materials Research* **1999,** *44*, 436-445.

(61) Fisher, R. G.; Woods, N. E.; Fuchs, H. E.; Sweet, R. M., *Journal of Biological Chemistry* **1980,** *255*, 5082-5089.

(62) Fu, J.; Schoch, R. B.; Stevens, A. L.; Tannenbaum, S. R.; Han, J., *Nature Nanotechnology* **2007,** *2*, 121-128.

(63) Clegg, G. A.; Fitton, J. E.; Harrison, P. M.; Treffry, A., *Progress in Biophysics and Molecular Biology* **1981,** *36*, 53-86.

(64) Yang, V. C.; Langer, R., *Analytical Biochemistry* **1985,** *147*, 148-155.

(65) Summer, H.; Dröge, P.; Grämer, R., *Journal of Visualized Experiments* **2009**, e1485.

CHAPTER 7

(1) Hughes, S.; Moody, A., *PCR (Methods Express)*. 1st ed.; Scion Publishing Ltd.: **2006**.

(2) Alkilany, A. M.; Lohse, S. E.; Murphy, C. J., *Accounts of Chemical Research* **2012,** *46*, 650-661.

(3) Fritzsche, W.; Taton, T. A., *Nanotechnology* **2003,** *14*, R63.

(4) Shendure, J.; Ji, H., *Nature Biotechnology* **2008,** *26*, 1135-1145.

(5) Viuf, C.; Bols, M., *Angewandte Chemie International Edition* **2001,** *40*, 623-625.

(6) Lamoureux, G. V.; Whitesides, G. M., *The Journal of Organic Chemistry* **1993,** *58*, 633-641.

(7) Lukesh, J. C.; Palte, M. J.; Raines, R. T., *Journal of the American Chemical Society* **2012,** *134*, 4057-4059.

(8) Chen, Y.; Kamlet, A. S.; Steinman, J. B.; Liu, D. R., *Nature Chemistry* **2011,** *3*, 146-153.

(9) Sletten, E. M.; Bertozzi, C. R., *Accounts of Chemical Research* **2011,** *44*, 666-676.

(10) Sletten, E. M.; Bertozzi, C. R., *Angewandte Chemie International Edition* **2009,** *48*, 6974-6998.